الجمهورية الجزائرية الديمقراطية الشعبية
People's Democratic Republic of Algeria
وزارة التعليم العالي والبحث العلمي
Ministry of Higher Education and Scientific Research

جامعة قاصدي مرباح ورقلة
University of Kasdi Merbah, Ouargla

كلية التكنولوجيات الحديثة للمعلومات والاتصالات
Faculty of New Technologies Information and Communication

قسم الإلكترونيك والاتصالات
Department of Electronics and Telecommunications

Thesis

Presented to obtain a Ph.D. degree ***in Automation***

Option: ***Automatic and systems***

Title:

Contribution to the development of a fault diagnosis technique for photovoltaic generators

Author:
Belkacem AOUFI

Publicly presented on: 05/03/2024

Jury:

President:	Mr. Djamel SAMAI	Prof. University of Kasdi Merbah, Ouargla.
Reporter:	Mr. Oussama HACHANA	Prof. University of Kasdi Merbah, Ouargla.
Co-reporter:	Mr. Mohamed Amine SID	Prof. Ferhat Abbas University, Setif1.
Examiner:	Mr. Billel MEGHNI	Prof. University of Badji Mokhtar, Annaba
Examiner:	Mr. Boubakeur ROUABAH	MCA. University of Kasdi Merbah, Ouargla.
Examiner:	Mr. Khaled BENSID	MCA. University of Kasdi Merbah, Ouargla.

Academic year: 2023/2024

Acknowledgment

First and foremost, I thank Allah, the Almighty, for assisting me and giving me the strength and willingness to conduct the research necessary to complete this work.

I gratefully acknowledge Prof. Oussama HACHANA, supervisor of my Ph.D. project, for his follow-up, patience, and availability, and for his suggestions as he oversaw my activities during all phases to perform coherent research work.

I want to express my gratitude to Prof. Mohamed Amine SID, professor, and researcher at the University of Sétif, for his co-supervision of my research activities, availability, politeness, guidance, and information sharing, from which I have always benefited.

In addition, I would like to thank all the scientific committee members, especially Prof. Djamel SAMAI, the doctoral project director, for his help and guidance during the whole project.

I sincerely thank my mother, my wife, and my children for their patience with me during these long four years and for their encouragement to conduct this work, despite constraints and some difficult moments.

Ouargla, 10/01/2024

Belkacem AOUFI

شكر وعرفــان

أولًا وقبل كل شيء أشكر الله تعالى الذي وفقني ومنحني القوة والإرادة لإجراء كل ما يلزم لإتمام هذا لإتمام هذا العمل.

أتقدم بالشكر الجزيل للأستاذ أسامة حشانة، المشرف على مشروع رسالة الدكتوراه الخاصة بي، وذلك لمتابعته وصبره، ولاقتراحاته البنّاءة طيلة مدة إشرافه على أنشطتي البحثية خلال جميع مراحلها من أجل إنتاج بحثي متماسك.

أود أن أعرب عن امتناني للأستاذ محمد أمين سيد، الأستاذ والباحث بجامعة سطيف، لمشاركته في الإشراف على أنشطتي البحثية، وتوجيهاته، وأدبه وتواضعه، ومعلوماته التي استفدت منها كثيرا.

بالإضافة إلى ذلك، أود أن أشكر جميع أعضاء اللجنة العلمية، وخاصة الأستاذ جمال سامعي، مدير مشروع الدكتوراه، لمساعدته وتوجيهه خلال المشروع بأكمله.

وأتقدم بالشكر الجزيل إلى أمي وزوجتي وأولادي على صبرهم معي طيلة هذه السنوات الأربعة وتشجيعهم الدائم للقيام بهذا العمل، رغم المعوقات وبعض اللحظات الصعبة.

ورقلة، 2024/01/10

بلقاسم عوفي

Table of contents

Acknowledgment ii
Table of contents iii
List of figures vi
List of tables ix
Acronyms x
Symbols xii
List of publications xv
Abstract xvi
General introduction 1
Preamble 2
Problem formulation and motivation to solve it 3
Contribution and novelty of the thesis 4
Thesis organization 4
Chapter 01: PV generator fault diagnosis methods: State-of-the-art 6
1.1. Introduction 7
1.2. Advantages of PV generator fault diagnosis 8
1.3. Basic definitions 8
1.3.1. Fault 9
1.3.2. Residual 9
1.3.3. Fault detection 9
1.3.4. Fault isolation 9
1.3.5. Fault identification (classification) 9
1.3.6. Fault diagnosis 9
1.4. Types of PV generator faults 10
1.4.1. Hot spot faults 11
1.4.2. Ground fault 12
1.4.3. Line-to-line fault 12
1.4.4. Series/parallel arc fault 13
1.4.5. Auxiliary diodes fault 13
1.4.6. Junction box fault 14
1.5. Causes of faults 15
1.6. Consequences of faults 15
1.7. Methods of PV generator fault diagnosis 15
1.7.1. Visual inspection method 15
1.7.2. Imaging-based methods 16

1.7.3. Electrical measurement-based methods 17
1.8. Conclusion 19
Chapter 02: Basic principles of photovoltaics 20
2.1. Introduction 21
2.2. Sunlight radiation 23
2.3. Photovoltaic effects 27
2.4. Photovoltaic materials and technologies 28
2.4.1. Crystalline silicon technology (PV first generation) 28
2.4.2. Thin film technology (PV second generation) 29
2.4.3. Emerging technology (PV third generation) 29
2.5. Trends and future PV technologies 30
2.6. Types and applications of PV generators 34
2.7. Conclusion 36
Chapter 03: Photovoltaic generator modeling 38
3.1. Introduction 39
3.2. Concept of modeling 39
3.3. Advantages of PV generator modeling 40
3.4. PV generator modeling 40
3.4.1. I-V characteristic of the PV generator 42
3.4.2. Electrical circuit-Based Models of the PV generator 42
3.5. Solving the PV generator modeling problem 49
3.5.1. Analytical methods 49
3.5.2. Numerical iterative methods 50
3.5.3. Metaheuristic methods 50
3.5.4. Lambert W function 51
3.5.5. Objective function for optimization methods 53
3.5.6. Objective function design for the PV generator modeling 55
3.6. Contribution to the PV generator modeling: Proposed methods 57
3.6.1. Bat Artificial Bee Colony Optimizer (BABCO) 57
3.6.2. Nested Loop Biogeography-based Optimization-Differential Evolution Optimizer (NLBBODE) 59
3.6.3. Results of the PV generator modeling using the proposed optimizers 61
3.6.4. Analysis of the statistical results 65
3.6.5. Results of convergence analysis 67
3.6.6. Validation of the proposed methods using experimental testing 69
3.7. Conclusion 72

Chapter 04: Photovoltaic generator simulator in normal and faulty conditions 73
4.1. Introduction 74
4.2. Description of the physical PV generator and the experimental setup 75
4.3. MATLAB/Simulink simulator of the PV generators 76
4.4. Simulator design procedure 77
4.5. PV Simulator outputs in healthy conditions 81
4.6. PV Simulator outputs in faulty conditions 84
4.6.1. Partial shading scenarios 84
4.6.2. Scenarios of other types of faults 89
4.7. Conclusion 92
Chapter 05: Contribution to the PV generator fault diagnosis: Proposed technique 94
5.1. Introduction 95
5.2. Hypothesis 96
5.3. Proposed PV generator fault diagnosis technique (Differential Shuffled Complex Evolution) "DSCE" 96
5.4. Modeling of the PV generator using "DSCE" 98
5.4.1 PV generator model parameter extraction in healthy conditions 98
5.4.2 Fault detection and diagnosis of the PV string using "DSCE" 101
5.5. Considered faulty scenarios 104
5.5.1 Partial shading scenarios 104
5.5.2 Other types of faults and simultaneous faults scenarios 104
5.6. Results, discussion and interpretation 105
5.7. Design of the PV string fault tree algorithm 106
5.8. Conclusion 108
General conclusion 115
Thesis conclusion 116
Perspectives and Future Works 117
Appendices 119
Appendix A: Extracts of the published journal and conferences papers 119
Appendix B: 123
B.1: Pseudo code of the BABCO algorithm 123
B.2: Pseudo code and flowchart of the NLBBODE algorithm 124
B. 3: Pseudo codes and flowchart of the DSCE algorithm 126
References 129

List of Figures

Fig. 0.1 Global net generating capacity of electricity using renewable energy 3
Fig. 1.1 Typical photovoltaic system. 8
Fig. 1.2 Thermographic image of (a) cell hotspot (b) module hotspot. 11
Fig. 1.3 Examples of PV Cell/module visible faults 12
Fig. 1.4 DC cable melted due to electrical arcing in PV plant. 13
Fig. 1.5 Examples of diodes faults 14
Fig. 1.6 Examples of fire occurred on a rooftop PV generator and junction box 14
Fig. 1.7 Relation between AI, ML, and EL 18
Fig. 2.1 Solar spectra at AM0 and AM1.5 23
Fig. 2.2 Types of the solar radiation 24
Fig. 2.3 Distribution of G0 over one year 26
Fig. 2.4 Distribution of the clearance Kt over one year 26
Fig. 2.5 Distribution of the variable S0 along one year 26
Fig. 2.6 Photovoltaic effect on a PV cell 27
Fig. 2.7 Structure of the 1st generation PV material 28
Fig. 2.8 Structure of the 2st generation PV material (Thin film cell & module) 29
Fig. 2.9 Example of mini perovskite PV module 30
Fig. 2.10 Best achieved efficiency of different PV technologies over the last decade's 33
Fig. 2.11 PV generators: cell, module, panel, and array 34
Fig. 2.12 Classification of PV systems 35
Fig. 2.13 Grid-connected PV system 36
Fig. 3.1 Graph of PV module I-V characteristic provided by Sandia Labs 43
Fig. 3.2 Electrical equivalent circuit of the single-diode model (SDM) 44
Fig. 3.3 Electrical equivalent circuit of the double-diode model (DDM). 47
Fig. 3.4 Electrical equivalent circuit of the triple-diode model (TDM) 48
Fig. 3.5 Electrical equivalent circuit of the PV module/String model 48
Fig. 3.6 Graph of the Lambert W function 52
Fig. 3.7. Convergence curves of NLBBODE, BBO, and DE optimizers for the PV cell model 68
Fig. 3.8. Convergence curves of NLBBODE, BBO, and DE optimizers for Photowatt-PWP-201 module model 68

Fig. 3.9 Convergence curves of NLBBODE, BBO, and DE optimizers for STM6-40/36 module model 68
Fig. 3.10 Convergence curves of BABCO and competing optimizers for R.T.C. France solar cell 69
Fig. 3.11 Convergence curves of BABCO and competing optimizers for the Photowatt-PWP-201 module 69
Fig. 3.12 Convergence curves of BABCO and competing optimizers for the STM6-40/36 module 69
Figure 3.13. Measured and estimated data based on the parameters identified by BABCO on CLS-220P module 71
Fig 3.14. Measured and estimated data based on the parameters identified by NLBBODE on the CLS-220P string 71
Fig. 4.1 Experimental setup of the PV generator and accessories 76
Fig. 4.2. SDM of PV module/string 78
Fig. 4.3. Matlab-Simulink emulator of one PV substring 78
Fig. 4.4. Matlab-Simulink emulator of the entire PV string 79
Fig. 4.5. Set of the I-V curves satisfying negative gradient condition 81
Fig. 4.6. AE between measured and simulated values of key electrical parameters of the PV string 82
Fig 4.7. PV string simulator results compared to real measured data 83
Fig 4.8. Scenario # 01 85
Fig 4.9. Scenario # 02 86
Fig 4.10. Scenario # 03 86
Fig 4.11. Scenario # 04 87
Fig 4.12. Scenario # 05 87
Fig 4.13. I-V curves of measured and simulated data of different scenarios 88
Fig 4.14. P-V curves of measured and simulated data of different scenarios 89
Fig 4.15. Results of other types and simultaneous faults scenarios 91
Figure 5.1. Results of the parameters extracted by DSCE on CLS-220P module model 100
Figure 5.2 Results of the parameters extracted by DSCE on the CLS-220P string model 101
Figure 5.3 Estimated and measured data in a scenario of 02 shaded substrings 101
Figure 5.4 Measured and estimated data of 05 shaded substrings 102
Figure 5.5 Measured and estimated data of scenario of one substring shaded, a bypass diode inverted, and connection resistance fault 103

Figure 5.6 Graphs of the estimated parameters using the DSCE technique in the different scenarios of case 1.1 109
Figure 5.7 Graphs of the estimated parameters using the DSCE technique for scenarios of case 1.2 110
Figure 5.8 Graphs of the estimated parameters using the DSCE technique for scenarios of case 1.3 111
Figure 5.9 Graphs of the estimated parameters using the DSCE technique for scenarios of case n° 02 112
Figure 5.10 Graphs of the estimated parameters using the DSCE technique for scenarios of case n° 03 113
Figure 5.11 Flowchart of the fault tree algorithm using the DSCE technique 114

List of tables

Table 1.1 Categorization of PV generator faults according to their causes and consequences ... 10
Table 2.1 Clearness index in different days ... 25
Table 3.1 PV generators characteristics and environment working conditions. ... 62
Table 3.2 Search range boundaries of the solar PV generators models ... 62
Table 3.3 Results of the proposed methods for R.T.C. France solar cell modeling ... 63
Table 3.4 Results of the proposed methods for the Photowatt-PWP-201 module modeling ... 64
Table 3.5. Results of the proposed methods for the STM6-40/36 module modeling ... 65
Table 3.6 Statistical results of RMSE obtained by the proposed methods ... 65
Table 3.7 Results of modeling of the CLS-220P module using the BABCO method ... 70
Table 3.8 Results of modeling of the PV CLS-220P string using NLBBODE method ... 71
Table 4.1 Lookup table for CLS 220P PV string ... 80
Table 4.2. PV string in healthy working conditions ... 82
Table 4.3. Partial shading scenarios ... 85
Table 4.4. Results of simulation of the partial shading scenarios ... 88
Table 4.5. Scenarios of other types and simultaneous faults ... 91
Table 4.6. Results of simulation of scenarios (S 2.1, …, S 2.5) ... 92
Table 5.1 Statistical results obtained by DSCE method and compared to recent methods ... 99
Table 5.2 Extracted parameters of the CLS-220P module using DSCE technique ... 99
Table 5.3 Extracted parameters of the CLS-220P string using DSCE technique ... 100
Table 5.4 Estimated parameters using the DSCE technique for scenarios of case 1.1 ... 109
Table 5.5 Estimated parameters using the DSCE technique for scenarios of case 1.2 ... 110
Table 5.6 Estimated parameters using the DSCE technique for scenarios of case 1.3 ... 111
Table 5.7 Estimated parameters using the DSCE technique in scenarios of case n° 02 ... 112
Table 5.8 Estimated parameters using the DSCE technique for scenarios of case n° 03 ... 113

Acronyms

A	ampere
ABC	artificial bee colony
ABC-DE	artificial bee colony-differential evolution
AC	alternating current
AE	absolute error
AI	Artificial intelligence
AM0	air mass zero (zero atmosphere)
AM1.5	air mass 1.5
a-Si	amorphous silicon
a-Si H	amorphous silicon hydrogenated
BABCO	Bat-Artificial Bee Colony Optimizer
BIPVS	building-integrated photovoltaic system
BPFPA	bee pollinator flower pollination algorithm
CCC	current-carrying conductor
CCE	competitive complex evolution
CdTe	cadmium telluride
CIGS	copper indium gallium selenide
DC	direct current
DDM	double diode model
DE	differential evolution
DHI	diffuse horizontal irradiance
DIEEI	Dipartimento di Ingegneria Elettrica, Elettronica e dei Sistemi
DSCE	Differential-Shuffled Complex Evolution
DT	decision tree
EL	ensemble learning
G	irradiance
GA	genetic algorithm
GCPSO	guaranteed convergence particle swarm optimization
GDI	global diffuse irradiance
GWO	grey wolf optimizer
GWOCS	grey wolf optimizer and cuckoo search
HS	harmony search
IEC TS	international electrotechnical commission, technical specification
IR	infrared

IRENA	International Renewable Energy Agency
ITLBO	improved teaching-learning-based optimization
I-V	current-voltage
K	kelvin
k-NN	K-nearest neighbors
LL	lower limit
MAE	mean absolute error
ML	machine learning
MPPT	maximum power point tracking
MRE	mean relative error
MSE	mean squared error
NCCC	non-current-carrying conductors
NFE	number of function evaluation
NLBBODE	Nested-Loop Biogeography-Based Optimization-Differential Evolution.
nm	nanometer
NNs	neural networks
NREL	national renewable energy laboratory
OC	open-circuit
PGJAYA	performance-guided Jaya
Positive-negative	P-N
PSO	particle swarm optimization
P-V	power-voltage
PV	Photovoltaic
QD	Quantum dots
RAMS	Reliability, availability, maintainability, and safety
RE	relative error
RF	random forest
RMSE	root mean squared error
s	second
SA	simulated annealing
SC	short-circuit
SCE	shuffled complex evolution
SDM	single diode model
Si	silicon
STC	standard test conditions

StD	standard deviation
STFT	special trans function theory
SVM	support vector machine
T	cells' temperature
TDM	triple diode model
TS	Taylor series
UL	upper limit
V	volt
W	watt
WOA	whale optimization algorithm

Symbols

d	day of the year.
Dim	dimension of problem
E	highest possible rate emigration
E_g	band gap energy of the semiconductor
FF	fill factor
$Freq_i$	frequency of the ultrasonic wave of the i^{th} bat
G_0	extraterrestrial radiation on a horizontal surface for a day
G_{Dif}	diffuse irradiance
G_{Dir}	direct irradiance
G_G	global solar irradiance
G_{Ref}	reflected irradiance
G_{STC}	solar irradiance at standard test conditions
H_i	number of species present in the habitats
I	highest possible rate of immigration
I_{Estim}	estimated current
IAE (I_L)	estimated individual absolute error
I_d	diode current
I_L	cell output current
$I_{L\ Meas}$	measured current
Impp	current at the maximum power point
I_{ph}	photocurrent
I_{out}	output current

I_{phSTC}	photo-current generated at standard test conditions
I_{sc}	short circuit current
I_{scSTC}	short circuit current at standard test conditions
I_{sd}	reverse saturation current of diode
I_{sdSTC}	nominal saturation current
I_{sh}	shunt resistor current
It_{Max}	maximum number of iterations
I-V	current-voltage characteristics
k	boltzmann constant
K_i	Current temperature coefficient
k_{max}	number of experimental data
K_r	keeping rate
K_t	daily clearness index
Mpp	maximum power point
n	diode ideal factor
n_1	diffusion diode ideal factor
n_2	recombination diode ideal factor
n_3	recombination defect diode ideal factor
N_p	number of solar cells in parallel
NP	number of populations
N_s	number of solar cells in series
$Ob_{Classic}$	classic objective function
$Ob_{Lambert}$	objective function using the Lambert W function
Pr_i	probability evaluation
P-V	power-voltage characteristics
q	electron charge
R_s	series resistance
R_{sh}	shunt resistance
S_0	time between sunrise and sunset
T_{STC}	temperature at standard test conditions
V_L	cell output voltage
Vmpp	voltage at the maximum power point
V_{oc}	open-circuit voltage
V_{th}	thermal voltage
W	lambert equation solution

X_i	position of the i^{th} individual
X_i^{new}	new position
X_{best}	best position closest to the pray so far
β_s	the hour angle of the sunset for the horizontal surface
λ	immigration rate
Ψ	group of top-performing bats
∂	declination.
$\emptyset$	latitude
μ	emigration rate

List of publications

International journal papers:

- Hachana O, Aoufi B, Tina GM, Sid MA, Photovoltaic mono and bifacial module/string electrical model parameters identification and validation based on a new differential evolution bee colony optimizer, *Energy Conversion and Management*, 248, 114667, 2021. https://doi.org/10.1016/j.enconman.2021.114667

- B Aoufi, O Hachana, MA Sid, GM Tina, Precise and fast parameter identification of mono-crystalline, poly-crystalline, and mono-facial photovoltaic modules using a new Bat Artificial Bee Colony optimizer, *Journal of Computational Electronics*, 2022; **21**, pages491–512. DOI: https://doi.org/10.1007/s10825-022-01870-4

- Aoufi B, Hachana O, Sid MA, Tina GM. NLBBODE optimizer for accurate and fast modeling of photovoltaic module/string generator and its application to solve real world constrained optimization problems. *Applied Soft Computing*. 2023 Sep 1; 145: 110597. DOI: https://doi.org/10.1016/j.asoc.2023.110597

International communication conferences:

- Aoufi B, Hachana O. A New Mutated-Firefly Algorithm for Parameters Extraction of Solar Photovoltaic Cell Model. In Hatti M. (eds) Artificial Intelligence and Renewables Towards an Energy Transition, ICAIRES. Lecture Notes in Networks and Systems, Springer 2021; 174. https://doi.org/10.1007/978-3-030-63846-7_52.
- Aoufi B, Hachana O, Mohamed Amine Sid, Parameter estimation of solar photovoltaic cell models using hybrid metaheuristic algorithm NLHSDE, in the first International Conference on Sustainable Energy and Advanced Materials, IC-SEAM'21 April 21-22, 2021, Ouargla.

Abstract (English)

In today's world, renewable energy is becoming increasingly popular due to growing concerns about the environment and increasing demand for energy. Of all forms of renewable energy, photovoltaic energy appears to be the most promising option for global production. However, PV power plants often encounter technical faults that can negatively affect the performance of PV panels and their components. These defects include partial shading, aging, cracks in photovoltaic cells, hot spots, short circuits, open circuit faults, and others. To effectively address these challenges, an automatic fault diagnosis system is crucial. This thesis proposes three new metaheuristic techniques for modeling photovoltaic generators quickly and accurately. The third technique was used for fault diagnosis through the process of the PV generator modeling itself. This strategy adopted for fault diagnosis is based on the assumption that I-V data acquired during healthy conditions produce correct model parameters, while I-V data acquired during faulty or abnormal conditions produce modeling parameters that contain the same faults' signatures. The results indicate that this strategy is innovative, reliable, and accurate and that the initial assumption was valid and proven.

Keywords: fault detection, fault diagnosis, PV generator modeling, metaheuristic technique, parameter identification, simulation, objective function.

ملخّـص (Arabic)

في وقتنا الحاضر يتزايد الطلب العالمي على الطاقة، وتكتسب الطاقة المتجددة شعبية متنامية باعتبارها بديلاً أكثر صداقة للبيئة من الوقود الأحفوري. من بين الأشكال المختلفة للطاقة المتجددة تظهر الطاقة الكهروضوئية المرشح الأوفر حظّا لتبوء الصدارة في الإنتاج العالمي. ومع ذلك، غالبًا ما تواجه محطات الطاقة الكهروضوئية أعطاباً فنية يمكن أن تؤثر على أداء الألواح الكهروضوئية ومكوناتها، مثل التظليل الجزئي وشيخوخة الخلايا الكهروضوئية والشقوق التي قد تصيبها والنقاط الساخنة والدوائر القصيرة ومشاكل الدائرة المفتوحة وغيرها. ولمواجهة هذه التحديات بشكل فعال، يعد وجود نظام تشخيص الأعطال التلقائي أمرًا بالغ الأهمية. تقترح هذه الأطروحة ثلاث تقنيات جديدة من نوع الاستدلال الأسمى، لنمذجة المولدات الكهروضوئية بسرعة ودقة. تمّ استخدام التقنية الثالثة لتشخيص الأخطاء من خلال عملية نمذجة المولد الكهروضوئي نفسها. استندت هذه الاستراتيجية المعتمدة لتشخيص الأخطاء على فكرة أن البيانات I-V التي تم الحصول عليها أثناء ظروف التشغيل العادية تنتج معلمات نموذجية صحيحة، في حين أن البيانات I-V التي تم الحصول عليها أثناء ظروف التشغيل التي بها أعطال (ظروف غير عادية) تنتج معلمات نمذجة تحتوي على توقيعات الأخطاء ذاتها. وتشير النتائج إلى أن هذه الاستراتيجية مبتكرة وموثوقة ودقيقة وأنّ فكرة الافتراض الأولى كانت صائبة.

الكلمات المفتاحية: اكتشاف الأخطاء، تشخيص الأخطاء، نمذجة المولّد الكهروضوئي، تقنية الاستدلال الأسمى، تحديد المعلمات، المحاكاة، الدالة الموضوعية.

Résumé (French)

Dans le monde d'aujourd'hui, les énergies renouvelables deviennent de plus en plus populaires en raison des préoccupations croissantes concernant l'environnement et de la demande croissante d'énergie. Parmi toutes les formes d'énergie renouvelable, le photovoltaïque semble être l'option la plus prometteuse pour la production mondiale. Cependant, les centrales photovoltaïques rencontrent souvent des défauts techniques qui peuvent nuire aux performances des panneaux photovoltaïques et de leurs composants. Ces

défauts incluent, autre autres, l'ombrage partiel, le vieillissement, les fissures des cellules photovoltaïques, les points chauds, le court-circuit, le circuits ouvert. Pour relever efficacement ces défis, un système de diagnostic automatique des défauts est crucial. Cette thèse propose trois nouvelles techniques métaheuristiques pour modéliser les générateurs photovoltaïques de manière rapide et précise. La troisième technique a été utilisée pour le diagnostic des défauts via le processus de modélisation du générateur photovoltaïque lui-même. Cette stratégie adoptée pour le diagnostic des défauts est basée sur l'hypothèse que les données I-V acquises lors des situations normales produisent des paramètres de modèle corrects, tandis que les données I-V acquises lors des situations présentant des anomalies produisent des paramètres de modélisation qui contiennent les mêmes signatures de défauts. Les résultats indiquent que cette stratégie est innovante, fiable et précise et que l'hypothèse initiale était valide et prouvée.

Mots clés : détection de défauts, diagnostic de défauts, modélisation de générateur PV, technique métaheuristiques, identification de paramètres, simulation, fonction objective.

General introduction

Preamble

Since the dawn of the Industrial Revolution, the world has faced serious global warming and climate change challenges. This is due to the continuously growing demand for energy, most of which is still made up of fossil fuels. [1, 2]. Fossil fuels produce energy through combustion, releasing tremendous quantities of greenhouse gases into the atmosphere. This pollution affects not only the environment but also threatens the health of the population with severe types of diseases.

To solve these issues, renewable energies are proposed as the ideal alternative to fossil fuels due to their sustainability and friendly effects on the environment, especially in the electrical power generation sector [3]. Solar photovoltaic (PV) energy is the most promising type of renewable energy, quickly rising to the top list of clean energy sources. Statistics provided by the International Renewable Energy Agency (IRENA) state that the capacity of photovoltaic-based electricity generation would reach 28% of the global renewable power capacity by the end of 2021. Fig. 01 illustrates the global net generating capacity of electricity that uses renewable energy over the years from 2011 to 2021 [4].

The factors that motivate investment in solar PV energy are economic and strategic. The solar energy used to produce photovoltaic-based electricity is abundant everywhere even under cloudy weather [5, 6]. It is noiseless, smokeless, and with no rotating parts. Furthermore, rapid development in solar PV technologies contributes significantly to lowering prices of the PV modules and encourages investment in the PV market [7].

The primary objective of installing PV systems is to harvest as much electrical power as possible. However, converting solar energy into electricity outdoors is susceptible to the constantly fluctuating weather, impacting regular power generation. These conditions make operations like control, monitoring, and fault diagnosis of photovoltaic systems extremely complicated. Therefore, accurate measurement of weather parameters, such as solar irradiance and ambient temperature, is essential for the performance of photovoltaic systems [8, 9]. Precise modeling of the solar PV generator plays a crucial role in ensuring and predicting the performance of the PV generator. Also, modeling is necessary for operations like supervision and control, and it is important for fault diagnosis for maintenance and safety purposes [10].

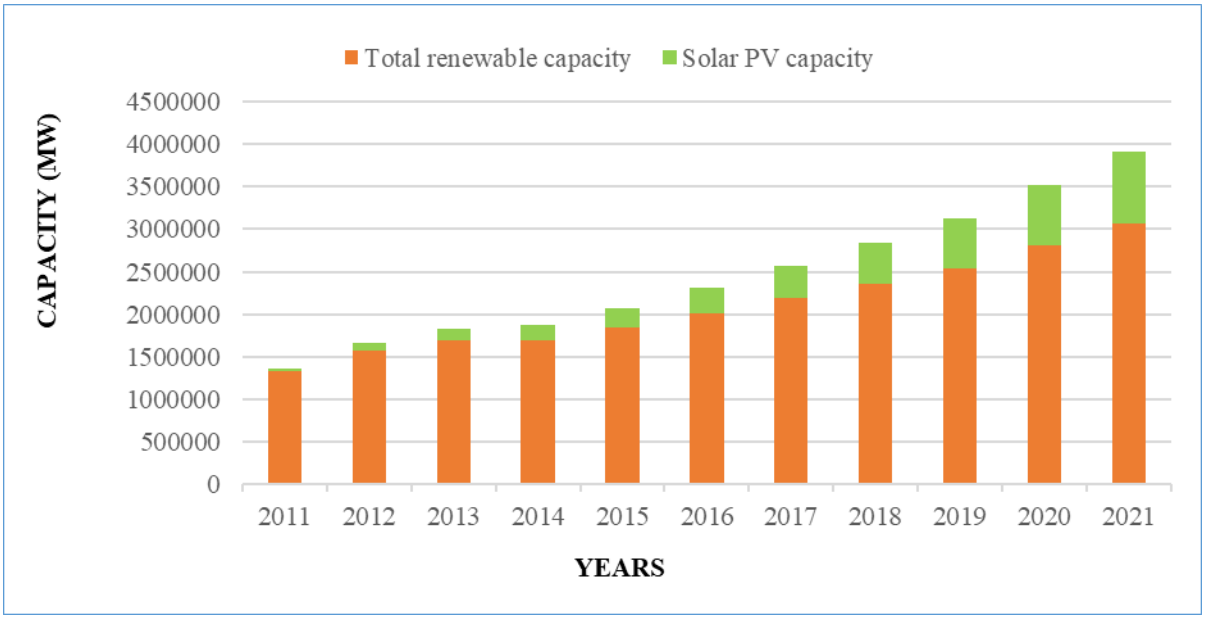

Fig. 0.1 Global net generating capacity of electricity using renewable energy (source of data IRENA)

During the life cycle of the PV generator (PV module), it can be impacted by several internal and external faults including, among others, hot spots, shadows, dust, soiling, cell degradation, cell cracks, open-circuit or short-circuit faults, arc faults line-to-line, or line-to-ground faults [11-14].

The solar PV system contains several elements. The primary element is the PV generator (the PV module, string, and array). It comprises PV-connected cells, where the sunlight is converted to electricity. The PV cells are made based on different categories of technologies.

Problem formulation and motivation to solve it

Photovoltaic generators are susceptible to various faults and malfunctions. To ensure their reliability and performance, a PV generator simulator should be developed, along with a reliable technique for fault detection and diagnosis. This simulator is dedicated to fault diagnosis and is a crucial step toward enhancing the efficiency and resilience of photovoltaic systems.

Moreover, fault diagnosis involves a lot of testing and validation, which means that some faults cannot be performed on a physical PV generator due to the risks involved. For instance, short-circuiting a PV module or the occurrence of fire can cause irreversible damage. Therefore, the motivation behind the development of a dedicated PV generator simulator as well as a diagnosis technique is the necessity for the safe and effective detection and diagnosis of faults to ensure the PV generator's performance and reliability.

Contribution and novelty of the thesis

The contribution and novelty of this thesis can be outlined in the following points:

Firstly, it proposes three hybrid algorithms that can accurately and quickly determine the parameters of a PV generator model. The first one is named Nested-Loop Biogeography-Based Optimization-Differential Evolution (NLBBODE). The second is called the Bat-Artificial Bee Colony Optimizer (BABCO) and the third one is called Differential-Shuffled Complex Evolution (DSCE). DSCE algorithm is also used to detect faults in the PV generator through modeling.

Secondly, the performance of the three algorithms is evaluated based on metrics such as accuracy, reliability, statistical performance, and conversion speed. These metrics are then compared with those of other techniques published in the literature.

Finally, a PV generator emulator has been created to imitate the behavior of a physical PV generator, both in healthy and faulty conditions. The purpose of developing this simulator is to safely and effectively detect and diagnose faults, as not all faults can be tested on a real PV generator.

Thesis organization

After the introduction, that sets the context for the study as well as the methods used in the field of PV generator modeling and fault diagnosis, this thesis is presented through the following main chapters:

- Chapter 01 discusses the state-of-the-art methods used for detecting and diagnosing faults in PV generators. The chapter begins by defining the terminology used in this field and classifying the various types of faults that can occur on a PV generator. It also identifies the appropriate locations for each type of fault, along with their probable causes and consequences. Finally, the chapter explains the different methods used for detecting and diagnosing faults in PV generators.
- Chapter 02 introduces the fundamental principles of the photovoltaic effect, which is the physical process of converting light into electricity. It begins with a brief overview of sunlight radiation and then investigates PV materials and technologies, including the history and prospects of PV technology generations. The chapter ends with a presentation of the various types of PV generators and their applications.

- Chapter 03 discusses the issue of identifying parameters in the PV generator model. It introduces two new metaheuristic methods to solve the problem. The chapter covers the concept of PV generator modeling and presents the various models used in literature to achieve it. The electrical circuit-based models (SDM, DDM, and TDM) are explained and analyzed to demonstrate how the mathematical equations that govern the physical PV generator are derived and verified. The chapter then provides a comprehensive explanation of the optimization process, presenting the results of the two proposed approaches used to solve the stated problem.
- Chapter 04 focuses on introducing and explaining the proposed PV generator simulator, along with the adopted procedure in its design. The simulator is tested under various healthy and faulty conditions to validate its performance. The simulated faults include partial shading and other types of faults that could affect the components of the PV generator, such as short-circuit or open-circuit modules, and bypass diode faults, among others.
- Chapter 05 introduces the main contribution to the fault detection and diagnosis of the PV generator through a proposed technique. The chapter begins by presenting the starting hypothesis and then thoroughly explains the proposed technique, along with the results obtained for modeling the PV generator in healthy conditions. Finally, it presents and discusses the results of using the proposed technique for fault diagnosis in various scenarios.
- A general conclusion is presented at the end of the thesis along with perspectives and future research in PV generator modeling and fault diagnosis.

Chapter 01:

PV generator fault diagnosis methods: State-of-the-art

Introduction

Like any other system, photovoltaic generators (PV generators) are exposed to a variety of faulty situations, which can reduce their efficiency, reliability, and availability, or even can result in dangerous events such as "fire" in some cases [13,14,15]. However, it is necessary for manufacturers as well as for operators to deal with PV generator faults in order to decrease investment risks, ensure correct maintenance plans, and improve PV generator longevity and performance.

Whether it is a stand-alone or in a grid-connected configuration, the primary goal of installing PV panels is to capture as much solar photovoltaic energy as possible. Nevertheless, converting PV energy into electricity outdoors is vulnerable to external circumstances such as shadows, dust, and soiling…. and internal conditions such as hot spots, cell aging, cell cracks, open-circuit or short-circuit faults, line-to-line, or line-to-ground faults…etc. all these conditions have a negative impact on PV system performance [13,14,15,16]. As a result, fault diagnosis of the PV generator systems is critical for optimizing produced power and minimizing functional failure [17]. Moreover, discovering the malfunctioning of the PV generator is not always straightforward, and certain problems may remain hidden for long periods during the lifecycle of the PV generator [18].

Regarding the rapid growth of the PV industry in the last few years and its associated complexity, many research efforts have focused on fault detection, isolation, and diagnosis methods, aiming to prevent the risk of PV system failure. these methods are used to deal with concerns about PV plants' reliability, availability, maintainability, and safety, commonly known as (RAMS) [19]. From a safety viewpoint, particular attention should be given to building-integrated PV (BIPV) systems, due to the direct threat to occupants in case of PV-related fire [20]. Therefore, prompt fault diagnosis strategies in this kind of system are vital.

Typically, as shown in Fig. 1.1, the PV system comprises the PV generator (modules/arrays), inverter, and load. PV system may be configured as a grid-connected or stand-alone system. This thesis focuses only on the faults that may occur in the PV generator (arrays, modules, cells, wiring…etc.). This is because the PV generator is the element the most exposed to extreme weather conditions, such as solar radiation, ambient temperature, wind, humidity …etc.

In general, the fault diagnosis process includes three principal phases [21]:

- *Fault detection:* This can be achieved by detecting when the measured data crosses a predefined threshold.

- *Fault classification*: In this phase, the fault is identified by relating it to its appropriate causes.
- *Fault localization and isolation:* This phase is for localizing the fault on the PV generator and then taking the right decision about it. It is a relatively difficult and still challenging process due to the cost of supplementary equipment such as sensors, sophisticated cameras …etc.

1.2. Advantages of PV generator fault diagnosis

Fault diagnosis of PV generators aims principally to detect the reduction of energy production below the optimal level. It aims as well to detect any deviation which could lead to safety issues hotspots fires etc. Prompt detection of faults on a PV generator helps considerably two Maintenance operations and cost reduction. In other words, it's insuring continuous electricity production without unplanned shutdown of the PV plant.

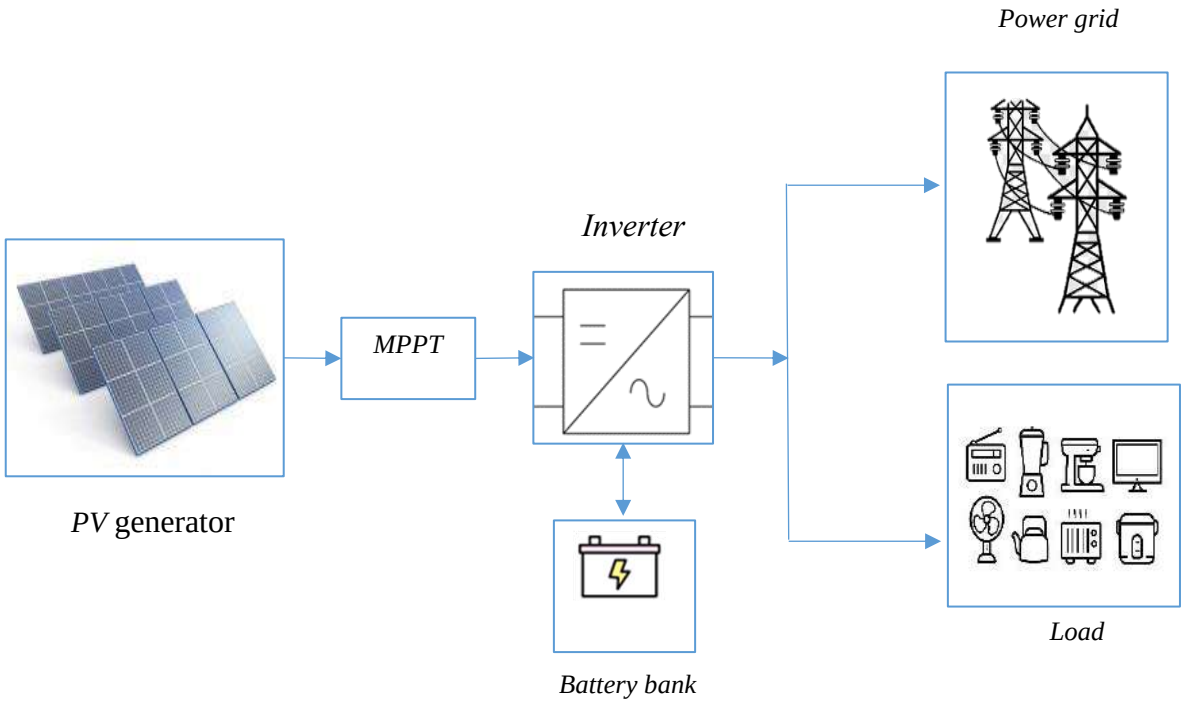

Fig. 1.1 Typical photovoltaic system.

1.3. Basic definitions

In the literature related to PV fault diagnosis, a kind of non-uniformity in the use of terminology can be observed. Therefore, providing the most relevant definitions to describe the PV fault

diagnosis process and the associated terminology is worthwhile. This is according to the available references related to fault diagnosis, as a branch of automatic control or automation engineering in general, and PV fault diagnosis system references in particular.

1.7.1. Fault

The fault is an undesired and unauthorized divergence of at least one parameter or characteristic property of the system from normal, accepted, or standard condition [22] . A fault is any defect that could affect any system component during fabrication or operations.

For PV generator systems, the fault is any degradation that could lead to a decrease in power, lifetime, reliability, and safety issues like fire or electrical shock for people.

1.7.2. Residual

The residual is the fault indicator resulting from a deviation between measured data and model-equation-based estimated data [22, 23].

1.7.3. Fault detection

Fault detection is the task of discovering the occurrence of a defect in the system (PV generator) before it reveals in the form of failure. It is the most crucial step of fault diagnosis as all subsequent steps depend on its precision [21, 23].

1.7.4. Fault isolation

Succeeds the fault detection process, fault isolation is the determination of the type, location, and time of detection of a fault [21, 23]. For maintainability purposes, fault isolation aims to determine the fault location at the lowest level of the replaceable component.

For PV generators, in the case of partial shading for example, the lowest level for isolating a fault is the substring level, where a bypass diode is activated to isolate the faulty substring. In case where removing the faulty module is required, the faulty components may be replaced or repaired, such as junction box components, soldering connection, faulty diode…etc.

1.7.5. Fault identification (classification)

Succeeds the fault isolation process, fault identification or classification is the process of referring the fault to its root cause and determining its size [21, 23]. The fault identification aims to identify the original failure mode.

1.7.6. Fault diagnosis

Fault diagnosis (diagnostic) is the process that defines the type, location, and size of fault detection. The fault diagnosis comprises both fault detection and fault identification [23].

Fault diagnosis methods may change from one engineering discipline to another, but its phases are mostly the same

1.4. Types of PV generator faults

A variety of PV generator faults have been categorized and discussed in the literature according to their nature and causes. Some references list several types of faults, but in reality, lots of faults are either causes or results of other faults. Particular attention must be given to faults that may be detected and diagnosed automatically under a monitoring and supervision environment.

Table 1.1 summarizes the principal types of faults that may occur on a PV generator with their appropriate locations (level), their probable causes, and consequences.

Table 1.1 Categorization of PV generator faults according to their causes and consequences

Type of fault	***Location level (PV generator component)***	***Possible causes***		***Consequences / Risks***
		Internal	***External***	
Hot spots	PV Cell/Module	-Aging & degradation -Glass breakage -Discoloration -Soldering defects with high resistance. -Mismatch (at cells level)	-Shading -Dust -Soiling -Snow	- Reduction in output power
Ground fault	Cell/module/array	-Cable insulators defects -Defects in the ground cable -Accidental contact between the current conductor and the ground network.	-Water infiltration	- Fire. - Reduction in output power
Line-to-line fault	-Junction box. -Sub-string/ module/array	-Cable insulators defects -Accidental contact between two conductors	-Water infiltration in the junction box	- Fire - Damage to the Substring/module/array - Electrical shock (fatality/severe injuries)

Arc faults (series/parallel)	-PV module/array	-Accidental contact (short bridge) in a conductor. - Two adjacent conductors with significantly different potentials. -Poor fixation in junction box connectors (due to corrosion, and aging…)	-Humidity - Rain ingress	- Fire - Damage of the PV generator - Worker's facial burn
Auxiliary diode fault	-By-pass diode -Blocking diode	-Partial shading. -Poor soldering.	-Overheating -Reverse connection during maintenance (human error)	- Damage to the diode - Open or short circuit of the diode. - Yield decrease
Junction box fault	Junction box	-Corrosion -Water and dust penetration	-Poor connection, -Inappropriate mounting.	-Rapid increase in connectors resistance. - Arc - Risk of fire

1.4.1. Hot spot faults

The hot spot manifests as a temperature rising of one cell or group of cells within a PV module/string. The hot spot is classified as a mismatch fault that occurs when the power circulation is not uniform within the PV module/string [24, 25].

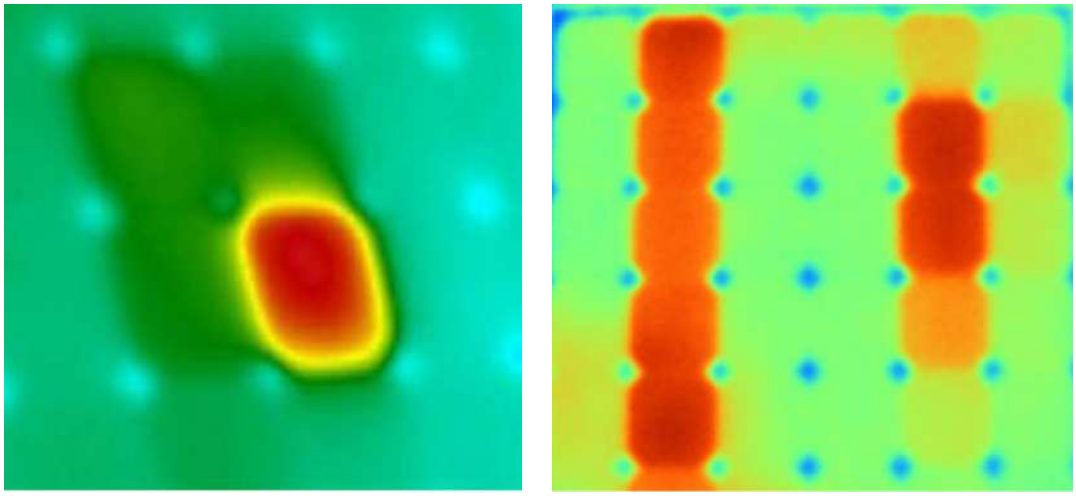

(a) **(b)**

Fig. 1.2 Thermographic image of **(a)** cell hotspot **(b)** module hotspot [26].

The principal causes of the hot spots are high resistance, cold soldering connections during the fabrication [19], and partial shading if the bypass diode is defective. As a result, the affected cells consume power instead of producing it [19, 25].

If no action is taken before the temperature of the hot spots exceeds a crucial threshold, the affected cells may be completely damaged, and in the worst case, a disastrous fire can occur on the PV module/string. The most relevant method for prompt detection of hot spots is thermography (Infrared) imaging. Fig 1.2 presents an example thermal imaging of hotspot fault, and some visible faults of PV cell/module are illustrated in Fig 1.3.

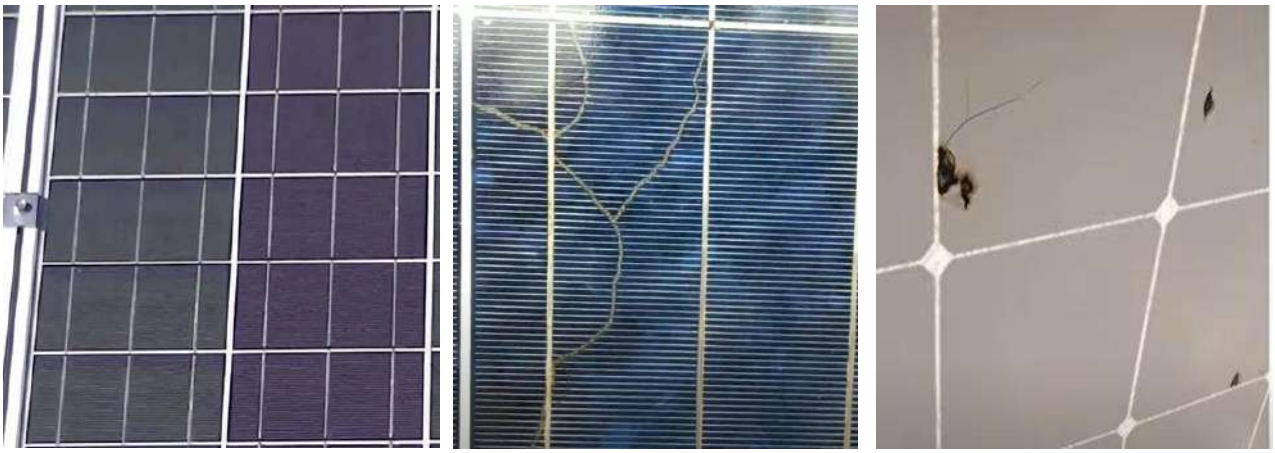

(a) **(b)** **(c)**

Fig. 1.3 Examples of PV Cell/module visible faults:
(a) Discoloration **(b)** Snail trail effect **(c)** Back sheet burns due to hot spots.

1.4.2. Ground fault

As with any other electrical equipment chassis, the external metallic parts of the PV arrays must be grounded. This procedure is intended to protect users from getting an electric shock if any leakage current is accidentally passed through these metallic parts.

A ground fault is an accidental contact between the current-carrying conductor (CCC) and the non-current-carrying conductors (NCCC) which are the grounded metallic parts of the PV array such as the PV modules frame and mounted racks [27].

The causes of the ground fault may be inadequate wiring or accidental contact between a CCC and the ground network due to a defective cable insulator. If the ground fault is not detected and corrected properly, it may result in generating DC arcs at the contact point and hazardous fire in the worst case [19].

1.4.3. Line-to-line fault

The line-to-line fault is an accidental contact between two points with different potentials within the current carrying network. It is commonly defined as a short circuit fault between two different potentials within the PV generator [28].

1.4.4. Series/parallel arc fault

Arc fault is defined as the accidental movement of the electrical current through an insulator material such as air or any other dielectric material [19]. The arc fault manifests in two forms:

a) Series arc fault: which occurs on the location of discontinuity of a current-carrying conductor (CCC). The discontinuity could be caused by defective soldering, cell damage, corrosion, mechanical abrasion…etc. [27].
b) Parallel arc fault: occurs on the location between two adjacent and different potentials current-carrying conductors (CCCs). This electrical discharge is due to defective insulation in most cases. [27].

If not detected and correctly maintained, the series or parallel arc fault may produce a hazardous fire on the PV generator or may cause severe burns to users. Fig 1.4 presents an example of an electrical arc discharge effect.

Fig. 1.4 DC cable melted due to electrical arcing in PV plant [29].

1.4.5. Auxiliary diodes fault

The auxiliary diodes are the bypass diode and blocking diode. These two diodes assure key roles in controlling PV generator performance in terms of recompensing for power loss and protecting the PV generator components.

The bypass diode serves as a barrier against the reverse voltage that can occur because of partial shading for example, whereas the blocking diode serves as a barrier against the reverse current that may be occurred because of line-to-line fault as an example [19, 30].

These two auxiliary diodes may be subject to faults short-circuit and open-circuit if the PV generator is partially shaded for a long time, reverse connection during maintenance, or poor wiring [31]. If not detected and corrected, these faults may lead to hazardous events such as electrical shock for users. An example of diode faults is shown in Fig. 1.5.

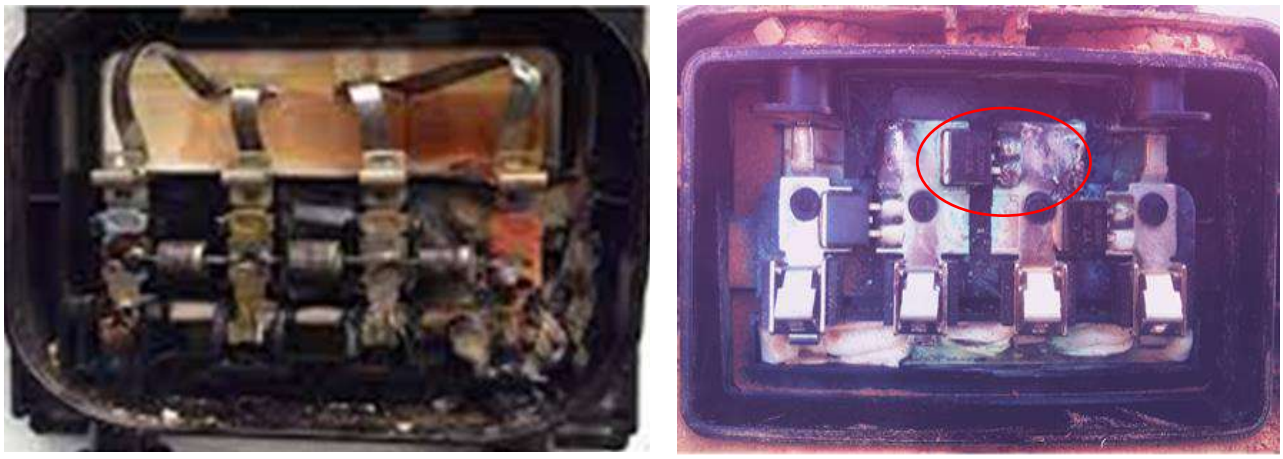

(a) **(b)**

Fig. 1.5 Examples of diodes faults:
(a) burnt diode in junction box. **(b)** defective soldering of a by-pass diode

1.4.6. Junction box fault

A junction box is an enclosure containing connectors that link the PV string cables and external terminals [32]. The junction box may be subject to several faults such as corrosion, water and dust penetration, poor connection, and inappropriate mounting.

(a) **(b)**

Fig. 1.6 Examples of fire occurred on: **(a)** Rooftop PV generator. **(b)** Junction box in a PV plant

Consequently, these faults may lead usually to a rapid increase in connector resistance and may produce arcs and fire on the whole PV generator [33]. Fig 1.6 shows example of fires taking place on a rooftop PV generator and junction box of a land PV plant.

1.5. Causes of faults

The main causes of faults that could occur on PV generators can be internal or external. Internal faults may occur due to errors in the fabrication process of PV modules, such as soldering errors or lack of materials. Human-related errors are common during transportation and installation. External factors related to the operating environment such as extreme temperatures, snow, dust storms, etc. are the main causes of faults that can affect PV generators.

1.6. Consequences of faults

In general, faults in photovoltaic (PV) generators can cause a reduction in power output or pose safety risks such as electrical shock or fire. Therefore, it is crucial to take all necessary precautions to prevent these faults from happening or to minimize their impact if all prevention measures fail.

1.7. Methods of PV generator fault diagnosis

Several PV generator fault diagnosis methods have been proposed by researchers to detect, classify, and localize faults. These methods differ from each other by the following features [19]:

- Fault detection speed.
- Capacity to distinguish between the types of faults.
- Ability to identify single or simultaneous faults at once.
- Sensor and wiring requirements.

In the literature, a sort of unevenness is remarkable in categorizing the PV generator fault diagnosis methods. This is because this discipline is relatively recent, and to the continuous development of new related techniques.

From a general perspective, the PV generator fault diagnosis methods can be categorized into the following main categories:

1) Visual inspection method
2) Imaging-based methods.
3) Electrical measurement-based methods.

1.7.1. Visual inspection method

Visual inspection is the initial and basic method used to detect visible faults with bare eyes in all kinds of systems [25]. Among the PV generator faults that can be detected visually, are partial shading, dust accumulation, discoloration, breaking glass, cell cracks, delamination...etc.

Visual inspection is the simplest method that contributes to collecting a large amount of data but has some drawbacks such as time consumption and skilled manpower, especially in large-scale PV plants. Nowadays, visual inspectcanould be assisted with drones equipped with cameras. However, a wide variety of hidden faults cannot be detected through a simple visual inspection. Advanced techniques using visual imagind sophisticated devices and appropriate software are in use.

1.7.2. Imaging-based methods

The imaging-based methods are qualitative methods used to reveal hidden faults such as hot spots [30, 34]. In this kind of method, sophisticated devices, such as thermography (infrared) cameras, and advanced image processing techniques are used to extract the information from images and precisely detect and locate faults [34]. This group of methods is classified into three subgroups:

a) Thermography imagining method

Thermography imaging is the result of the captured infrared (IR) radiation emitted from the local overheating PV cells caused by partial shading, defective soldering, short circuit …etc. This process is performed using appropriate IR detectors [35].

b) Electroluminescence imagining method

Electroluminescence imaging is a photographic technique that involves surface contact with a PV cell/module to inject an electric current. This method is used to reveal surface and subsurface faults by receiving IR radiation in a dark location. The bright areas represent healthy cells while the darker ones represent faulty such as cell cracks, snail trails, fissures, and defective connections [30].

c) Photoluminescence imagining method

Photoluminescence imagining is a qualitative contactless method used for fault detection, especially during fabrication and for quality control. A laser source spreads the light on the surface of the PV module, then a special camera receives the reflected photoluminescence

image which will be thoroughly inspected. This method can reveal several kinds of faults such as degradation, open circuits, poor soldering, and diode faults [34].

1.7.3. Electrical measurement-based methods

The electrical measurement-based methods are used to identify PV system faults on both sides

DC and AC. This category of methods uses the electrical measured data such as the current-voltage (I-V) and power outputs, as well as the weather measurements like ambient temperature, solar irradiance, wind speed…etc.

Five subcategories could be identified under this group of electrical measurement methods, they are:

a) Methods based on statistical and signal processing:

This category of fault diagnosis methods uses electrical signal waves to be injected into the PV module, received back, and processed. The PV module/string must be disconnected from the array to be tested.

These techniques include time domain reflectometry [36], speared spectrum time domain reflectometry [34], and earth capacitance measurement. These techniques are used to reveal defaults such as disconnected modules and degradation. [37]

b) Methods based on power loss investigation

The power loss investigation is the simplest and most common method. Indeed, the fault diagnosis procedure logically begins with examining the output power of the PV generator. These methods use generally may detect and identify faults, like hotspots, partial shading, open-circuited modules, and poor connection.

In general, methods of this category analyze the output power losses and compare results to the simulated model. The fault detection and classification are performed by computing the deviation errors between the healthy and faulty conditions [19, 30]

c) Methods based on I-V curves analysis

The I-V curves analysis techniques use the current-voltage (I-V) characteristics to monitor the behavior of the PV module/string. The fault occurrence affects the referential I-V curves according to the fault's type and impact. In general, these methods compare the healthy I-V curves with the faulty ones [38].

The I-V curves analysis techniques as well as the first and second derivative of the function *I=f(V)*, have shown their efficiency to detect and diagnosing faults like different partial shading scenarios, mismatch faults, ground faults, open-circuited modules, by-pass diode faults…etc. [39]. Using the I-V curves as inputs, other techniques may be involved in fault detection and diagnosis, such as Fuzzy logic and metaheuristic algorithms [40].

d) Voltage and current measurement methods

These methods detect and locate different types of faults using the measurement of the output current and voltage of the PV generator (PV module/string/array). After determining thresholds, online measurements are compared to a simulated PV generator model to detect and locate faults. Several related works are proposed in the literature to correctly detect and locate faulty PV modules/strings and other faults like partial shading, open circuit modules, arc faults, and line-to-line faults [39].

e) Methods based on artificial intelligence

Artificial intelligence (AI) approaches are very strong tools that have lately been used in many engineering fields, medicine, language processing, and various other disciplines. They have also demonstrated notable efficacy in control, modeling, and PV system forecasting. [41]. Artificial intelligence is a set of techniques that comprises machine learning (ML) techniques, which includes in its turn the ensemble learning (EL) methods [42], as illustrated in Fig. 1.7.

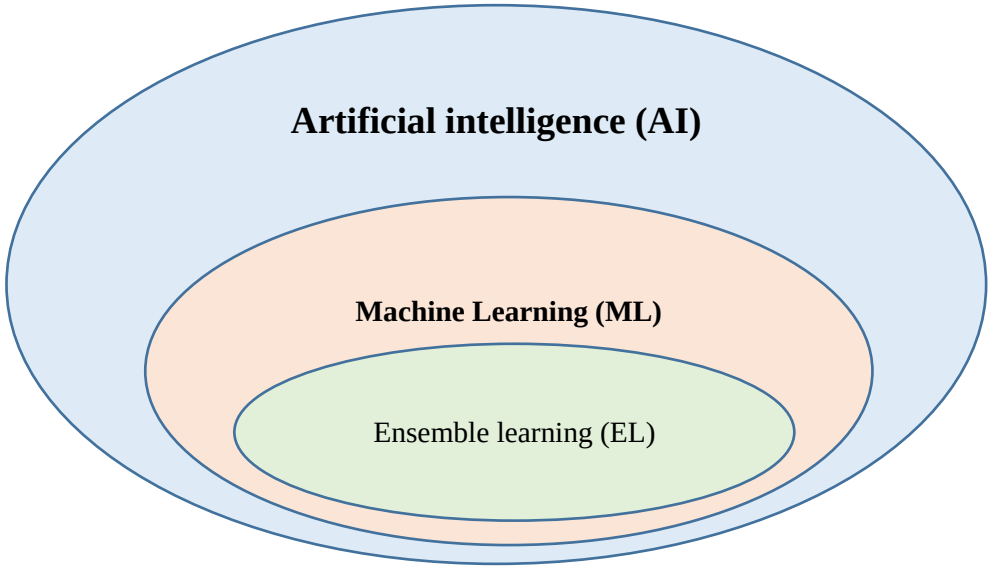

Fig. 1.7 Relation between AI, ML, and EL.

In the last two decades, many research papers concerning PV system fault diagnosis have been published using AI approaches. The most related ML methods in this field are decision tree (DT), K-nearest neighbors (k-NN), random forest (RF), support vector machine (SVM), neural networks (NNs) and its improved version, as well as ensemble learning (EL) [42].

1.8. Conclusion

This chapter provides a detailed review of the methods used in fault detection and diagnosis of PV generators. In addition, the chapter outlines the typical faults that may occur on PV generator, their causes, and their impacts on reducing the PV generator performance and other related safety issues such as fire.

The chapter begins by giving basic definitions of terms used in the fault detection and diagnosis domain, and then a listing of types of PV generator faults is provided. Finally, methods used for PV fault detection and diagnosis are described. For instance, visual inspection methods can be used to detect faults such as cracks and hot spots in the PV modules. While imaging-based methods can be used for detecting defects in the PV cells. The electrical measurement-based methods are the widespread used methods due to their capability in online application and monitoring. This type of method includes I-V curves analysis, power loss investigation, and artificial intelligence based techniques

Chapter 02: Basic principles of photovoltaics

2.1 Introduction

With a growing focus on sustainable and renewable energy sources, photovoltaic energy is emerging as a transformative technology. It provides a promising solution to our ever-growing energy needs while decreasing our dependence on fossil fuels as a result. This revolutionary technology converts sunlight directly into electricity, a process that could revolutionize energy consumption.

The term "*photovoltaic*", which means literally light-electricity, is composed of two parts "*photo*" and "*voltaic*", the first part is derived from the Greek word "phos" meaning light, and the second "voltaic" is a reference to the Italian scientist Alessandro Volta, who is widely regarded as a pioneer in electricity science [43].

Photovoltaic generators are devices that convert sunlight into electricity with specialized materials known as solar cells. In these cells, electrons are produced by converting photons, the particles of light, into energy. Direct current is generated by this process.

In 1839, the French physicist "Edmund Becquerel" observed a voltage exhibited by two identical electrodes illuminated in a weak conducting solution. This was the first time the photovoltaic effect was known. The first solid photovoltaic cell was built with selenium in the 1880s, and it converted light into electricity with (1-2) % efficiency. The price of selenium cells relative to the tiny amount of power they produce has prevented them from being practical as energy converters [44]. In 1954, the Bell Telephone Laboratories announced the first silicon photovoltaic cell with a 4% efficiency, which soon developed to 8% efficiency in 1958 [45].

Furthermore, photovoltaic generators offer numerous advantages compared to other sources of energy generation, which can be summarized as follows [44, 46]:

- Photovoltaic generators are noiseless and have low visual impact since they have no moving or rotating parts compared to the classical energy generators.
- Photovoltaic generators reach its full generation capacity rapidly when exposed to the sunlight, without any mechanical risks compared to classical generators.
- There is no risk of leak or explosion since there are no combustible fluids to operate.
- There is no risk of greenhouse gas emissions or air pollutants when producing electricity, despite the waste of panel manufacturing or after being fully exploited.

- Require low operating and maintenance costs.
- Photovoltaic generators offer flexibility in system size. They can be easily scaled up or down to meet various energy demands. From small residential installations to large utility-scale solar farms.
- Photovoltaic generators offer an ideal solution for providing electricity to off-grid areas that lack access to traditional power sources, improving the quality of life and enabling economic development.

On the other hand, photovoltaic generators have many limitations that can be summarized as follows [44, 46]:

- Photovoltaic generators' operation is intermittent since it depends on sunlight, which varies with weather conditions and time of day. It is unavailable during nighttime and reduced on cloudy or rainy days.
- Implementing energy storage solutions to store excess energy for use during periods of low sunlight can be expensive, and the efficiency of energy storage technologies may vary.
- Large-scale solar photovoltaic farms or extensive rooftop installations require a significant amount of land or space.
- Energy losses during conversion, which are thermal usually. At the same time, high temperatures reduce efficiency.
- even though photovoltaic generators can significantly reduce energy bills and offer long-term cost savings, the payback period for the initial investment may be long.

Despite the advantages and limitations of photovoltaic generators, they are well worth studying, researching, developing, and investing in. Due to this, the purpose of this chapter is to illustrate several basic principles of photovoltaics, including the general concept of how this physical phenomenon operates and the mechanism of converting sunlight to electricity. According to their architecture and the energy demand, a classification of photovoltaic systems is given at the end of this chapter.

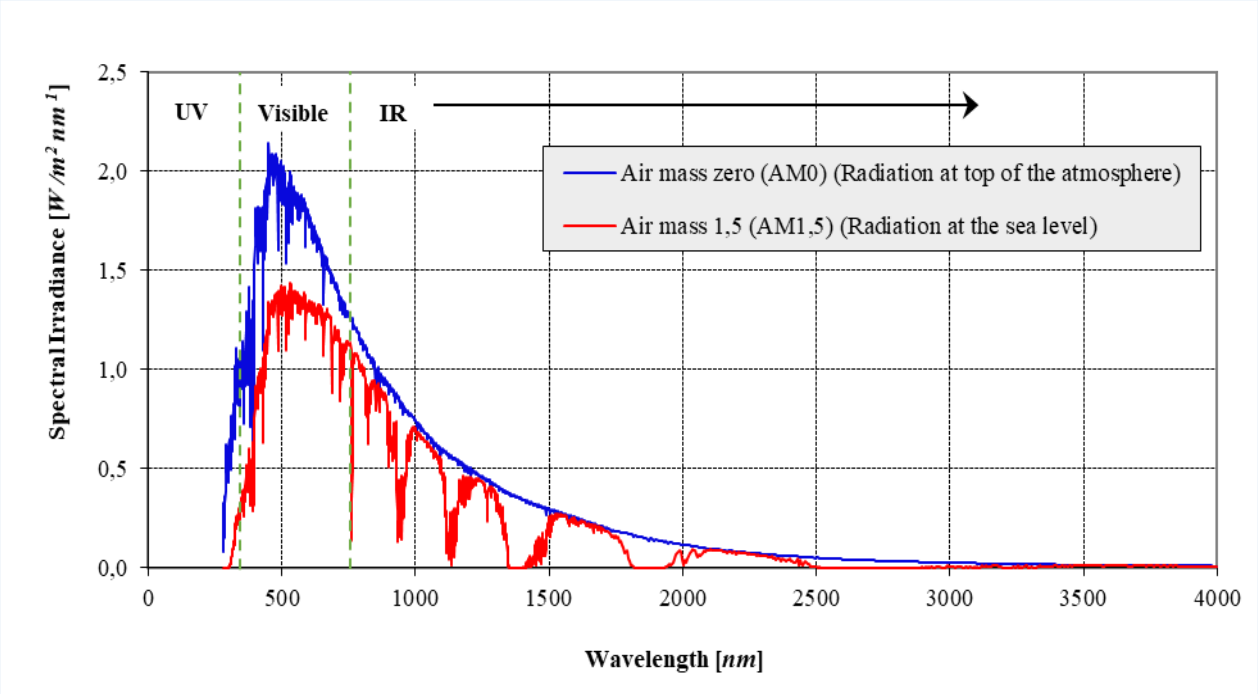

Fig. 2.1 Solar spectra at AM0 and AM1.5.

2.2 Sunlight radiation

The sunlight is emitted as radiated electromagnetic waves with wavelengths ranging from 300 nanometer (nm) to 4000 nanometers (nm). In general, renewable energy applications in terrestrial environments utilize radiation, or photons, which have this wavelength range [300, 4000] nanometers.

The sunlight is made of a range of colors called a spectrum and contains waves including infrared, visible light, and ultraviolet waves [47, 48].

The solar radiation emitted toward the Earth is either absorbed, reflected, or diffused by particles in the atmosphere or on the Earth's surface [48]. Fig 2.1 illustrates two levels of the sunlight spectrums; the extraterrestrial at the top of the atmosphere with an air mass equal to zero (AM0), and the one at the level of sea with an air mass equal to 1.5 (AM1.5).

As can be seen in Fig 2.1, the range of the wavelength of visible light is from 400 nm to 750 nm, while the ultraviolet radiation is inferior to 400 nm, and the infrared is superior to 750 nm.

Researchers estimate that the earth's surface receives more solar energy each minute than the entire earth's population consumes in a year [48]. In addition to time of day, season, geographic

location, weather, and landscape, many other factors affect solar radiation that reaches the surface of the Earth. In terms of their form, solar radiation can be divided into three major types that are illustrated in Fig 2.2 [47, 48]:

- *Direct radiation:* Also known as global solar radiation is the radiation that falls perpendicular to the surface of the Earth and is measured using pyranometers or solarimeters.
- *Diffuse Radiation:* Often-called diffuse sky radiation is the type of sunlight scratched into the atmosphere layers before reaching the earth surface. This type of sun radiation is divided into two types: global diffuse irradiance (GDI) and diffuse horizontal irradiance (DHI). The measurement of the diffuse solar radiation is realized using either a solarimeter, or pyrheliometer.
- *Reflected radiation:* a phenomenon known as the Albedo effect, which occurs when solar radiation bounces off the earth's surface or objects such as cars, buildings, or solar panel reflectors.

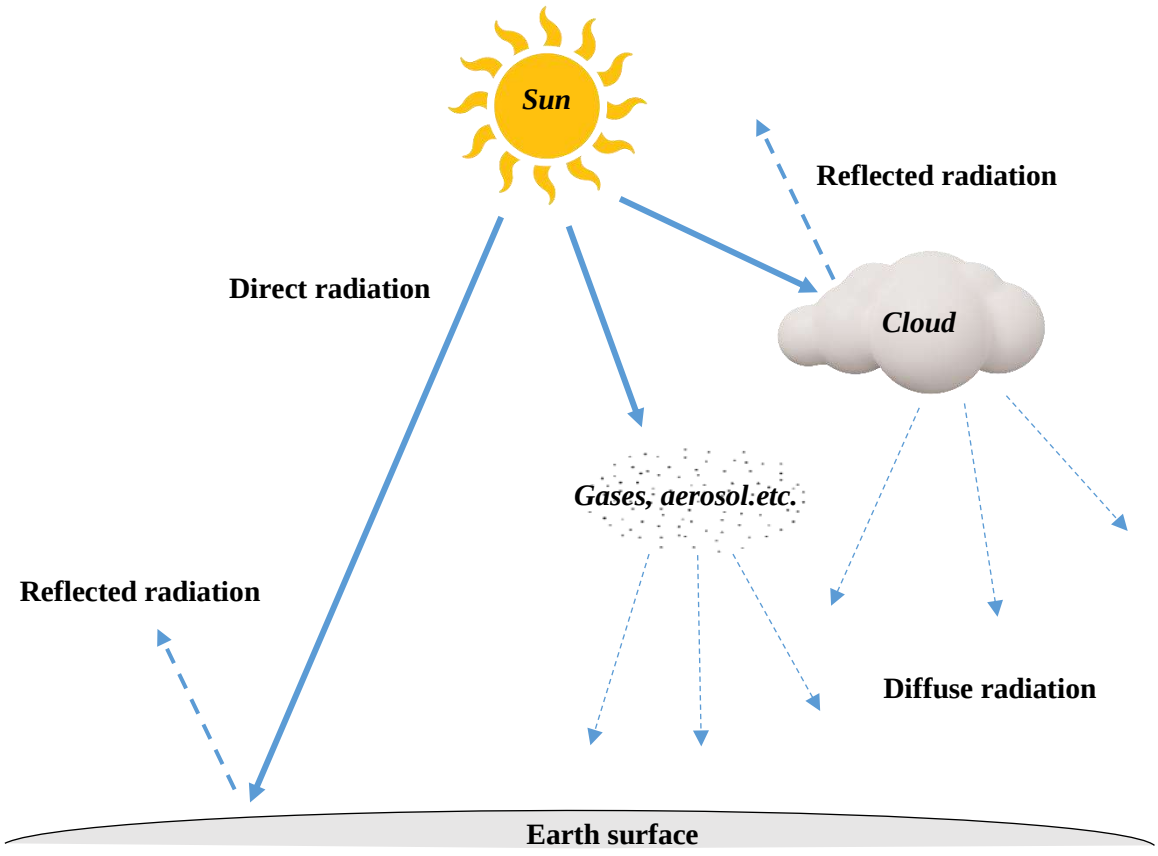

Fig. 2.2 Types of the solar radiation

Solar radiation reaching the earth in a given day is known as "insolation" and is measured in kWh/m^2/day. Meanwhile, the extraterrestrial radiation on a horizontal surface for a day (G_0) is given by the following equation [21]:

$$G_0 = \frac{24}{\pi}\left[1 + 0.033cos\left(\frac{2\pi d}{365}\right)\right][cos(\emptyset)cos(\partial)sin(\omega_s) + \beta_s sin(\emptyset)\, sin(\partial)] \quad (2.1)$$

where:

- d is a day of the year.
- $\emptyset$ indicates the latitude
- ∂ indicates the declination.
- β_s the hour angle of the sunset for the horizontal surface, which is given as follows [21]:

$$\beta_s = cos^{-1}[-tan(\emptyset)tan(\partial)] \quad (2.2)$$

S_0 is the time between the sunrise and the sunset is considered as a variable in the classical Angstrom equation:

$$\cos(S_0) = -tan(\emptyset)tan(\partial) \quad (2.3)$$

A definition of the daily clearness index K_t is given as the ratio between the daily global radiation applied to a horizontal surface and the daily extraterrestrial radiation applied to a horizontal surface. K_t can be formulated as follows:

$$K_t = \frac{G}{G_0} \quad (2.3)$$

An example of the clearance is given in Table 2.1.

Table 2.1 Clearness index in different days [49]:

Day characteristic	K_t
Cloudy	$0.0 \leq K_t < 0.3$
Partially cloudy	$0.3 \leq K_t < 0.7$
Clear	$0.7 \leq K_t < 0.9$

The figures Fig 2.3, Fig 2.4 and Fig 2.5 illustrate examples of the extraterrestrial radiation on horizontal surface for a day (G_0), the daily clearness index K_t, and the length of the day S_o versus the total numbers of days in a given year [21].

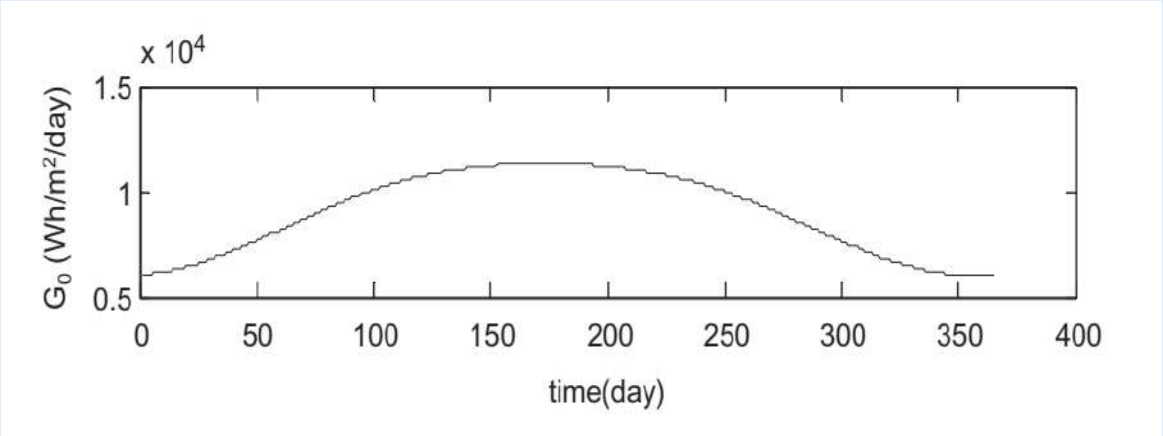

Fig. 2.3 Distribution of G_0 over one year

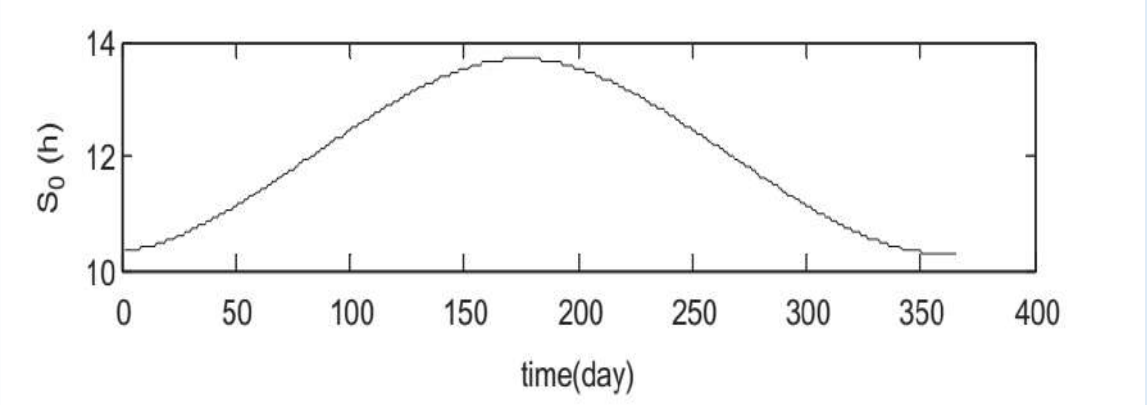

Fig. 2.4 Distribution of the clearance K_t over one year

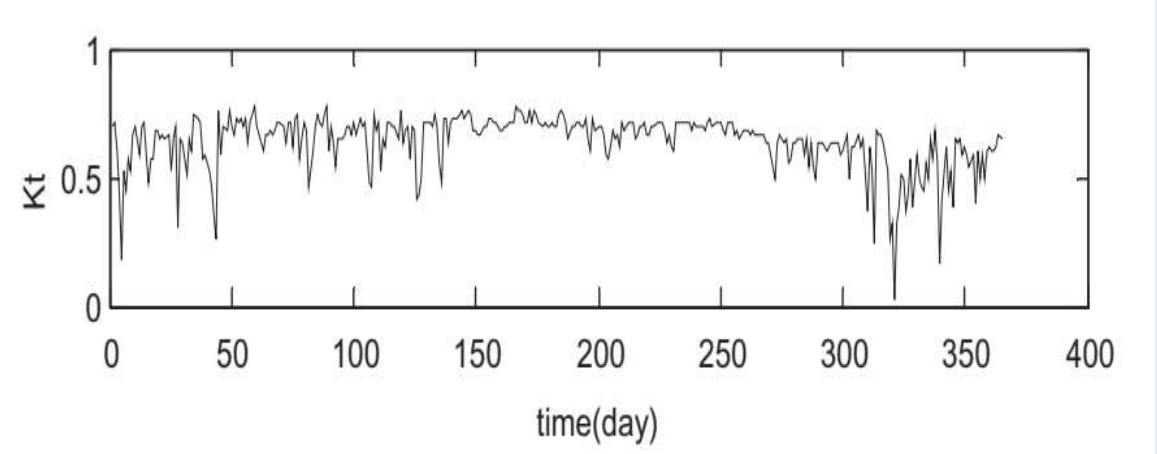

Fig. 2.5 Distribution of the variable S_0 along one year

2.3 Photovoltaic effects

The photovoltaic effect occurs when light causes a material to produce voltage and DC current. This physical and chemical process is called photosynthesis. In 1839, the French experimental physicist Alexandre Edmond Becquerel discovered the photovoltaic effect while conducting experiments on an electrolytic wet cell consisting of two metal electrodes. He noticed that the voltage of the cell increased when its silver plates were exposed to sunlight [21, 50]. Since then, many scientists have attempted to develop technologies to generate electricity based on this principle.

Currently, it is a consensus that the photovoltaic effect occurs when sunlight hits a semiconductor's boundary layer resulting in the generation of a DC electric current. An illustration of the principle of the PV effect on a PV cell is given in Fig 2.6, where the PV cell has two layers of semiconductor material with a P-N junction. This junction acts as a diode permitting electrons to flow in one direction only, i.e. from the N-type layer to the P-type layer. Upon the hit of the sunlight photons on the PV cell, a part of the photons' energy is absorbed by the PV cell generating pairs of electron holes. When an external load is connected to the positive and negative electrodes, an electric current then flows from the N-side to the P-side of the junction.

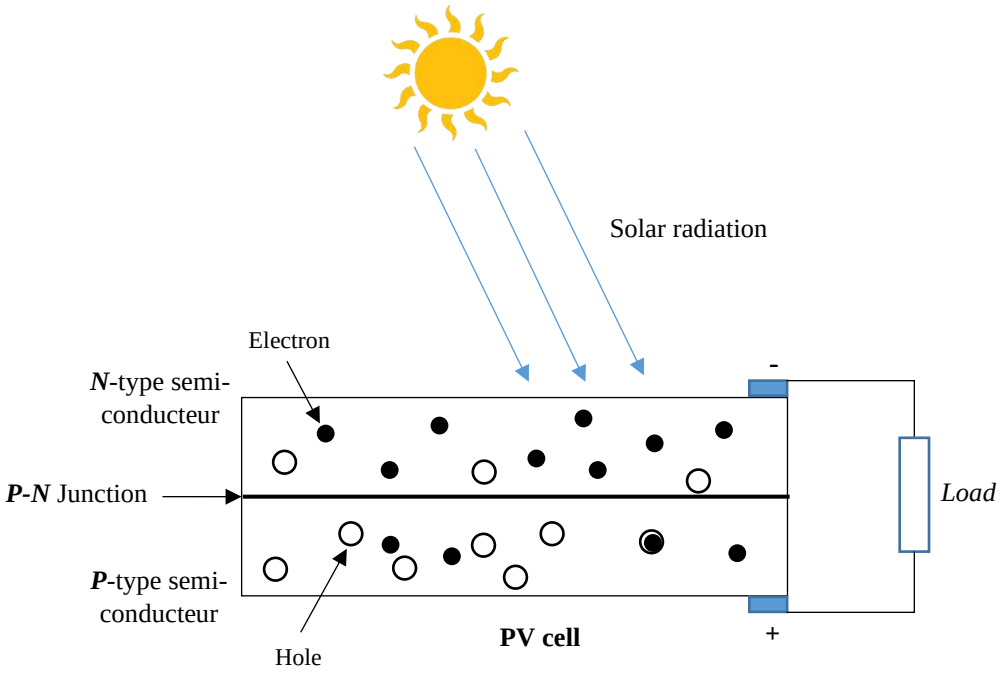

Fig. 2.6 Photovoltaic effect on a PV cell

2.4 Photovoltaic materials and technologies

Since the discovery of the PV effect, the fabrication of PV semiconductor materials has increased continuously. Indeed, silicon-based solar cells dominate the commercial PV market. However, many innovative cells are being developed aiming to enhance efficiency and reduce costs.

PV technologies are broadly classified into three generations based on their technical attributes: first-generation solar cells made of crystalline silicon, second-generation solar cells using thin films, and third-generation solar cells employing emerging materials [21, 50].

2.4.1. Crystalline silicon technology (PV first generation)

Among the first-generation technologies are monocrystalline and polycrystalline silicon PV cells, both of which use the Silicon (Si) wafer as their basic technology. These cells have universally single-junction structures, and their best-known highest efficiency has reached 26.7% [51]. First-generation cells are the most efficient and widely used, but they more costly among all three generations of cells. They are also and are known by their susceptibility to performance degradation at higher temperatures. An illustration of the structure of the PV cell and module for monocrystalline and polycrystalline technologies is shown in Fig 2.7.

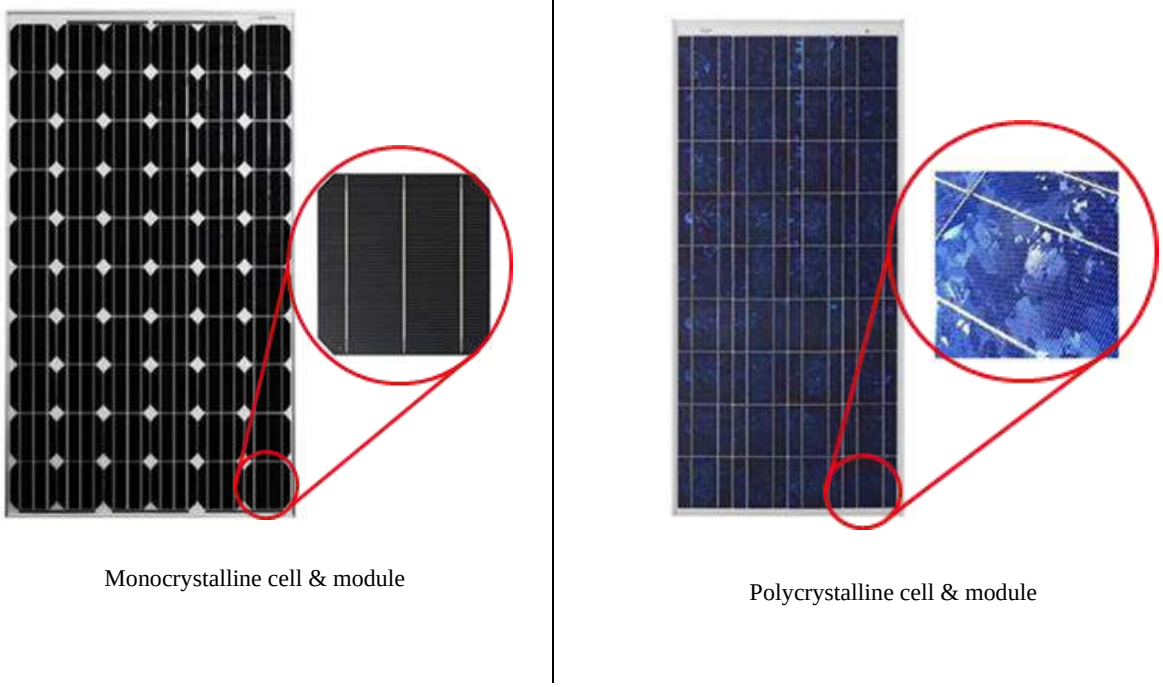

Monocrystalline cell & module

Polycrystalline cell & module

Fig. 2.7 Structure of the 1st generation PV material

2.4.2. Thin film technology (PV second generation)

Solar PV cells of the second generation, known as thin films PV cells, use diverse technologies comprise:

- Cadmium telluride (CdTe),
- Copper indium gallium selenide (CIGS),
- Amorphous silicon (a-Si),
- Amorphous silicon hydrogenated (a-Si H).

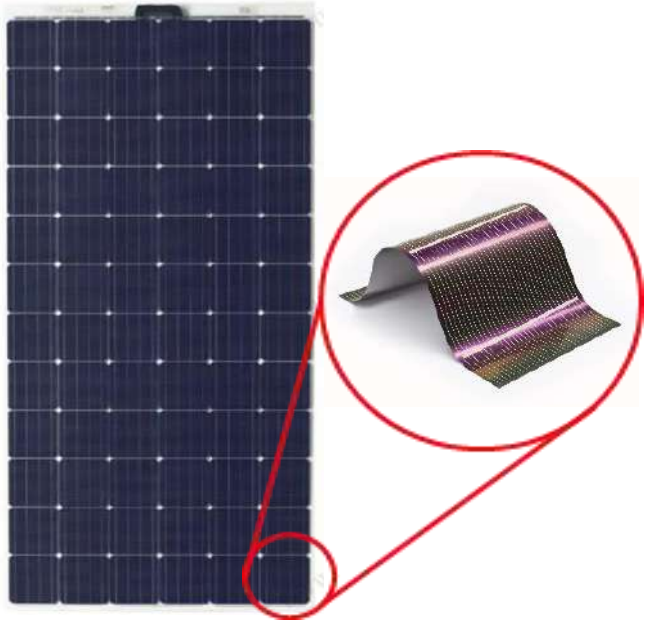

Fig. 2.8 Structure of the 2st generation PV material (Thin film cell & module)

Compared to the first generation (wafer-based Si), this technology is easier to implement and low cost due to its simpler fabrication process involving thin layers that consume less semiconductor materials. However, the efficiency is still less than that of first-generation cells, which was reported to have reached 23.35% by the CIGS-based PV cells [50, 51]. Fig 2.8 illustrates an example of the structure of thin film PV cells and modules.

2.4.3. Emerging technology (PV third generation)

Still in ongoing devolvement in laboratories, the third generation so-called PV emerging technology uses the thin film layers of the second generation to fabricate the solar PV cells. The

main objective of the emerging technologies is to reduce production costs and increase efficiency which is reported to have reached 25.2% (recorded by the perovskite PV cells) [7, 10]. This objective was attained by using materials including organic dyes, solar inks, conductive plastics, and nanotubes. The PV emerging technologies can be classified into five subcategories:

- Perovskite,
- Quantum dots (QD),
- Multi-junction cells,
- Organic,
- Dye-sensitized solar cells.

Fig 2.9 illustrates an example of mini perovskite PV module.

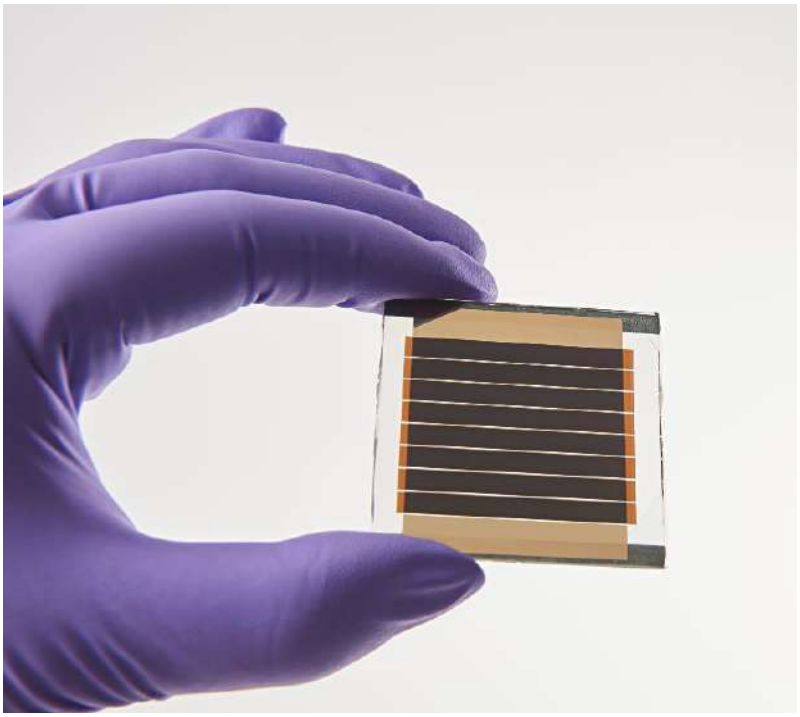

Fig. 2.9 Example of mini perovskite PV module

2.5. Trends and future PV technologies

It has been reported that a quarter of global electricity needs will be supplied by solar PV by 2050, making it one of the most prominent generation sources. The solar PV industry is forecast to become the second-largest power generation source by 2050, just behind wind power [52].

To provide insight into the trends and future of the PV market, technical, economic, and statistical studies have been conducted. The main factors considered were efficiency and cost.

Fig 2.10 presents a recent chart of the best reached-cell efficiencies for the different PV technologies of the world market since 1976. This chart was provided by provided by the National Renewable Energy Laboratory (NREL) [53]. As can be seen, the multi-junction PV technology outperforms the existing technologies by reaching 47.6% efficiency.

In many ways, photovoltaic research seems to be advancing quickly. Even though many PV methods and products are still in premature phases inside laboratories and not commercialized, they are promised to be the leaders of the PV industry in the future [54].

As illustrated in Fig 2.10, the multi-junction PV cells with four or more junctions are beating the records of efficiency for consecutive years. Despite their high cost, this type of PV technology could reach more records in the future. Their application can be beneficial in fields such as space and some specific mobile applications, especially with the intensive effort of scientists and companies to reduce their costs. Another possible development way of this technology is the idea of PV cells with multi-layers by tuning the doping of the band gap. In this concept, every layer would have a band gap tuned to a particular wavelength of light [54].

Perovskite-Si tandem PV cells from the emerging generation look like a promising type since their efficiency has sharply increased in the last few years to reach the threshold of 40%.

Despite their modest efficiency, crystalline Si and thin film technologies remain dominant in the PV market due to their low cost and their long lifetime. It seems that this technology will remain preferable for investments such as PV power plants and Building-Integrated Photovoltaics (BIPV) for the next decade.

The development of power storage technology is another important factor to consider in the future PV industry perspectives. The PV power storage systems can play a crucial role in the enforcement of efficiency, reliability, and cost-effectiveness of the whole PV system.

Photovoltaic generators are solar PV devices that use the photovoltaic effect to convert sunlight into electricity [55]. This means that PV cells, modules, strings, and arrays are all PV generators.

Figure 2.11 clarifies that the photovoltaic cell is the elementary generator of photovoltaic energy. While a photovoltaic cell produces a small amount of electrical energy, typically less than 2 watts, it is not practical to use it alone as a photovoltaic generator. Instead, it is commonly

employed as a photoelectric sensor in instrumentation and automation applications, such as light detectors (photodetectors).

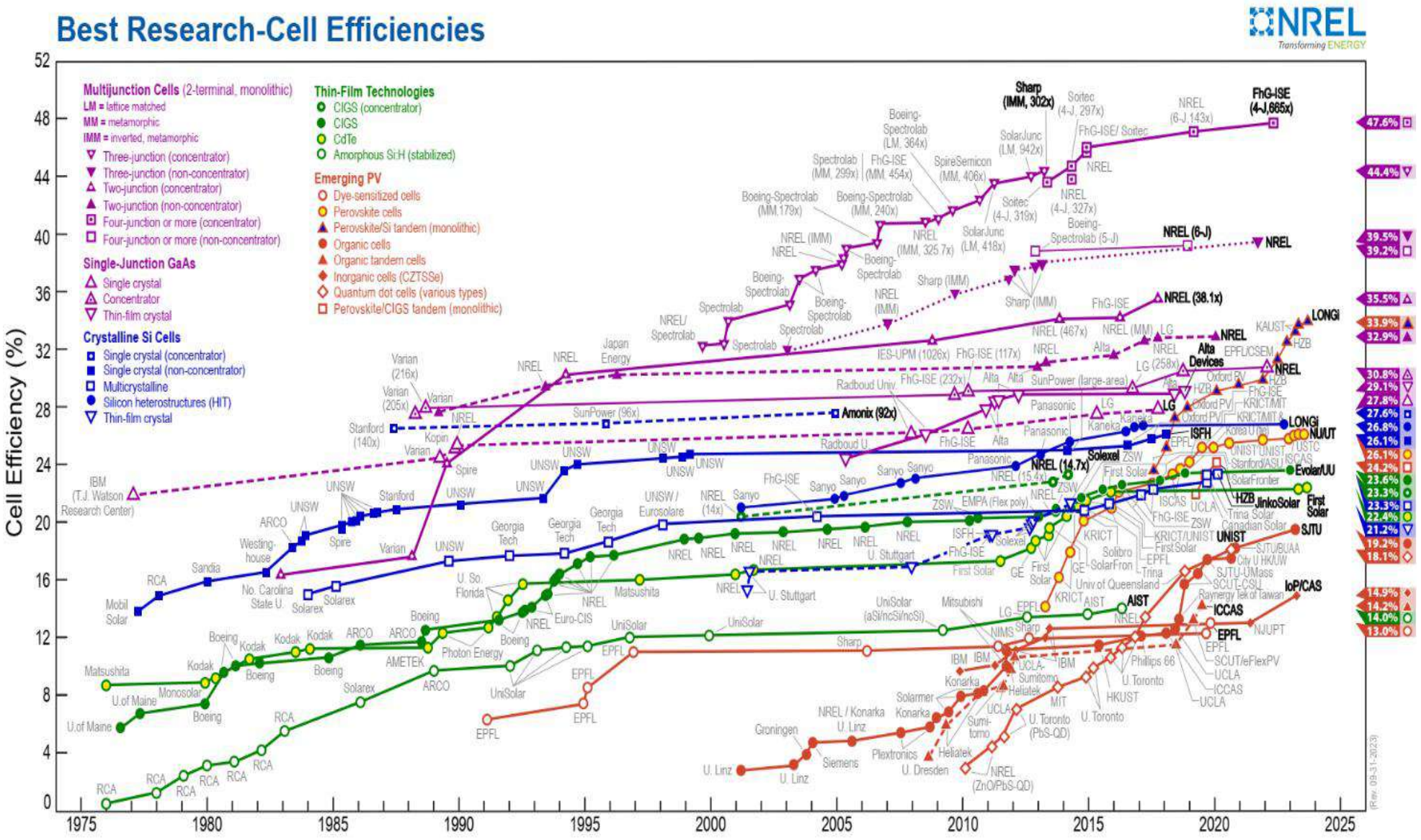

Fig. 2.10 Best achieved efficiency of different PV technologies over the last decades, provided by the National Renewable Energy Laboratory (NREL)

2.6. Types and applications of PV generators

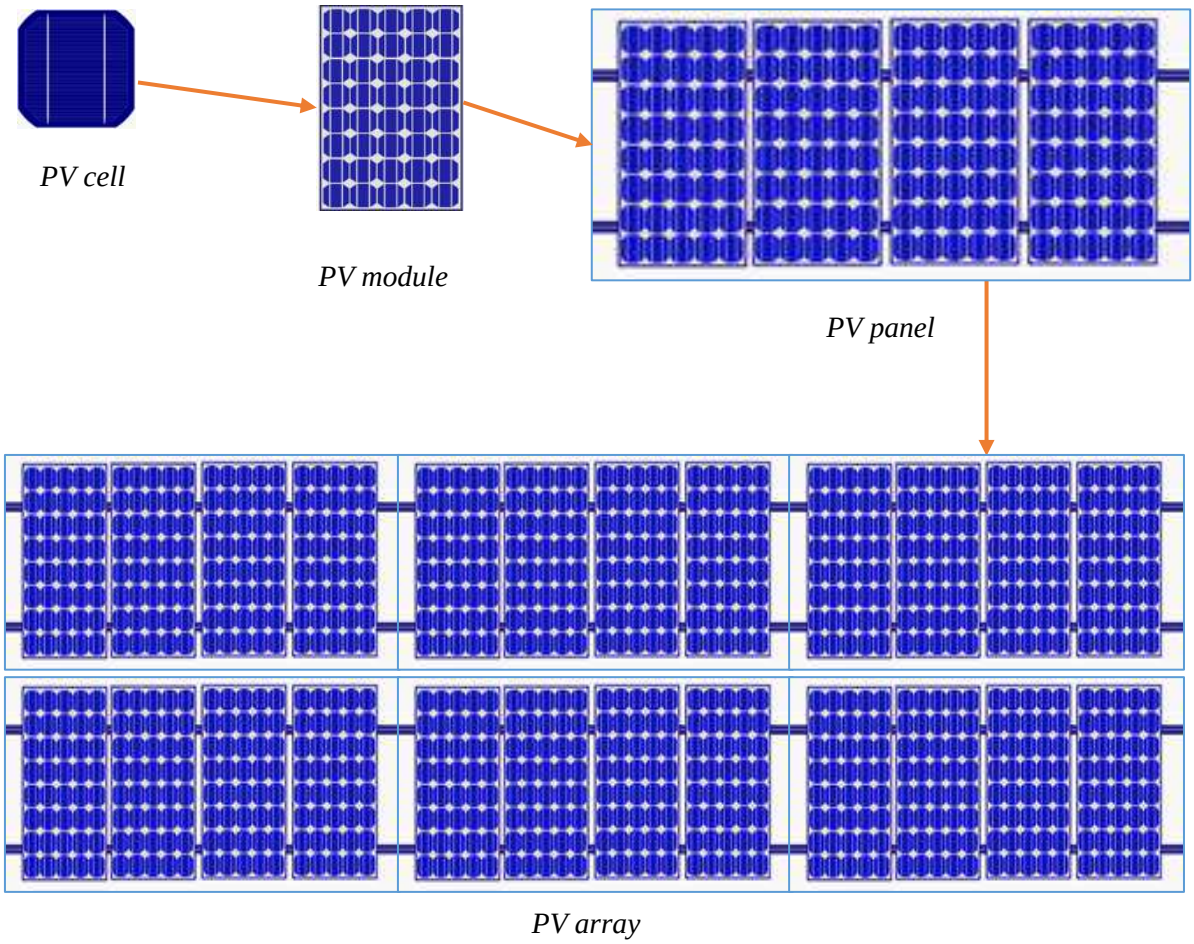

Fig. 2.11 PV generators: cell, module, panel, and array.

The photovoltaic module, on the other hand, consists of a series of photovoltaic cells connected in series to harness solar photovoltaic energy efficiently. PV modules are assembled and consolidated using the appropriate materials to protect their cells from degradation during transportation and to extend their lifecycles while in use. A PV module size is about one square meter and can produce up to 150~300 watts.

A PV panel is a collection of PV modules that are physically joined and wired together. It is worth noting that this definition is sometimes mistakenly used to describe a PV string in literature. However, according to the standard definition provided by the IEC TS 61836, a PV string is a grouping of PV modules connected in a series [55].

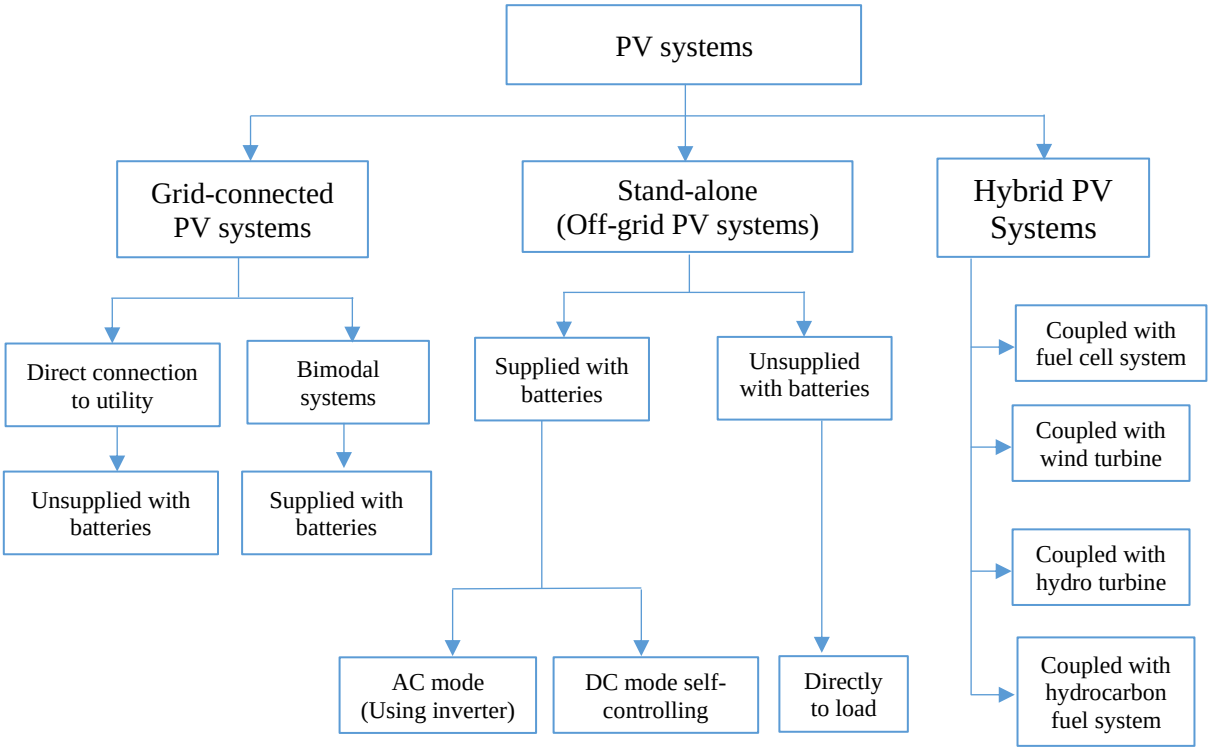

Fig. 2.12 Classification of PV systems.

Solar PV arrays consist of electrically connected solar panels mounted in a PV plant or on top of a building. Their size depends on the area allocated and the energy required.

PV systems are generally classified according to their exploitation mode requirements and the configuration of their components, as follows:

- *Grid-connected PV systems:* In this type of PV system, clients are supplying the grid utility with the overproduced energy and consuming energy from the grid utility only when their PV systems are not generating electricity, or when their local production is not sufficient. This configuration can reduce the costs of utility bills or even generate extra revenues by selling the overproduced energy to electricity companies. As illustrated in Fig 2.12, this type of PV system can be designed either directly connected to the grid without any energy storage or can be supplied with batteries to store excess power for nighttime usage. This last type of PV system is called a Battery Backup PV System or Bimodal PV System. Fig. 2.13 presents a typical PV system tied to the utility grid equipped with batteries and an inverter.

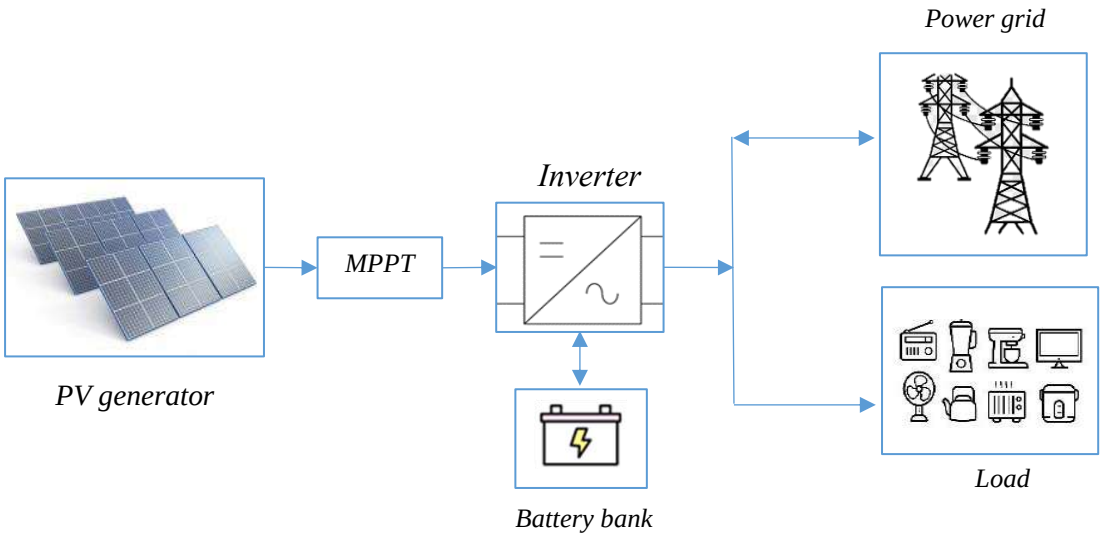

Fig. 2.13 Grid-connected PV system.

- *Stand-alone (off-grid) PV systems:* The stand-alone PV system is designed to generate electrical energy independently from the electricity grid, making it suitable for rural areas and distant agglomerations. As shown in Figure 2.12, this system can either be equipped with batteries to store excess energy or operate without batteries. In the latter case, the PV generator is directly connected to the loads, and the system must be designed to meet the energy demand without exceeding it.
- *Hybrid Solar PV Systems:* In hybrid PV systems, the solar PV generator is connected to other types of electricity generation systems. By coupling PV systems with various electricity generation systems, it can ensure reliable backup power. Whether with classic or renewable systems, this approach provides an almost uninterruptible power supply. Fig. 2.12 presents some kinds of systems that could be tied to the PV systems. For instance, fuel cell systems, wind turbine systems, hydro turbine systems, and hydrocarbon-based fuel generators (diesel, natural gas…etc.).

2.7. Conclusion

In conclusion, this chapter presents the basic concepts and principles of Photovoltaics are presented. The discovery of photovoltaic energy has triggered a continuous revolution of innovation and progress, from its humble beginnings in the observations of Edmund Becquerel to the significant advancements made at Bell Telephone Laboratories in the mid-20th century, photovoltaic energy has come a long way. Today, it stands as an inspiration of hope in mankind's

quest for sustainable and renewable energy sources, and the middle of the battle against climate change and global warming.

The advantages of photovoltaic generators, as highlighted, offer a compelling case for their adoption as a primary source of energy generation. Its ability to generate electricity silently, rapidly harness the power of sunlight, and its minimal environmental impact make it a notable solution. With the flexibility to scale from small residential installations to vast solar farms, photovoltaic generators promise a dynamic future for energy production.

During the presentation, the intricate process of converting sunlight into electricity was thoroughly explained, covering both physical and chemical aspects. One of the key concepts discussed was the photovoltaic effect, where solar radiation is converted into the movement of electrons, which ultimately generates a flow of current within the PV cell material.

In addition, the presentation includes a discussion on the types of photovoltaic technologies, their current trends, and future directions. The PV market and research institutions have identified three generations of photovoltaic technologies. The first generation is based on crystalline silicon technology, while the second generation is based on thin film technology. The third generation is represented by the newest and most advanced so-called emerging technologies.

Finally, a discussion is given to explain various kinds of photovoltaic generators and their integration with different systems based on their architecture and the energy demand. Three types of PV systems are available - grid-connected PV systems, stand-alone (off-grid) PV systems, and hybrid Solar PV Systems. The primary goal of configuring these systems is to reduce the cost of electricity bills and provide greater flexibility to generate power, even when off-grid or using batteries or hybrid backups.

Chapter 03:

Photovoltaic generator modeling

3.1. Introduction

The growing global need for sustainable and renewable energy sources has led to the rapid adoption of photovoltaic (PV) systems as an essential part of contemporary methods of electricity generation.

The efficiency of PV systems is highly dependent on their optimal configuration, accurate performance prediction, and reliable grid integration. To achieve these objectives, it is crucial to develop precise and sophisticated models of PV generators for their control, monitoring, simulation, and fault diagnosis. However, because of the weather conditions' instability, PV systems present a high level of complexity while producing electricity. Unfortunately, manufacturers provide PV generator data only for specific conditions of solar irradiance and temperature. These provided data are not sufficient when modeling the solar power outputs under real operating circumstances [56, 57].

For this reason, reliable and precise PV generator models play a vital role in grid integration, energy management, and planning. Understanding the behavior of PV systems under dynamic and fluctuating environmental conditions, such as changing solar radiation and temperature, enables efficient management of energy flow and stability in off-grid and grid-connected applications.

In this state of affairs, integrating automatic supervision and monitoring techniques in PV plants presents big challenges nowadays and in the future. This is because of the cost and complexity of these techniques, especially for big PV plants.

In this chapter, the modeling of PV generators (cell, module, string, arrays) is investigated to provide a comprehensive understanding of this topic, as well as their underlying principles, methodologies, and applications.

In general, PV modeling can be performed in two steps:

- First, the PV parametric model is developed from fundamental physics-based principles and simplified assumptions;
- Second, the emphasized parameters are estimated using experimental data and specialized algorithms.

3.2. Concept of modeling

From an engineering viewpoint, a standard definition of the model of a given system is a comprehensive description of a single component of the system that can be built, used,

and analyzed to predict the operational characteristics of the finished product [58].

A model of the PV generator is an informative representation that describe it and illustrate relations between its inputs and outputs. Since the solar PV cell is the smallest unity that represent the PV generator, the model of the PV module, string and array, are can be generalized from the PV cell model.

3.3. Advantages of PV generator modeling

There are several advantages of PV generator modeling that can be categorized as follows:

Technically: PV models help in simulating the behavior of the PV generator and evaluate the feasibility in different scenarios before implementation. One of the most important applications of PV generator modeling is the design of maximum power point tracking (MPPT) techniques and devices.

Economically: During exploitation, the PVG model contribute in control, in monitoring and in fault detection. This contributes in maintenance planning and reduce costs significantly.

Safety compliance: PV generator models contribute in identifying and managing risks associated with PVG operations, such as hot spot or fire. Operators can evaluate the reliability of a system and take corrective action promptly.

3.4. PV generator modeling

The PV generator produces electricity from the energy of the photon by the interaction of several physical phenomena. The performance of a PV generator is influenced by a variety of parameters related to meteorological and environmental circumstances. Considering these parameters is vital for optimizing PV generator performance and predicting energy output correctly. These parameters are listed as follows:

a) Solar Irradiance:

The first physical factor that influences the performance of the PV generator is solar irradiance which represents the solar power intensity per unit area measured in watts per square meter (W/m^2). The global solar irradiance (G_G) is the sum of three types of irradiances [59]:

$$G_G = G_{Dir} + G_{Dif} + G_{Ref} \tag{3.1}$$

where:

- G_{Dir} *is the direct irradiance:* The intensity of sunlight that directly reaches the PV surface without any scattering or absorption in the atmosphere. It depends on the

angle of incidence between the sunlight and the PV surface, with maximum irradiance occurring when the sun is perpendicular to the surface.

- G_{Dif} *is the diffuse irradiance:* The intensity of sunlight that is scattered and spread out in the atmosphere before reaching the PV surface. Diffuse irradiance depends on factors like cloud cover and atmospheric conditions.
- G_{Ref} *is the reflected irradiance:* Reflected irradiance is the solar radiation that reaches the PV surface after being reflected from surrounding surfaces, such as the ground, nearby buildings, or other objects. Reflected irradiance contributes to the total solar energy incident on the PV generator.

The instrument that measures the global irradiance is the Pyrometer and the reflected irradiance can be neglected and the equation of the global irradiance is given as follows:

$$G_G = G_{Dir} + G_{Dif} \tag{3.2}$$

b) Temperature:

The electrical efficiency of the PV generator is influenced by the ambient temperature. Higher temperatures can lead to increased electron-hole recombination rates, resulting in reduced power output. Temperature coefficients are used to model this behavior and estimate the temperature-dependent efficiency of PV cells.

c) Wind Speed:

Wind speed affects the convective cooling of PV modules. A higher wind speed can help dissipate heat from the PV surface, potentially leading to a decrease in PV cells' temperature and an improvement in electrical efficiency.

d) Humidity:

Humidity affects atmospheric conditions and can impact the amount of scattering and absorption of sunlight. In arid regions, lower humidity levels may lead to less attenuation of solar irradiance.

The performance of the PV generator is also impacted by other internal and external factors such as dust accumulation, hotspots, cells' aging, deterioration…etc.

The PV generator model identification is performed usually in the Standard Test Conditions (STC). Some factors such as wind speed and humidity are neglected in the PV generator model identification process. The above-mentioned factors impact, although, due to experimental

constraints and for simplifying equations, some neglect factors the influence of wind speed and solar spectrum.

3.4.1 I-V characteristic of the PV generator

The characterization of a PV generator predominantly relies on its current-voltage (I-V) characteristic. However, due to the inherent nonlinearity of this characteristic, accurately simulating and predicting the PV generator's behavior becomes challenging, particularly in the context of continuously varying outdoor conditions.

Moreover, PV generator manufacturers typically provide limited data about their modules, primarily acquired under standardized test conditions (STC). Utilizing this data as a basis to infer power degradation necessitates either the development of a model capable of instantaneously converting all collected data from the actual PV generator to the reference conditions or the identification of the PV generator under the precise peculiarities of these reference conditions. This is often resulting in unit disconnection and consequently, a cessation of power generation.

Other PV generator models are proposed in the literature, the most widespread are the electrical circuit-based models.

3.4.2. Electrical circuit-Based Models of the PV generator

In photovoltaic technology, the PV generator's smallest element is the PV cell, which serves as a semiconductor device equipped with a *p-n* junction, fabricated within a thin wafer or layer of semiconductor material. Upon exposure to incident light, it initiates a photocurrent on the premise that the photon energy exceeds the material's band gap. The intensity of the produced photocurrent is proportional to the power of solar radiation [60].

However, in the absence of solar radiation, the current-voltage (I-V) characteristics of a solar cell demonstrate an exponential behavior akin to that of a diode. Specifically, the I-V curve exhibits a rectifying nature, allowing current to flow more readily in the forward bias direction, while presenting substantial resistance in the reverse bias direction.

An example of the shape of output current as a function of the output voltage of a PV module is illustrated in Fig 3.1, which is provided by Sandia labs, five critical points are also provided: Open circuit (I_{sc}, 0), short-circuit (0, V_{oc}), maximum power point (I_{mp}, V_{mp}), (I_x, ½V_{oc}), and (I_{xx}, ½(V_{oc}+V_{mp}). It has been proven as well that the equations describing the performance of the PV generators can be applicable at any level starting from the PV cells, to PV modules, or even PV arrays [61].

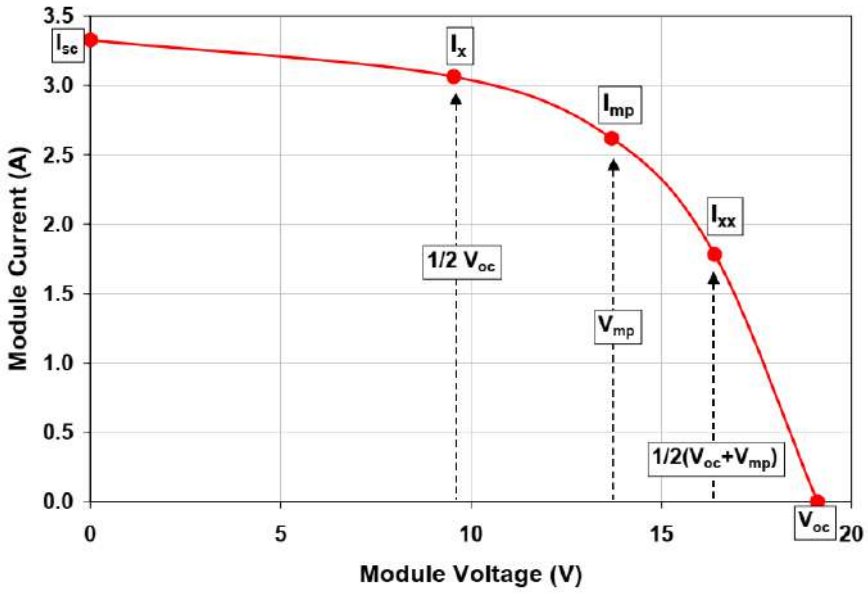

Fig. 3.1 Graph of PV module I-V characteristic provided by Sandia Labs [61]

a) Single-diode model

The single-diode model SDM is the simplest electrical circuit-based model of the PV generator used to simulate and predict the electrical behavior of the PV generator. This model is widely applied in photovoltaic research and industry applications due to its simplicity [62]. Fig. 3.2 illustrates the electrical equivalent circuit of the SDM and their related physical parameters.

In the SDM electrical equivalent circuit, G represents the solar irradiance. The ideal photo-generated current I_{ph} is flowing from the current source as a result of the incident irradiance. In parallel, a diode that has an ideality factor n is inserted and through which passes the forward diode current I_D. Two internal resistances (shunt resistor: R_{sh}, series resistor: R_s) are presented in the SDM equivalent circuit to consider the load current and the leakage current respectively. I_L and V_L are the output current (the load current) and the output voltage (the load voltage) respectively.

According to Kirchhoff's law, the output current can be written as follows [63]:

$$I_L = I_{ph} - I_D - I_{sh} \tag{3.3}$$

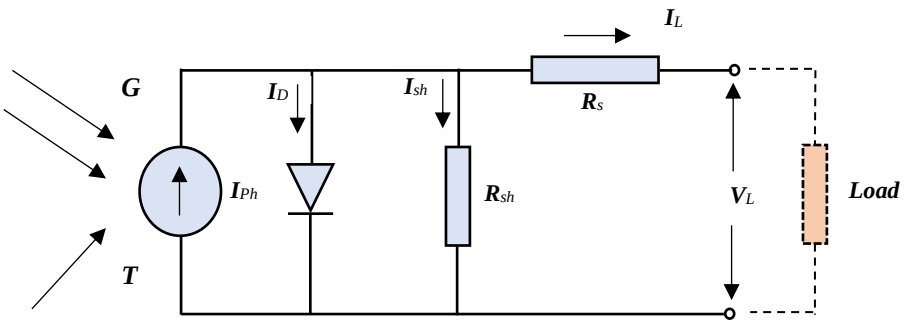

Fig. 3.2 Electrical equivalent circuit of the single-diode model (SDM).

Using the Shockley diode law, the forward diode current I_D is obtained as follows [64]:

$$I_D = I_{sd}.\left[exp\left(\frac{V_L+R_S.I_L}{n.V_{th}}\right) - 1\right] \tag{3.4}$$

where I_{sd} is the reverse saturation current. V_{th} refers to the thermal voltage of the diode and it is given as follows:

$$V_{th} = \frac{k.T}{q} \tag{3.5}$$

where:

- T is the cell's temperature in Kelvin,
- k = 1.380653×10^{-23} J/K is the Boltzmann's constant,
- q = 1.60217646 ×10^{-19} C is the electron charge.

The current flowing through shunt resistor I_{sh} can be expressed as follows:

$$I_{sh} = \frac{V_L+R_S.I_L}{R_{sh}} \tag{3.6}$$

From the four equations, the output current can be expressed as follows:

$$I_L = I_{ph} - I_{sd}.\left[exp\left(\frac{q.(V_L+R_S.I_L)}{n.k.T}\right) - 1\right] - \frac{V_L+R_S.I_L}{R_{sh}} \tag{3.7}$$

As can be seen in Eq 3.7, the SDM includes both linear and nonlinear (exponential) characteristics. Their five unknown parameters are:

- The photocurrent I_{ph};
- The diode saturation current I_{sd};

- The shunt resistance R_{sh};
- The series resistance R_s;
- The diode ideality factor n.

On the other hand, the photo-current I_{ph} is influenced by the cell surface irradiance G and the temperature T, and it can be obtained as follows [65]:

$$I_{ph} = \frac{G}{G_{STS}}\left[I_{phSTS} + K_i(T - T_{STC})\right] \tag{3.8}$$

Where:

- G is the solar irradiance measured on the cell surface;
- G_{STC} =1000 W/m², is solar irradiance;
- I_{phSTC} is the photo-current generated at the STC environment;
- T is the temperature measured at the cell surface;
- T_{STC} = 25° C = 298 Kelvin, is the temperature measured at the STC environment;
- K_i is Current temperature coefficient (A/K), also, known as short circuit current coefficient.

The diode saturation current function of temperature is given as follows [65]:

$$I_{sd} = I_{sdSTC}\left(\frac{T}{T_{STC}}\right)^3 exp\left[\frac{qE_g}{n.k}\left(\frac{1}{T_{STC}} - \frac{1}{T}\right)\right] \tag{3.9}$$

where:

- E_g is the band gap energy of the semiconductor;
- I_{sdSTC} is the nominal saturation current.

The photo-current I_{ph} and the diode saturation current I_{sd} can be calculated analytically using Eq. 3.8 and Eq.3.9 at the given irradiance G and temperature T. But still, the three remaining parameters need to be computed. Several research works have been performed, and are still ongoing, with the aim of identifying the PV generator model parameters analytically and employing by employing PV module manufacturers' data as well as the measured weather parameters at STC.

Usually, the analytical methods are used to determine the PV model parameters at STC data provided by PV module manufacturer. The identified parameters are then translated to

operational conditions using Eq. 3.8 and Eq. 3.9 as functions of irradiance and temperature [10]. Some assumptions are performed as well to simplify calculation due to the complexity and the nonlinearity of the current-voltage equation.

Even though the SDM is widely employed for PV generator modeling due to its simplicity, it has some inherent drawbacks such as [66, 67]:

- The SDM was introduced upon the assumption that in the depletion region, the recombination loss is absent, but in reality, this is not true;
- SDM efficiency deteriorates upon temperature variations;
- SDM accuracy decreases at low irradiance levels, particularly at open-circuit voltage (V_{oc}).

b) Double-diode model

Due to the over-mentioned drawbacks of the SDM, several attempts have been conducted to propose other models capable of accurately expressing the PV generator behavior. Therefore, to consider the effects of recombination current loss in the depletion region, the double-diode model (DDM) is proposed [10]. The electrical equivalent circuit of the DDM is presented in Fig 2.3 and the mathematical formulation of the DDM output current is given as follows [68]:

$$I_L = I_{ph} - I_{D1} - I_{D2} - I_{sh} \tag{3.10}$$

$$I_L = I_{ph} - I_{sd1} \cdot \left[exp\left(\frac{q.(V_L+R_S.I_L)}{n_1.k.T}\right) - 1\right] - I_{sd2} \cdot \left[exp\left(\frac{q.(V_L+R_S.I_L)}{n_2.k.T}\right) - 1\right] - \frac{V_L+R_S.I_L}{R_{sh}} \tag{3.11}$$

Compared to Eq.3.7 governing the SDM, two supplementary parameters related to the second diode are added to describe the I-V characteristic of the DDM, as mentioned in Eq.3.11. Hence, seven unknown parameters are considered in the DDM: I_{ph}, I_{sd1}, I_{sd2}, R_s, R_{sh}, n_1, and n_2.

The two exponential parts in the equation of the DDM raise its nonlinearity and complexity, and consequently, raise the computational efforts of any employed technique to determine the explicit relationship between the output current and the load voltage.

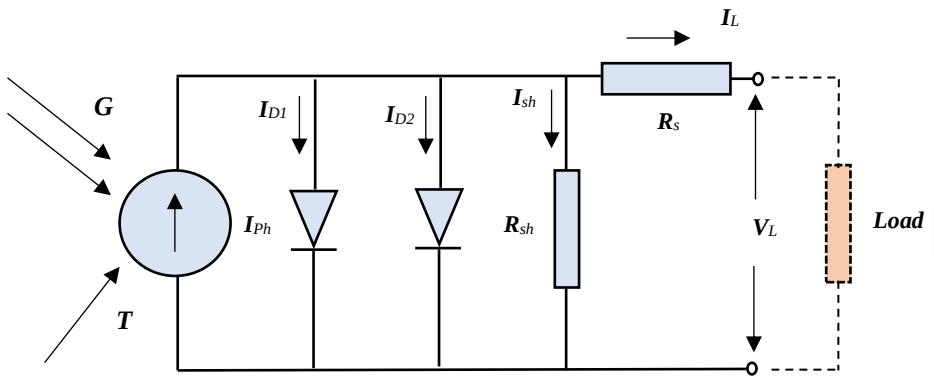

Fig. 3.3 Electrical equivalent circuit of the double-diode model (DDM).

c) Triple-diode model

In the last few years, the triple-diode model (TDM) has attracted the attention of researchers to solve the PV generator modeling problem. Since 2007, when the TDM was introduced in reference [69], several works have been published in the literature using the TDM as a more accurate option to deal with this problem.

The TDM is considered the most accurate PV generator model due to its capacity to represent the current leakage through a small-sized solar cell's peripheries, which was missed in SDM and DDM [70]. Also, due to its efficiency in providing a more comprehensive representation of the electrical behavior of photovoltaic cells, especially under a wide range of operating conditions. In the TDM, a third diode is inserted in parallel with the two diodes as well as the shunt resistor as illustrated in Fig .3.4. Consequently, a third exponential part is added to the Eq.3.10 to represent the physical properties of this third diode, and the final equation that describes the TDM is as follows:

$$I_L = I_{ph} - I_{D1} - I_{D2} - I_{D3} - I_{sh} \tag{3.12}$$

$$I_L = I_{ph} - I_{sd1}\left[exp\left(\frac{q(V_L + R_s I_L)}{n_1 kT}\right) - 1\right] - I_{sd2}\left[exp\left(\frac{q(V_L + R_s I_L)}{n_2 kT}\right) - 1\right] - I_{sd3}\left[exp\left(\frac{q(V_L + R_s I_L)}{n_3 kT}\right) - 1\right]$$

$$- \frac{V_L + R_s I_L}{R_{sh}} \tag{3.13}$$

Nine unknown parameters have to be identified in the process of PV generator modeling in the TDM: I_{ph}, I_{sd1}, I_{sd2}, I_{sd3}, R_s, R_{sh}, n_1, n_2, and n_3. Even though TDM is the most accurate model, three exponential parts in the equation that describe the relation between its electrical parameters increase the level of its complexity and computational resources to solve it.

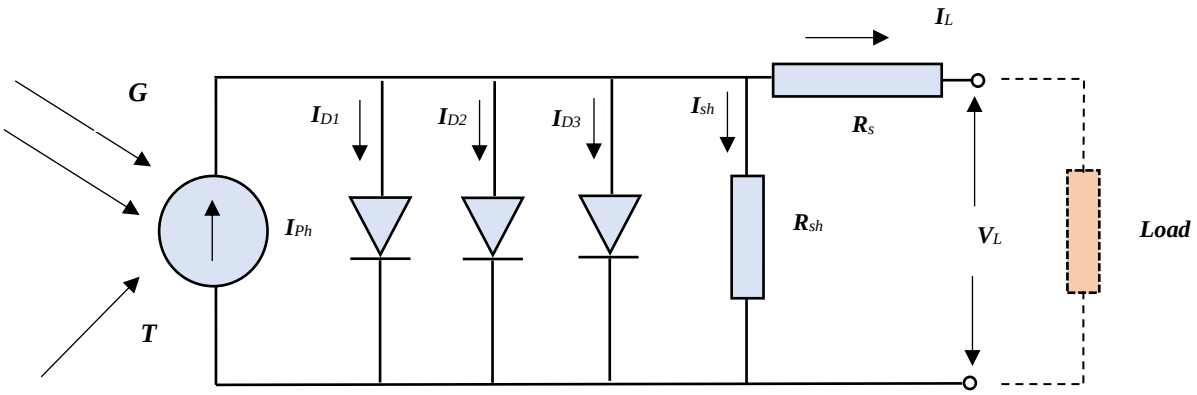

Fig. 3.4 Electrical equivalent circuit of the triple-diode model (TDM).

d) Solar PV module/string model

The equivalent electrical circuit of the PV module and the PV string model is illustrated in Fig.3.5. According to the standard definition provided for the PV generators by the International Electrotechnical Commission (IEC-TS 61836) [71]:

- PV cell is the most elementary photovoltaic device;
- PV module is a complete and environmentally protected assembly of interconnected photovoltaic cells.
- PV string is a larger unit formed by PV modules connected in series or parallel. In general, the PV string is a group of modules connected to one inverter device

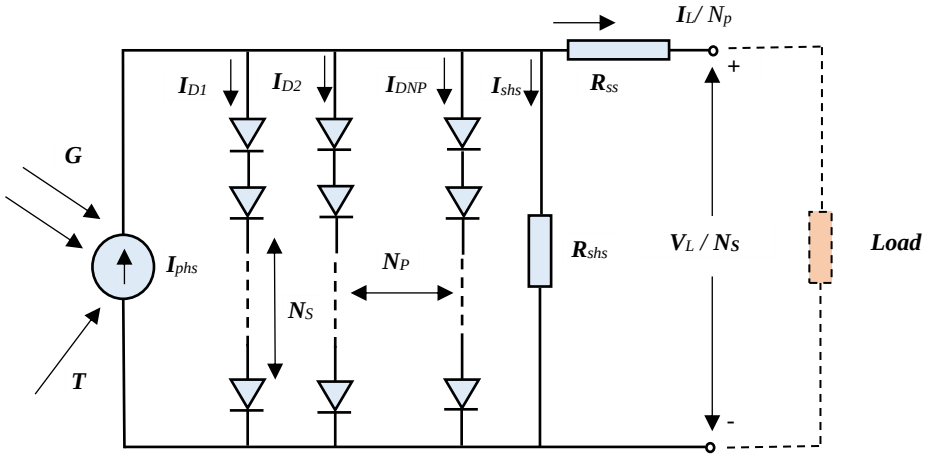

Fig. 3.5 Electrical equivalent circuit of the PV module/String model.

Hence, the output current of the PV cell, PV module or PV string can be expressed either in SDM, DDM, or TDM.

The output current of the PV module/string represented in SDM is given as follows [72]:

$$I_L = I_{phs} - I_{sds} \cdot \left[exp\left(\frac{V_L - I_L R_{ss}}{n_s . V_{thm}}\right) - 1\right] - \frac{V_L - I_L \cdot R_{ss}}{R_{shs}} \quad (3.14)$$

where:

$(I_{phs} = N_p \cdot I_{ph});\ \ (I_{sds} = N_p \cdot I_{sd});\ (R_{ss} = \frac{N_s}{N_p} \cdot R_s);\ \ (R_{shs} = \frac{N_s}{N_p} \cdot R_{sh})\ ;\ (n_s = N_s \cdot n);$

and $(V_{thm} = \frac{kT}{q})$.

The output current of the PV module/string represented in DDM can be formulated by adding a second exponential part to Eq.3.14, is given as follows:

$$I_L = I_{phs} - I_{sds1} \cdot \left[exp\left(\frac{q(V_L - I_L R_{ss})}{n_{s1} kT}\right) - 1\right] - I_{sds2} \cdot \left[exp\left(\frac{q(V_L - I_L R_{ss})}{n_{s2} kT}\right) - 1\right] - \frac{V_L - I_L \cdot R_{ss}}{R_{shs}} \quad (3.15)$$

In the same way, the output current of the PV module/string represented in TDM can be formulated by adding a third exponential part to Eq.3.15, is given as follows:

$$I_L = I_{phs} - I_{sds1} \cdot \left[exp\left(\frac{q(V_L - I_L R_{ss})}{n_{s1} kT}\right) - 1\right] - I_{sds2} \cdot \left[exp\left(\frac{q(V_L - I_L R_{ss})}{n_{s2} kT}\right) - 1\right]$$
$$- I_{sds3} \cdot \left[exp\left(\frac{q(V_L - I_L R_{ss})}{n_{s3} kT}\right) - 1\right] - \frac{V_L - I_L \cdot R_{ss}}{R_{shs}} \quad (3.16)$$

3.5. Solving the PV generator modeling problem

In literature, several methods have been proposed to solve the problem of the PV generator model parameters identification. In general, the proposed methods are categorized into two groups: analytical methods, and metaheuristic methods [70].

3.5.1. Analytical methods

The analytical methods were used earlier and they usually use numerical techniques to estimate the unknown parameters of the PV generator model. These methods are characterized by their simplicity in implementation and the use of approximations and assumptions leading sometimes to less accuracy [73].

In the analytical methods, the unknown parameters of the PV generator model are determined at three reference points: open-circuit (OC), short-circuit (SC), and the maximum power point (MPP), and by using manufacturers' data sheets under standard test conditions (STC). Using a series of empirical equations, the I-V curve is then generalized to real operating conditions.

It is obvious that these methods become more complicated when dealing with DDM and TDM PV generator models [73].

3.5.2. Numerical iterative methods

The numerical iterative methods are considered classical optimization approaches conducting by the minimization of the error between the measured and the estimated data. This type of method is more accurate than the analytical ones, due to their capability of handling the nonlinearity of the problem and the multivariable equations. However, these methods need a larger execution time compared to analytical methods, and they are highly dependent on the initial solutions [74]. These methods include among others: Newton Raphson, Levenberg Marquardt, Least Square Error, Lambert *W* function… [62].

3.5.3. Metaheuristic methods

This kind of method becomes more popular in the last few years and still attracts more researchers' attention. Numerous works were published in the literature involving metaheuristic approaches for PV generator modeling.

Generally, the task of determining the parameters of the PV generator model using metaheuristic methods is addressed by transforming it into a numerical optimization problem. The optimization process using metaheuristic methods aims to minimize the difference between the measured and the estimated I-V data by minimizing an objective function that governs the optimization. This type of method is more powerful and more robust than the previous methods, due to its stochastic character and random initialization of the solutions. Particularly when dealing with complex nonlinear problem like the TDM PV model [74].

The most notable classification of metaheuristic methods is the following [75]:

- Nature-inspired methods (from biology, swarm-based algorithms, animal behavior while foraging or hunting…);
- Evolutionary-inspired algorithms (using hypotheses of evolution like mutation and crossover…);
- Physics-based methods (Physics laws like gravity, magnetism, quantum…);
- Mathematical-based methods (Arithmetic operations, geometry …);
- Social phenomena-based methods (Teaching learning process, Games, Culture …);

Based on their inspiration, these methods have their own strengthens and drawbacks.

Compared to the analytical and the numerical iterative methods, the metaheuristic methods are characterized by the following features:

- They are population-based methods, where each individual is a candidate solution, versus the singularity of the solution in the other methods. This feature multiplies the chance of finding the optimal solution by the population size.
- They are stochastic, which complies perfectly with the search strategy in real-world life.
- They are random initialized methods, which makes them independent from the wrong initial conditions.
- They are characterized by two important features: *exploration*, which indicates the capability of covering the search space, and *exploitation* which designates the ability to promptly catch the optimal solution when entering its neighbor zone.

In the last decades, numerous metaheuristic approaches have been proposed to solve the problem of PV generator modeling, such as Particle Swarm Optimization (PSO), Artificial Bee Colony (ABC), Simulated Annealing (SA), Genetic Algorithm (GA), Differential Evolution (DE), Harmony Search (HS), Whale Optimization Algorithm (WOA), Grey Wolf Optimizer (GWO)…etc.

However, a lot of metaheuristic methods suffer from different kinds of insufficiencies which prompted researchers continuously to develop new reliable methods to cope with that numerical issue and the high computational complexity of the problem.

Another way to enhance the performance of the metaheuristic methods is to hybridize two or more methods, by employing the best method in one algorithm in the aim of having more powerful methods. For that reason, researchers tend to develop new hybrid methods to improve the accuracy, reliability, and convergence speed of the new methods. For example, among these hybrid or enhanced metaheuristic methods: hybrid Artificial Bee Colony and Differential Evolution (ABC-DE), Guaranteed Convergence Particle Swarm Optimization (GCPSO), Performance-Guided JAYA (PGJAYA), Improved Teaching-Learning-Based Optimization (ITLBO), hybrid Grey Wolf Optimizer and Cuckoo Search (GWOCS), hybrid Bee Pollinator Flower Pollination Algorithm (BPFPA)… etc.

Considering the above-mentioned features of metaheuristic methods, special attention will be given to them in this thesis. In addition, this research work contributes to hybrid metaheuristic approaches in terms of methodology.

3.5.4. Lambert *W* function

The nonlinearity in the equation describing the relation between the output current and the

output voltage of the PV generator is due to the expression of that output current in the exponential part of this equation. In other words, if the output current $I_L = x$ the equation is a function represented in the following form:

$$f(x) = xe^x = \varphi \tag{3.17}$$

To obtain *x*, it is necessary to apply the inverse function as follows:

$$x = f^{-1}(xe^x) = W(\varphi) \tag{3.18}$$

Eq. 3.18 which provides the solution *x* of the Eq.3.17 is known in mathematics as the Lambert *W* function. Many engineering problems can be addressed using this function. A graphical representation of the Lambert *W* function is shown in Fig.3.6, where it is composed of two parts, the first is when $x \geq -1$ and the second when $x < -1$. Many iterative and analytical techniques can be applied to solve the Lambert *W* function such as: software package solvers (Example: MATLAB, Mathematica, Maple…), Taylor series (TS), Special Trans Function Theory (STFT), which is more accurate as reported in many papers [76].

It has been proven through many published papers that the most accurate method to solve the Lambert *W* function is the STFT method whatever the value of φ. In contrast, the TS method has acceptable accuracy only for small values of φ [77].

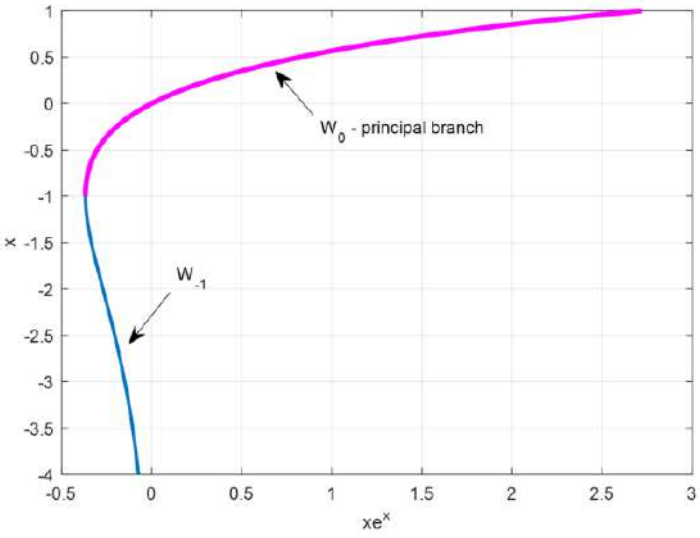

Fig. 3.6 Graph of the Lambert *W* function, $x = W(xe^x)$ [76].

Hence, the solution of Eq.3.17 using the STFT method can be formulated as follows [77]:

$$x = W(\varphi) = \varphi \frac{\sum_{k=0}^{N} \frac{\varphi^k (N-k)^k}{k!}}{\sum_{k=0}^{N+1} \frac{\varphi^k (N+1-k)^k}{k!}} \tag{3.19}$$

where *N* is a positive integer.

To determine the explicit relation between the output current-voltage of the PV generator models, either for SDM, DDM, or DMD, the Lambert *W* function was employed to give accurate PV generator modeling [78].

The application of the Lambert *W* function in the problem of the PV generator modeling represented in SDM is performed through the following arrangement of Eq.3.7:

$$I_L = \frac{R_{sh}(I_{ph}-I_{sd})-V_L}{R_s+R_{sh}} - \frac{k.T}{q.R_s}.n.W(\varphi) \tag{3.20}$$

where *W* represents the solution of the Lambert equation and:

$$\varphi = A.exp\left[\frac{R_{sh}q(R_sI_{ph}-R_sI_{sd})+V_L}{nkT(R_s+R_{sh})}\right] \tag{3.21}$$

$$A = \left[\frac{qR_{sh}R_sI_{sd}}{nkT(R_s+R_{sh})}\right] \tag{3.22}$$

For the DDM the equation is rearranged as follows:

$$I_L = \left[\frac{R_{sh}(I_{ph}+I_{sd1}+I_{sd2})-V_L}{R_s+R_{sh}} - \frac{k.T}{q.R_s}\right].[n_1W(\varphi_1)+n_2W(\varphi_2)] \tag{3.23}$$

$$\varphi_1 = \frac{qI_{sd1}R_sR_{sh}}{n_1.k.T(R_{sh}+R_s)}exp\left(\frac{qR_{sh}(I_{ph}R_s+I_{sd1}R_s+V_L)}{n_1.k.T(R_{sh}+R_s)}\right) \tag{3.24}$$

$$\varphi_2 = \frac{qI_{sd2}R_sR_{sh}}{n_2kT(R_{sh}+R_s)}exp\left(\frac{qR_{sh}(I_{ph}R_s+I_{sd2}R_s+V_L)}{n_2kT(R_{sh}+R_s)}\right) \tag{3.25}$$

For the TDM the equation is reformed as follows:

$$I_L = \left[\frac{R_{sh}(I_{ph}+I_{sd1}+I_{sd2}+I_{sd3})-V_L}{R_s+R_{sh}} - \frac{k.T}{q.R_s}\right].[n_1W(\varphi_1)+n_2W(\varphi_2)+n_3W(\varphi_3)] \tag{3.26}$$

$$\varphi_1 = \frac{qI_{sd1}R_sR_{sh}}{n_1.k.T(R_{sh}+R_s)}exp\left(\frac{qR_{sh}(I_{ph}R_s+I_{sd1}R_s+V_L)}{n_1.k.T(R_{sh}+R_s)}\right) \tag{3.27}$$

$$\varphi_2 = \frac{qI_{sd2}R_sR_{sh}}{n_2kT(R_{sh}+R_s)}exp\left(\frac{qR_{sh}(I_{ph}R_s+I_{sd2}R_s+V_L)}{n_2kT(R_{sh}+R_s)}\right) \tag{3.28}$$

$$\varphi_3 = \frac{qI_{sd3}R_sR_{sh}}{n_3kT(R_{sh}+R_s)}exp\left(\frac{qR_{sh}(I_{ph}R_s+I_{sd3}R_s+V_L)}{n_3kT(R_{sh}+R_s)}\right) \tag{3.29}$$

3.5.5. Objective function for optimization methods

The objective function (or the fitness function) serves as a mathematical representation of

the primary goal of the optimization problem [79]. It guides optimization process towards finding the optimal solution that aligns with the specific objectives and requirements of the problem.

In the literature, various types of objective functions used in the optimization methods are reported. Among others:

- *Absolute Error (AE)*: AE measures the absolute differences between the predicted data and the actual one of the PV generator models for each data point. It provides a simple and interpretable measure of the model's performance.
  The formula for calculating AE is given as follows:
  $$AE = |I_{measured} - I_{estimated}| \tag{3.30}$$

- *Mean Absolute Error (MAE)*: MAE measures the average absolute difference between estimated and measured values.
  The formula for calculating AE is given as follows:
  $$MAE = \frac{1}{N} \sum_{k=1}^{N} AE_k \tag{3.31}$$
  (*N* denotes the number of the measured data).

- *Relative error (RE)*: RE measures the relative difference between predicted values and actual target values. The relative error is useful for understanding the accuracy of predictions in proportion to the magnitude of the true values. It is commonly used in situations where the absolute magnitude of errors is less critical, and the relative discrepancy is more important. The formula to calculate the relative error is as follows:
  $$RE = \left|\frac{I_{measured} - I_{estimated}}{I_{measured}}\right| \tag{3.32}$$

- *Mean Relative Error (MRE)*: MRE measures the average relative difference between the predicted data and the actual one (ground truth) of the PV system. Relative error is useful when the scale of the target variable varies significantly, and the focus is on understanding the accuracy in proportion to the true values.
  The formula for calculating MRE is given as follows:
  $$MRE = \frac{1}{N} \sum_{k=1}^{N} RE_k \tag{3.33}$$
  (*N* denotes the number of the measured data).

- *Mean Squared Error (MSE)*: The most widely used objective function for regression problems. It measures the average squared difference between estimated and measured values.

  The formula for calculating MSE is given as follows:

$$MSE = \frac{1}{N} \sum_{k=1}^{N} \left(I_k^{measured} - I_k^{estimated}\right)^2 \quad (3.34)$$

  (*N* denotes the number of the measured data).

- *Root Mean Squared Error (RMSE)*: RMSE is the square root of the MSE and provides a measure of the standard deviation of the prediction errors. RMSE is sensitive to outliers since the squared differences amplify their impact.

  For these reasons, RMSE is the most popular and the most suitable for the PV generator modeling problem [72].

  The formula for calculating RMSE is given as follows:

$$RMSE = \sqrt{MSE} = \sqrt{\frac{1}{N} \sum_{k=1}^{N} \left(I_k^{measured} - I_k^{estimated}\right)^2} \quad (3.35)$$

  (*N* denotes the number of the measured data).

Using metaheuristic methods in solving the problem of PV generator modeling aims to find the optimal solution to the vector of the unknown parameters of the PV generator model. This optimization process is subject to minimizing the objective function that evaluates the difference between the measured output current and the calculated one.

In this thesis, the objective function adopted is the RMSE for the PV generator modeling as well as for fault detection and diagnosis.

3.5.6. Objective function design for the PV generator modeling

As discussed above, the objective function used for the optimization of the unknown parameters of PV generator model is the root mean square error (RMSE) which is defined as follows:

$$Ob(x, I_L, V_L) = \sqrt{\frac{1}{L_{max}} \sum_{L=1}^{L_{max}} \left(I_L^{meas} - I_L^{estim}\right)^2} \quad (3.36)$$

where *x* is the vector containing the unknown parameters (five parameters for the SDM, Seven for the DDM, and nine for the TDM). I_L^{meas}, V_L^{meas} represent the measured output current and voltage at the L^{th} point respectively, L_{max} denotes the number of experimental measured *I-V* data.

a) Classic objective function:

To formulate the classic objective function, Eq.3.36 is expressed in a form demonstrating the implicit relation between the output measured current and voltage, which is given as follows:

$$Ob_{Classic}(x) = \sqrt{\frac{1}{L_{max}} \sum_{k=1}^{L_{max}} [f(V_L, I_L, x)]^2} = \sqrt{\frac{1}{L_{max}} \sum_{k=1}^{L_{max}} \left(I_L^{meas} - I_L^{estim}\right)^2} \quad (3.37)$$

A general equation of the classic objective function is given to the PV module/string represented in TDM by considering Eq. 3.37 and the function "*f*" is then given as follows:

$$f(V_L, I_L, x) = I_L^{meas} - I_{phs} - I_{sds1} \cdot \left[exp\left(\frac{q(V_L^{meas} - I_L^{meas} R_{ss})}{n_{s1} kT}\right) - 1\right]$$

$$- I_{sds2} \cdot \left[exp\left(\frac{q(V_L^{meas} - I_L^{meas} R_{ss})}{n_{s2} kT}\right) - 1\right] - I_{sds3} \cdot \left[exp\left(\frac{q(V_L - I_L^{meas} R_{ss})}{n_{s3} kT}\right) - 1\right]$$

$$- \frac{V_L - I_L^{meas} \cdot R_{ss}}{R_{shs}} \quad (3.38)$$

With: $x = (I_{phs}, I_{sds1}, I_{sds2}, I_{sds3}, R_{ss}, R_{shs}, n_{s1}, n_{s2}, n_{s3})$ is the vector of the unknown parameters, and $(I_{phs} = N_p \cdot I_{ph})$; $(I_{sds} = N_p \cdot I_{sd})$; $(R_{ss} = \frac{N_s}{N_p} \cdot R_s)$; $(R_{shs} = \frac{N_s}{N_p} \cdot R_{sh})$; and $(n_{si} = N_s \cdot n_{si}, i = \{1,2,3\})$

For DDM then: $i = \{1,2\}$;

For SDM then: $i = \{1\}$;

For solar PV cell then: $N_s = 1$ and $N_p = 1$.

b) Objective function using Lambert *W* function:

The objective function using the Lambert *W* function is more precise because it expresses the explicit relation between the output measured current and voltage. So, for the PV module/string which is taken as a general case, in Eq.3.36, the function "*f*" is expressed as follows:

$$Ob_{Lambert}(x) = f(V_L, I_L, x) = I_L^{meas} - \left[\frac{R_{shs}(I_{phs} + I_{sds1} + I_{sds2} + I_{sds3}) - V_L^{meas}}{R_{ss} + R_{shs}} - \frac{k.T}{q.R_{ss}}\right] . [n_{s1} W(\varphi_1) + n_{s2} W(\varphi_2) + n_{s3} W(\varphi_3)] \quad (3.39)$$

Where:

$$\varphi_1 = \frac{q I_{sds1} R_{ss} R_{shs}}{n_{s1}.k.T(R_{shs} + R_{ss})} exp\left(\frac{q R_{shs}(I_{phs} R_{ss} + I_{sds1} R_{ss} + V_L^{meas})}{n_{s1}.k.T(R_{shs} + R_{ss})}\right)$$

$$\varphi_2 = \frac{q I_{sds2} R_{ss} R_{shs}}{n_{s2} kT(R_{shs} + R_{ss})} exp\left(\frac{q R_{shs}(I_{phs} R_{ss} + I_{sds2} R_{ss} + V_L^{meas})}{n_{s2} kT(R_{shs} + R_{ss})}\right)$$

$$\varphi_3 = \frac{qI_{sds3}R_{ss}R_{shs}}{n_{s3}kT(R_{shs}+R_{ss})} exp\left(\frac{qR_{shs}\left(I_{phs}R_{ss}+I_{sds3}R_{ss}+V_L^{meas}\right)}{n_{s3}kT(R_{shs}+R_{ss})}\right)$$

With: $x = (I_{phs}, I_{sds1}, I_{sds2}, I_{sds3}, R_{ss}, R_{shs}, n_{s1}, n_{s2}, n_{s3})$ is the vector of the unknown parameters, and $(I_{phs} = N_p \cdot I_{ph})$; $(I_{sds} = N_p \cdot I_{sd})$; $(R_{ss} = \frac{N_s}{N_p} \cdot R_s)$; $(R_{shs} = \frac{N_s}{N_p} \cdot R_{sh})$; and $(n_{si} = N_s \cdot n_{si}, i = \{1,2,3\})$

For DDM then: $i = \{1,2\}$;

For SDM then: $i = \{1\}$;

For solar PV cell then: $N_s = 1$ and $N_p = 1$.

In this thesis, the objective function adopted is the RMSE which takes into account the Lambert *W* function due to its accuracy compared to the classic one.

3.6. Contribution to the PV generator modeling: Proposed methods

During the research work project, three new metaheuristic methods were proposed, denominated respectively, Bat-Artificial Bee Colony Optimizer (BABCO), Nested-Loop Biogeography-Based Optimization-Differential Evolution (NLBBODE), and Differential-Shuffled Complex Evolution (DSCE).

The three methods were designed to solve the problem of PV generator modeling and to overtake the limitations observed in the state-of-the-art optimization algorithms. In addition, the three techniques have been created to more accurately identify the unknown parameters of PV generator models in a short amount of time.

The goal is to use these parameters to create a dependable PV generator emulator and develop an online fault diagnosis application that relies on accurate parameters during normal operation.

In this chapter, the two methods NLBBODE and BABCO will be presented and their related results will thoroughly be discussed, while the third proposed method DSCE will be presented in Chapter 05 where it is used for PV generator fault detection and diagnosis.

3.6.1. Bat Artificial Bee Colony Optimizer (BABCO) [68]

This optimizer is a combination of the “Bat algorithm”, proposed by Yang et al. in 2010, [80] and the “Artificial Bee Colony” proposed by Karaboga. [81]. Evolutionary strategies (crossover and mutation) are used in the design of the BABCO to boost it while searching the optimal solution a long with the search space.

a) Initialization: The BABCO method begins with random initialization of the bats' positions as follows:

$$X_i = X_{min} + \omega.(X_{max} - X_{min}) \quad (3.40)$$

where:

- $\omega \in [0, 1]$ is a random number;
- X_i is the i^{th} bat position;
- X_{min} and X_{max} are the lower and the upper limits of the search space, respectively.

BABCO assesses the fitness of the bats position before ordering them from best to worst.

b) Bats' movement (search strategy): The bats move around the search area by varying the frequency of their ultrasonic pulse as described in the following equation:

$$Freq_i = Freq_{min} + rand.(Freq_{max} - Freq_{min}) \quad (3.41)$$

where $Freq_{max}$ and $Freq_{min}$ are the upper and lower frequency limits of the emitted waves, and "*rand*" is a random number from the space [0, 1].

The new position is then updated as follows:

$$X_i^{new} = X_i + Freq_i.(X_{best} - X_i) \quad (3.42)$$

where X_{best} is the best position closest to the pray so far.

Only when two conditions are fulfilled, the new position is accepted:

- The new position fitness evaluation is better than the current one.
- The loudness A_i is higher than a randomly selected number *rand* $\in [0, 1]$.

The loudness is updated using the following equations respectively:

$$A_i = (A_0 - A_\infty)\left[\frac{it+It_{Max}}{1-It_{Max}}\right] + A_\infty \quad (3.43)$$

where:

- It_{Max} is the maximum number of iterations and *it* is the current iteration.
- A_0, A_∞ are the loudness lower and upper boundaries respectively.

c) Probability evaluation: Inspired from the ABCO algorithm, the probability evaluation is performed using the following equation:

$$Pr_i = \frac{Ob(X_i)}{\sum_i^{NP} Ob(X_i)} \quad (3.44)$$

Where *NP* refers to the number of the bats' swarm, and *Ob* (X_i) is the fitness function that guide the optimization process.

d) Selection process: Two groups of bats, leaders, and scouts, are chosen using the above-mentioned probability. The leaders are the bats with the best echolocation fitness, and the scouts are those with the worst.

So, the group of top-performing bats called "Ψ" is selected based on the selection factor f as follows:

$$X_i^f = \begin{cases} X_{NP-1+i}^f & if\ i \in \delta \\ X_i^f & Othewise \end{cases} \quad (3.45)$$

The maximum number of leaders based on f is represented by δ. An example is if NP = 30 and f = 2, then δ would equal 15. The dimension index is represented by f. The same factor f is utilized in defining the group of the worst bats, denoted as Φ, using the same equation (3.46).

e) Crossover strategy: The crossover strategy will enhance exploration by motivating the worst bats to seek more precise solutions. This involves the leader bats interacting with the worst scout bats to exchange information on how to find better solutions. The process entails randomly selecting four indices (j_1, j_2, j_3, and j_4) $\in$ {*1, 2, …, D*} indices of bats from the group "Ψ" and the same indices from the group Φ, to replace each other respectively.

f) Mutation process: After the crossover operation, the resulting bats undergo a mutation process which occurs as follows:

$$X_i^{new} = X_{best} + \alpha.(X_{r_1} - X_{r_2}) + \beta.(X_{r_3} - X_{r_4}) \quad (3.46)$$

where:

- α and $\beta \in [0, 1]$, are random numbers;
- X_{r_1}, X_{r_2}, X_{r_3}, and X_{r_4} are four individuals randomly selected from the current population, with the condition that they are all different from each other as well as from X_i;

The new position is determined by the interaction of these four bats and will only be accepted if its fitness evaluation is superior to the current location [82].

The pseudocode of proposed BABCO is given in Appendix B.1.

3.6.2. Nested Loop Biogeography-based Optimization-Differential Evolution Optimizer (NLBBODE) [83].

The BBO algorithm uses migration, emigration, and mutation operators to create new solutions. During migration, good solutions share their advantageous information with poor ones, making

BBO effective at exploring within the current population. However, BBO has some disadvantages such as poor exploitation, generation of infeasible solutions, and lack of selection of the best members in each generation [84].

On the other hand, the DE algorithm uses mutation and crossover operators to produce new offspring generations. DE is a simple and efficient method for solving real-world problems effectively, with good exploration of the search space and localization of the global minimum region. However, DE's drawback is that solution exploitation is lacking [85].

To overcome the limitations mentioned earlier, the capabilities of DE and BBO can be combined. Specifically, BBO's exploration can be merged with DE's exploitation.

The resulting hybrid NLBBODE method utilizes BBO's population set, which is subjected to DE's mutation and selection processes. The offspring, also known as the new generation of islands, are then sorted, retaining only the good members according to DE's selection process. The hybrid approach excludes BBO's mutation operator and DE's crossover operator. Instead of the trial vector generated by DE's crossover operator, the donor vector is used. The next step is the selection process, where the decision to keep either the donor vector V_i or the target vector Xi in the next generation is based on their fitness. Lastly, the BBO elitism process is implemented, keeping only the best individuals among the population for the next iteration to prevent corruption due to emigration as stated in the original BBO approach.

a) Initialization: The NLBBODE method starts with random initialization of the individuals. This step is inspired from the original version of the BBO.

b) Immigration and emigration rates assignment: Once the population has been sorted, each individual X_i will be assigned an immigration rate (λ) and an emigration rate (μ), calculated using the following equation:

$$\lambda_i = I\left(1 - \frac{H_i}{NP}\right) \tag{3.47}$$

$$\mu_i = E\left(\frac{H_i}{NP}\right) \tag{3.48}$$

The symbols I and E stand for the highest possible rates of immigration and emigration, respectively. If λ is equal to I, it signifies an island without any species. Meanwhile, when μ is equal to E, it means that the island has the most species. Usually, I and E are both 1. H_i denotes the number of species present in the habitats. The candidate solutions share information by using their λ and μ. The emigration rate μ is utilized to choose which solutions should migrate randomly to the selected solution.

c) Mutation: Instead of the BBO's mutation process, the population are submitted to the DE's mutation operation according to the following equation:

$$V_i = X_{r_1} + F.(X_{best} - X_{r_1}) + F.(X_{r_2} - X_{r_3}) \quad (3.49)$$

where F is the mutation scaling factor and X_{best} is the best solution so far discovered in the current population. r_1, r_2, and r_3 are random indices $\in \{1, 2, ..., NP\}$ that are mutually distinct and also chosen to be different from the running index i.

It is worth noting that the BBO's mutation and DE's crossover operators are both excluded in the hybrid NLBBODE method.

d) Selection: In the next phase of the hybrid method, the selection process determines whether to keep the target vector X_i or the donor vector V_i according to their fitness, according to the following aquation:

$$X_{i+1} = \begin{cases} V_i & if\ Ob(V_i) \leq Ob(X_i) \\ X_i & otherwise \end{cases} \quad (3.50)$$

where $Ob(X_i)$ is the fitness function of the individual X_i.

e) Elitism: Lastly, the BBO elitism process is implemented in the hybrid method, keeping only the best individuals among the population for the next iteration to prevent corruption due to emigration as stated in the original BBO approach. This phase is performed according the following equation:

$$X_h = \begin{cases} X_{NP+i-h} & if\ h \leq Kr \\ X_h & otherwise \end{cases} \quad (3.51)$$

where K_r is the predefined keeping rate, an NP is the number of the population.

The pseudocode of the NLBBODE technique is given in Appendix B.2.

3.6.3. Results of the PV generator modeling using the proposed optimizers

The two proposed methods are used to solve the problem of the parameter identification of multiple PV generator models, namely, the RTC France silicon PV cell, the poly-crystalline Photowatt-PWP201, the mono-crystalline STM6-40/36, the CLS-220P modules, and the CLS-220P string. The data used for the CLS-220P module and string are provided by the power system laboratory of DIEEI at the University of Catania, Italy.

All the above-mentioned PV generator modeling problems are solved by identifying the parameters of their models in the three equivalent electrical based-circuits: SDM, DDM, and TDM.

The experimental I-V characteristic used to extract the parameters of the PV generator models' is obtained under conditions presented in the following table:

Table 3.1 PV generators characteristics and environment working conditions

PV generator	*Number of series cell*	*Incident solar irradiance (W/m^2)*	*PV temperature (Kelvin)*
RTC France solar cell	1	1000	306.15
Poly-crystalline Photowatt PWP-201 module	36	1000	318.15
Mono-crystalline STM6-40/36 module	36	1000	328.15
Mono-facial CLS 220P PV module	60	**Case n° 1:** 810	322.645
		Case n° 2: 661.897	661.897
		Case n° 3: 523.444	315.909
		Case n° 4: 149	313
Mono-facial CLS 220P PV string	180	**Case n° 1:** 952.36	322.86
		Case n° 2: 879.21	323.34
		Case n° 3: 661.9587	319.532
		Case n° 4: 474.0594	317.022

The search range boundaries of the unknown parameters for the five models are given in the following table:

Table 3.2 Search range boundaries of the solar PV generators models

Unknown Parameter	***RTC France solar cell***		***Poly-crystalline Photowatt PWP-201 module***		***Mono-crystalline STM6-40/36 module***		***Mono-facial CLS-220P module/string***	
	Lower limit	Upper limit	Lower limit	Upper limit	Lower limit	Upper limit	Lower limit	Upper limit
I_{ph} *(A)*	0	1	0	2	0	2	0	10
I_{sd} , I_{sd1}, I_{sd2} I_{sd3} *(μA)*	0	1	0	50	0	50	0	1E-04
R_s *(Ω)*	0	0.5	0	2	0	0.36	0	5
R_{sh} *(Ω)*	0	100	0	2000	0	1000	0	5000
n , n_1, n_2 , n_3	1	2	1	50	1	60	1	2

To validate their effectiveness, the proposed methods are compared to the state-of-the-art metaheuristic methods, so far published in literature, as well as to the original versions of fundamental techniques. The references of the competing techniques are reported in the references provided in front of title of each table.

Table 3.3 presents the results obtained by the proposed methods and compares them with some recent model parameter extraction algorithms of the RTC France cell. As can be noticed, the best results are obtained by the two proposed methods, BABCO and NLBBODE, and they are presented in bold font.

The two propose methods reached the best RMSE value of (7.7300062E-04) in SDM, followed by AOE, FC-EPSO, ELPSO, and TVACPSO. For the DDM, the best results are obtained by two propose methods (6.7451339E-04), followed by ELPSO and TVACPSO.

For TDM, as can be seen, the proposed methods outperform the competing techniques, where both of them obtain the best value of the RMSE (6.2853937E-04).

Table 3.3 Results of the proposed methods for R.T.C. France solar cell modeling [72, 83]

Model	Algorithm	I_{ph} (A)	n_1	n_2	n_3	R_s(Ω)	R_{sh}(Ω)	I_{sd1} (μA)	I_{sd2} (μA)	I_{sd3} (μA)	RMSE
SDM	GWOCS	0.76077	1.4808	-	-	0.03639	53.6320	0.32192	-	-	9.8607E-04
	CWOA	0.76077	1.4812	-	-	0,03636	53.7987	0.3239	-	-	9.8602E-04
	MADE	0.76080	1.4812	-	-	0.03640	53.7185	0.32300	-	-	9.8602E-04
	NoCuSa	0.76078	1.48118	-	-	0.03638	53.71853	0.32302	-	-	9.86022E-04
	TLABC	0.76078	1.48118	-	-	0.03638	53.71636	0.32302	-	-	9.86022E-04
	Rcr-IJADE	0.76077	1.481184	-	-	0.03637	53.71852	0.32302	-	-	9.8602E-04
	BBO-M	0.76078	1.47984	-	-	0.03642	53.36227	0.31874	-	-	9.8634E-04
	DE/BBO	0.7605	1.4817	-	-	0.0364	55.2627	0.32477	-	-	9.9922E-04
	BHCS	0.76078	1.48118	-	-	0.03638	53.71852	0.32302	-	-	9.86022E-04
	ABC-DE	0.76077	1.47986	-	-	0.03637	53.7185	0.32302	-	-	9.8602E-04
	LCJAYA	0.7608	1.4819	-	-	0.0364	53.7185	0.3230	-	-	9.8602E-04
	AOE	0.76079	1.4771	-	-	0.03654	52.8891	0.31067	-	-	7.7301E-04
	EPSO	0.76075	1.4627	-	-	0.03718	50.637	0.26887	-	-	8.0621E-04
	FC-EPSO1	0.76079	1.4773	-	-	0.03653	52.944	0.31131	-	-	7.7301E-04
	ELPSO	0.76078	1.47525	-	-	0.03654	52.8893	0.31067	-	-	7.7301E-04
	TVACPSO	0.76078	1.47525	-	-	0.03654	52.8896	0.31068	-	-	7.7301E-04
	BABCO	0.76078	1.47726	-	-	0.03654	52.8897	0.31068	-	-	**7.7300062E-04**
	NLBBODE	0.76078	1.47726	-	-	0.03654	52.8897	0.31068	-	-	**7.7300062E-04**
DDM	NoCuSa	0.76078	1.45141	2.00000	-	0.03674	55.46103	0.22705	0.74019	-	9.82485E-04
	BBO-M	0.76083	2	1.45798	-	0.03664	55.0494	0.59115	0.24523	-	9.8272E-04
	MADE	0.7608	1.9963	1.4505	-	0.03680	55.4329	0.7394	0.2246	-	9.8261E-04
	GWOCS	0.76076	2	1.4588	-	0.03666	54.7331	0.53772	0.24855	-	9.8334E-04
	TLABC	0.76081	1.90750	1.45671	-	0.03667	54.66797	0.42394	0.24011	-	9.84145E-04
	Rcr-IJADE	0.760781	1.451017	2	-	0.03674	55.48544	0.225974	0.749347	-	9.8248E-04
	MPSO	0.76078	1.44978	1.99927	-	0.03674	55.4860	0.22614	0.75097	-	9.8247E-04
	BHCS	0.76078	2	1.45102	-	0.03674	55.48544	0.74935	0.22597	-	9.8248E-04
	DE/BBO	0.76072	1.48429	1.97515	-	0.03627	55.49417	0.33306	0.00517	-	9.89182E-04
	CWOA	0.76077	1.45651	1.9899	-	0.03666	55.2016	0.24150	0.6	-	9.8272E-04
	LCJAYA	0.7608	1.4518	2.0000	-	0.0367	55.4815	0.22596	0.74640	-	9.8250E-04
	AOE	0.76081	1.4111	1.8662	-	0.03723	55.5501	0.89974	0.13523	-	7.6068E-04
	EPSO	0.76076	1.4379	1.9032	-	0.036718	56.806	0.18875	0.78495	-	7.6312E-04
	FC-EPSO1	0.76082	1.3948	1.8450	-	0.037567	54.928	0.10974	0.93626	-	7.4489E-04
	ELPSO	0.76080	1.386091	1.835767	-	0.037551	55.92047	1E-06	0.09916	-	7.4240E-04
	TVACPSO	0.76080	1.327160	1.735315	-	0.03797	56.54960	0.404E-02	0.92746	-	7.4365E-04
	BABCO	0.76119	1.310936	1.844264	-	0.06531	56.52733	1.984E-02	0.99999	-	**6.7451339E-04**
	NLBBODE	0.76119	1.310936	1.844264	-	0.06531	56.52733	1.984E-02	0.99999	-	**6.7451339E-04**
TDM	FC-EPSO1	0.76081	1.3324	1.7035	1.7906	0.037959	56.588	4.2896E-02	0.38552	0.58921	7.4300E- 04
	DE	0.760909	1.433005	4.204524	1.833772	0.038472	69.833667	0.1879183	0.0001	0	6.922665E-04

	Mu-FA	0.760787	1.999952	1.477264	1.476888	0.036546	52.889791	0	0.310684	0	7.730062E-04
	ABC-DE	0.761148	1.263258	1.712923	2.733502	0.060322	70.669069	0.0144989	20.762276	0.055782	5.7289457E-04
	ELBA	0.760804	0.351293	1.466889	1.869366	0.037326	51.825628	3.136E-26	0.279342	2.720E-04	7.514890E-04
	BABCO	0.7613286	1.233561	1.824338	1	0.075343	58.067357	4.927E-03	0.9999999	0.999999	**6.2853937E-04**
	NLBBODE	0.7613286	1.233561	1.824338	1	0.075343	58.067370	4.927E-03	1	0.999999	**6.2853937E-04**

Table 3.4 Results of the proposed methods for the Photowatt-PWP-201 module modeling [68, 83]

Model	*Algorithm*	I_{ph} *(A)*	n_1	n_2	n_3	R_s*(Ω)*	R_{sh}*(Ω)*	I_{sd1} *(μA)*	I_{sd2} *(μA)*	I_{sd3} *(μA)*	*RMSE*
SDM	MLBSA	1.0305	48.6428	-	-	1.2013	981.9823	3.4823	-	-	2.4251E-03
	CPSO	1.031135	47.68264	-	-	1.233794	861.48573	2.730950	-	-	2.0530E-03
	TLBO-ABC	1.0305	48.6432	-	-	1.2013	982.1815	3.4826	-	-	2.4251E-03
	LCJAYA	1.0305	48.6684	-	-	1.2024	981.9828	3.4823	-	-	2.425075E-03
	IJAYA	1.0305	48.6298	-	-	1.3016	977.3752	3.4703	-	-	2.4251E-03
	MADE	1.0305	48.6428	-	-	1.2013	981.9823	3.4823	-	-	2.4250E-03
	FPA	1.032091	48.13128	-	-	1.217583	811.3721	3.047538	-	-	2.7425E-03
	TVACPSO	1.031435	47.55665	-	-	1.235611	821.59514	2.638610	-	-	2.0530E-03
	ISCE	1.0305143	48.642835	-	-	1.201271	981.98228	3.48226304		-	2.425075E-03
	Rcr-IJADE	1.0305	48.6428	-	-	1.2113	981.9822	3.4823	-	-	2.4251E-03
	MPCOA	1.03188	48.50646	-	-	1.20295	849.6927	3.3737	-	-	2.4251E-03
	BABCO	1.0307108	47.49956	-	-	1.241294	745.91763	6.52051	-	-	**2.0465243E-03**
	NLBBODE	1.032382	47.422839	-	-	1.239289	744.712668	2.512893	-	-	**2.0465243E-03**
DDM	CPSO	1.031431	58.675729	47.56070	-	1.235456	822.14431	1E-12	2.641508	-	2.0530E-03
	TVACPSO	1.031434	47.555958	100	-	1.235632	821.65280	2.638124	1E-12	-	2.0530E-03
	BABCO	1.034753	47.821141	42.20106	-	1.999999	591.476886	0.132561	0.312026	-	**1.397480E-03**
	NLBBODE	1.034753	47.821141	42.20106	-	1.999999	591.476886	0.132561	0.312026	-	**1.397480E-03**
TDM	**BABCO**	1.4259914	48.965817	31.10416	42.986906	0.786684	15.6931849	15.695499	46.988542	24.803228	**1.305461E-03**
	NLBBODE	1.0349059	1.1606679	1.298064	1	1.999999	579.699677	0.276234	8.9215E-02	4.276E-08	**1.305461E-03**

Table 3.4 presents the results of the parameter identification of the polycrystalline Photowatt-PWP201 module model. As can be noticed, the two methods obtained the best RMSE value (2.0465243E-03) for the SDM, (1.397480E-03) for the DDM, and (1.305461E-03) for the TDM respectively.

Table 3.5 displays the solution for the parameter identification problem of the monocrystalline STM6-40/36 module model. The two proposed methods indisputably achieved the best RMSE values of (1.721921E-03) for the SDM, (1.6828785E-03) for the DDM, as well as for the TDM.

Table 3.5. Results of the proposed methods for the STM6-40/36 module modeling [68, 83]

Model	*Algorithm*	I_{ph} *(A)*	n_1	n_2	n_3	R_s*(Ω)*	R_{sh}*(Ω)*	I_{sd1} *(μA)*	I_{sd2} *(μA)*	I_{sd3} *(μA)*	*RMSE*
SDM	ILCOA	1.2001	1.2067	-	-	4.9000	9.6991	7.4812	-	-	1.6932E-02
	TLBO	1.66248	1.56749	-	-	0.00312	19.67204	2.63871	-	-	2.0888E-03
	TLBO-ABC	1.66317	1.54354	-	-	0.00363	17.25952	2.14043	-	-	1.8061E-03
	GWOCS	1.6641	1.5207	-	-	0.00424	15.7326	1.7449	-	-	1.7337E-03
	Rcr-IJADE	1.6639	1.5203	-	-	0.0043	15.9283	1.7387	-	-	1.7298E-03
	MADE	1.6639	1.5203	-	-	0.0043	15.9283	1.7387	-	-	1.7298E−03
	EPSO	1.6505	1.4640	-	-	0.019018	31.196	0.73874	-	-	2.6358E-03
	FC-EPSO1	1.6640	1.5328	-	-	0.0029309	15.855	2.0000	-	-	1.7889E-03
	ELPSO	1.666268	50.45864	-	-	0.5	497.7473	0.459614	-	-	2.1803E-03
	SDO	1.6639	1.5203	-	-	0.0043	15.9283	1.7387	-	-	1.7298E-03
	MCSWOA	1.6639	1.5203	-	-	0.0043	15.9294	1.7390	-	-	1.7298E-03
	STBLO	1.7000	1.5000	-	-	0.0050	15.4000	1.4127	-	-	1.9000E-03
	BABCO	1.663903	1.520463	-	-	0.0042677	15.93149	2.048509	-		**1.7219215E-03**
	NLBBODE	1.663903	1.520463	-	-	0.0042677	15.93149	2.048509	-	-	**1.7219215E-03**
DDM	EPSO	1.6644	1.7577	1.4527	-	0.26591	560.55	7.4011	1.4338	-	2.0573E-03
	FC-EPSO1	1.6634	1.5818	1.5445	-	0.011010	597.29	1.8519	0.097148	-	1.7721E-03
	ELPSO	1.664843	41.993481	67.344	-	0.50000	606.88830	6.210924	0.0016701	-	1.8307E-03
	SDO	1.6639	1.5203	54.5816	-	0.0043	15.9372	1.7385	49.9985	-	1.7298E-03
	MCSWOA	1.66390	1.4224	2.1992	-	0.0054	16.9519	0.61030	11.7629	-	1.7061E-03
	BABCO	1.663963	1.3638560	1.917464	-	0.2969723	621.142422	0.24120606	6.5967308	-	**1.6862785E-03**
	NLBBODE	1.664091	1.8337599	1.3113	-	0.0099999	17.348667	5.4156600	0.1055997	-	**1.6828785E-03**
TDM	**BABCO**	1.664079	1.3113561	1.833760	59.99480	0.3599999	624.552036	0.10560005	5.4156739	11.825081	**1.6828785E-03**
	NLBBODE	1.664091	1.3113561	1.833759	1	0.3600000	624.552012	0.10559971	5.4156576	6.4932E-10	**1.6828785E-03**

3.6.4. Analysis of the statistical results

In order to thoroughly assess the performance of the two proposed methods, it is imperative to conduct a statistical test of the results. This test is carried out over 30 independent runs to obtain a comprehensive understanding of the reliability of the methods compared to other optimizers. The outcomes of this test in provided in Table 3.6.

Table 3.6 Statistical results of RMSE obtained by the proposed methods [68, 83]:

PV generator	*Model*	*Algorithm*	*Best*	*Mean*	*Worst*	*StD*	*CPU time (s)*	*NFE*
RTC France solar cell	**SDM**	EPSO	8.0621E-04	-	-	4.3109E-04	13.670	-
		AEO	7.7301E-04	-	-	1.6402E-05	40.5233	-
		ELPSO	7.7301E-04	7.7314E-4	7.7455E-4	3.4508E-07	-	-
		FC-EPSO1	7.7301E-04	-	-	1:5688E-10	11.519	-
		TVACPSO	7.7301E-04	7.7301E-04	7.7301E-04	5.5805E-10	-	-
		BA	2.448688E-02	2.618039E-02	2.007289E-01	5.408680E-02	>300	>200000
		ABCO	2.699086E-03	3.043528E-03	4.403956E-03	6.118694E-04	>300	>200000
		BBO	4.4598531E-02	3.396547E-02	2.654123E-01	6.565482E-02	>300	>200000
		DE	7.730062E-04	7.730062E-04	7.730062E-04	2.323002E-12	12.019	17300
		BABCO	**7.730062E-04**	7.730062E-04	7.730062E-04	**3.268102E-17**	**2.845**	**8800**
		NLBBODE	**7.730062E-04**	7.730062E-04	7.730062E-04	**1.347862E-17**	**2.965**	**12500**
	DDM	AEO	7.6068E-04	-	-	1.4844E-04	**10.413**	-
		EPSO	7.6312E-04	-	-	1.5424E-04	15.485	-

		ELPSO	7.4240E-04	7.5904E-04	7.9208E-04	9.4291E-06	-	-
		FC-EPSO1	7.4489E-04	-	-	**2.1153E-10**	12.036	-
		TVCPSO	7.4365E-04	7.5883E-04	7.8476E-04	1.1044E-05	-	-
		BA	2.505467E-03	1.364431E-02	9.352746E-02	2.511031E-02	>300	>200000
		ABCO	2.276628E-03	4.069399E-03	6.549287E-03	1.462832E-03	>300	>200000
		BBO	4.523497E-03	2.154876E-02	5.4558722E-02	3.589531E-02	>300	>200000
		DE	7.730062E-04	7.738952E-04	8. 4988435E-04	1.309852E-04	65.200	125000
		BABCO	**6.7451340E-04**	7.3992908E-04	7.7288420E-04	**2.759472E-05**	**29.942**	**38090**
		NLBBODE	**6.7451339E-04**	6.7451339E-04	7.7300626E-04	**3.347776E-05**	**45.917**	**49324**
	TDM	EPSO	7.5440E-04	-	-	-2.6967E-04	43.0147	-
		FC-EPSO1	7.4300E-04	-	-	**9.1140E-11**	39.5212	-
		BABCO	**6.2853937E-04**	6.5725960E-04	6.7379416E-04	8.003333E-05	**36.882**	**220000**
		NLBBODE	**6.2853937E-04**	6.8421617E-04	6.7379416E-04	7.754547E-05	**25.456**	**130000**
Photowatt-PWP-201 module	**SDM**	GWOCS	2.4251E−03	2.4261E−03	2.4275E−03	1.196700E-06	-	-
		TLBO	5.212918E-03	7.0276795E-02	8.247839E-01	1.454545E-01	3.7754e-05	-
		LCJAYA	2.425075E-03	2.425075E-03	2.425075E-03	**2.415229E-16**	-	-
		MLBSA	2.425075E-03	2.7425077E-02	4.7853972E-02	1.029790E-01	-	-
		CPSO	2.0530E-03	2.0531E-03	2.0576E-03	8.6188E-07	-	-
		TVACPSO	2.0530E-03	2.0530E-03	2.0537E-03	1.3400E-07	-	-
		BA	9.771899E-03	3.589675E-02	1.718934E-01	4.450036E-02	>300	>200000
		ABCO	8.071293E-03	9.906737E-03	1.296355E-02	1.561538E-03	>300	>200000
		BBO	5.254875E-01	4.552148E-01	2.548745E-01	2,013338E-01	>300	>200000
		DE	2.046524E-03	2.046524E-03	2.046524E-03	1.345602E-06	40.622	125000
		BABCO	2.0465243E-03	2.0465243E-03	2.0465243E-03	**9.434855E-18**	**1.882**	**6080**
		NLBBODE	2.046524E-03	2.046524E-03	2.046524E-03	**1.468211E-17**	**4.992**	**10563**
	DDM	CPSO	2.0530E-03	2.0644E-03	2.1002E-03	1.3423E-05	-	-
		TVACPSO	2.0530E-03	2.0583E-03	2.1125E-03	1.3101E-05	-	-
		BA	9.635465E-03	2.362236E-01	4.404159E-01	1.850432E-01	>300	>200000
		ABCO	1.821143E-02	6.846875E-02	1.604345E-01	5.539901E-02	>300	>200000
		BBO	2.236598E-01	5.362236E-01	7.254699E-01	2.021586E-01	>300	>200000
		DE	2.053475E-03	2.165453E-03	2.252960E-03	2.372752E-03	>300	>200000
		BABCO	**1.3974800E-03**	1.397481E-03	1.397488E-03	**2.907850E-09**	**51.120**	**68180**
		NLBBODE	**1.3974800E-03**	1.397480E-03	1.397480E-03	**4.951744E-06**	**180.252**	**202587**
	TDM	**BABCO**	**1.3054614E-03**	1.6846680E-03	2.0529606E-03	**2.986153E-04**	**60.254**	**150000**
		NLBBODE	**1.3054614E-03**	1.6975487E-03	2.0554871E-03	**1.021547E-04**	**63.332**	**140000**
STM6-40/36 module	**SDM**	GWOCS	1.7337E-03	1.7457E-03	1.7528E-03	1.0447E-05	-	-
		MLBSA	1.7434148E-03	4.2973330E-03	3.32960904E-02	5.677849E-03	-	-
		TLBO	1.7298184E-03	2.9262854E-03	3.3684813E-03	4.952945E-04	-	-
		EPSO	2.6358E-03	-	-	4.7034E-03	4.171	-
		FC-EPSO1	1.7889E-03	-	-	7.3391E-10	**3.944**	-
		ELPSO	2.1803E-03	2.2503E-03	3.7160E-03	2.9211E-04	-	-
		SDO	1.7298E-03	1.7703E-03	1.9500E-03	4.5108E-05	-	-
		BA	4.316935E-02	2.805906E-01	3.589394E-01	1.214878E-01	>300	>200000
		ABCO	5.493811E-02	1.443224E-01	3.088941E-01	7.791709E-02	>300	>200000
		BBO	4.9852681E-02	1.239566E-01	3.182965E-01	8.589255E-02	>300	>200000
		DE	2.0589625E-03	2.258634E-03	1.0502502E-02	4.510825E-04	18.871	84100
		BABCO	**1.7219215E-03**	1.7219215E-03	1.7219215E-03	**1.637363E−17**	**4.978**	**10783**
		NLBBODE	**1.7219215E-03**	1.7219215E-03	1.7219215E-03	**6.191583E-18**	**6.035**	**13459**
	DDM	EPSO	2.0573E-03	-	-	7.4923E-04	6.382	-

		ELPSO	1.8307E-03	2.0351E-03	2.1178E-03	8.4271E-05	-	-
		FC-EPSO1	1.7721E-03	-	-	**3.0719E-10**	**5.998**	-
		SDO	1.7298E − 03	1.8118E-03	2.0288E-03	7.2421E-05	-	-
		BA	3.716638E-02	1.847427E-01	3.536434E-01	1.390727E-01	>300	>200000
		ABCO	3.576209E-02	8.984339E-02	1.825520E-01	5.081732E-02	>300	>200000
		BBO	2.3588528E-01	3.2896153E-01	4.2589612E-01	2.756957E-01	>300	>200000
		DE	2.1856991E-03	2.3975541E-03	2.9137584E-03	8.489536E-04	>300	>200000
		BABCO	**1.6829064E-03**	1.6912799E-03	1.6988491E-03	**3.481031E-06**	50.619	**83890**
		NLBBODE	**1.6828785E-03**	1.6907274E-03	1.7219215E-03	**1.506684E-05**	54.206	**48834**
	TDM	**BABCO**	1.6828784E-03	1.6869796E-03	1.7022926E-03	**6.148503-06**	69.254	**450000**
		NLBBODE	1.6828784E-03	1.6869792E-03	1.7001222E-03	**2.148503-06**	31.657	**140000**

Note that the best and worst values of the RMSE are indicated by *Best* and *Worst*, respectively. *Mean* represents the average of RMSE values, whereas *StD* denotes the standard deviation of the RMSE, which is an accurate reflection of the precision of the identified parameters and the overall reliability of the optimizer.

As can be noticed, it is evident that for the RTC France solar cell model, the two proposed methods have achieved *StD* values of (1~3E-17) for the SDM and (2~3E-05) for the DDM. Although FC-EPSO1 has obtained a StD of (2.1153E-10), its minimum RMSE is significantly higher than the two methods minimum RMSE. The same observation is for the TDM.

The two methods achieved StD values of (9E-18~1E-17) for the SDM and (1E-06~1E-09) for the DDM for the Photowatt-PWP-201 module. While the value of the StD is about 1E-04 for the TDM.

As for the STM6-40/36 module, the two methods yielded the best StD results for the SDM (6E-18~1E-17) and the DDM (3E-06~1E-05). Although the FC-EPSO1 optimizer obtained (3.0719E-10), its minimum RMSE is still higher than the two methods.

The above outcomes clearly demonstrate that the two methods outperform other optimizers in terms of accuracy and reliability.

3.6.5. Results of convergence analysis

3.7. To assess the computational performance of the two proposed methods, further investigation on the convergence rates is made and illustrated in Fig (3.7, 3.8, and 3.9) that show the results of the convergence rate of the NLBBODE optimizer compared to the original versions of the BBO and DE approaches. The three algorithms (BBO, DE, and NLBBODE) were run with the same number of function evaluations (NFE). As can be noticed, NLBBODE got the faster conversion rate compared to the BBO and DE optimizers in all cases of the RTC France PV cell, the Photowatt-PWP-201, and the STM6-40/36 modules

by using SDM, DDM, and TDM. While in Fig (3.10, 3.11, and 3.12), the convergence rate of the BABCO method is evaluated and compared to three other techniques: Differential Evolution (DE), Shuffled Complex Evolution (SCE), and Enhanced Lévy flight bat algorithm (ELBA). It is evident that the two proposed methods convergence speed outperforms the other three approaches in all cases.

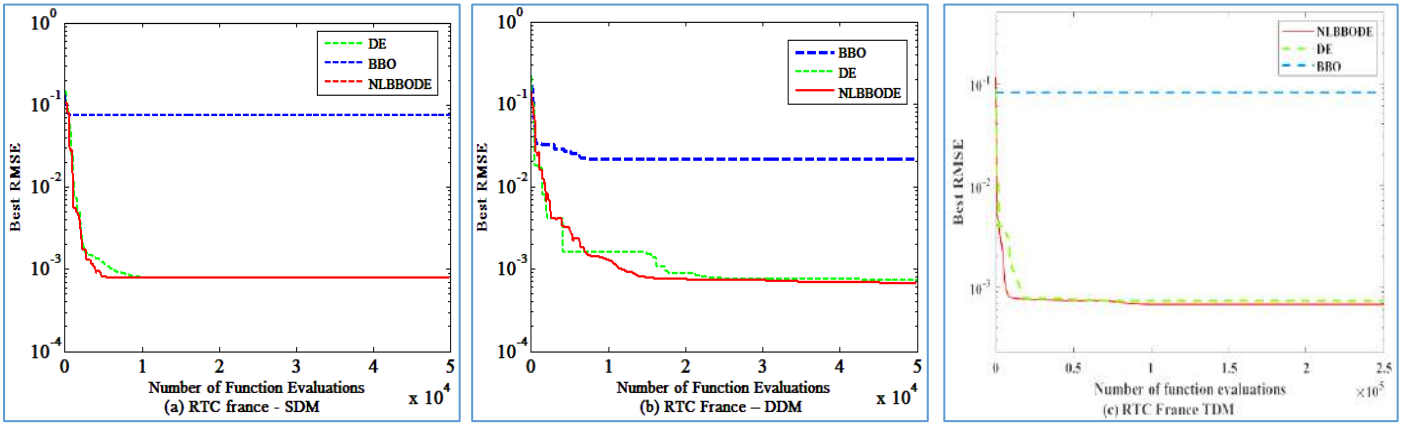

Fig. 3.7. Convergence curves of NLBBODE, BBO, and DE optimizers for the RTC France PV cell model: **(a)** SDM, **(b)** DDM, **(c)** TDM

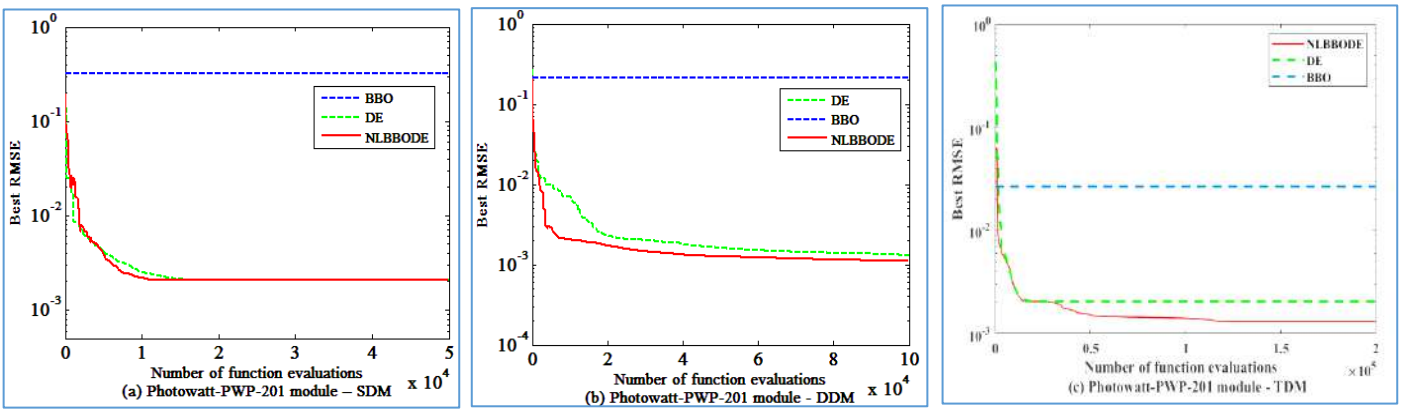

Fig. 3.8. Convergence curves of NLBBODE, BBO, and DE optimizers for Photowatt-PWP-201 module model: **(a)** SDM, **(b)** DDM, and **(c)** TDM

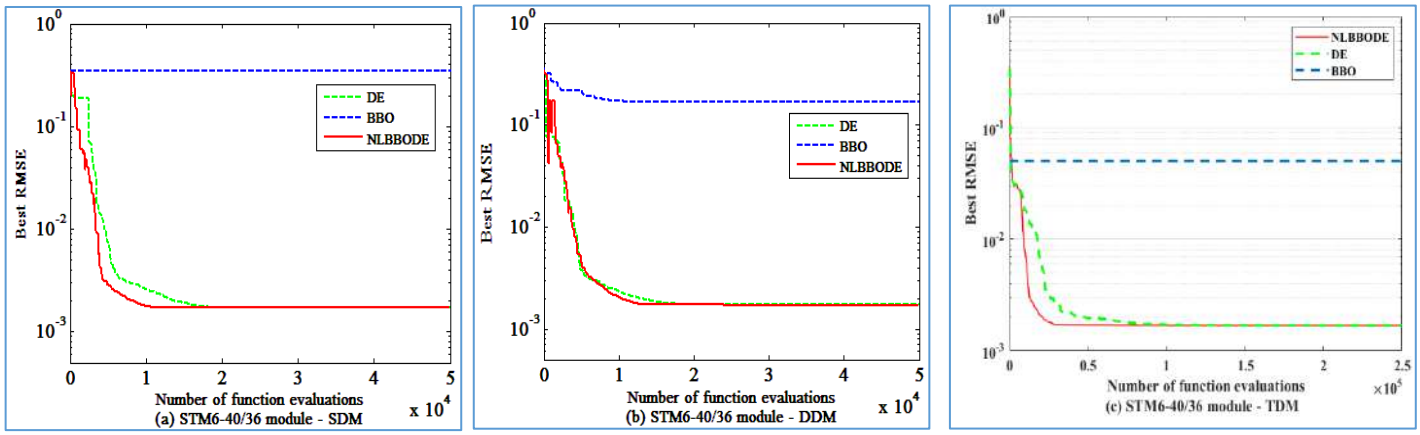

Fig. 3.9 Convergence curves of **NLBBODE**, BBO, and DE optimizers for STM6-40/36 module model: **(a)** SDM, **(b)** DDM, **(c)** TDM

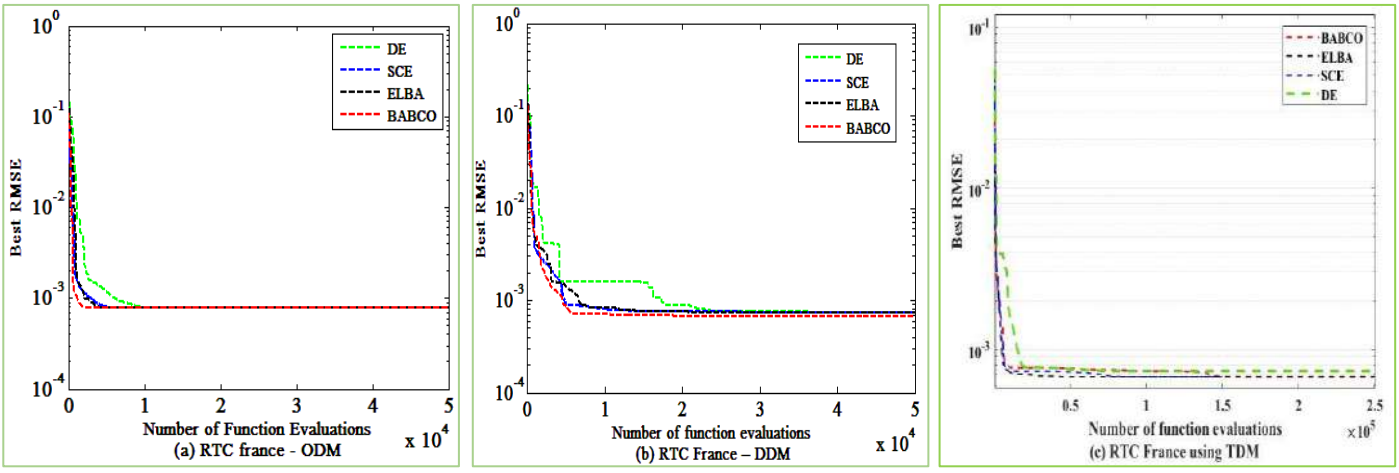

Fig. 3.10 Convergence curves of BABCO and competing optimizers R.T.C. France solar cell:

(a) SDM, **(b)** DDM, **(c)** TDM.

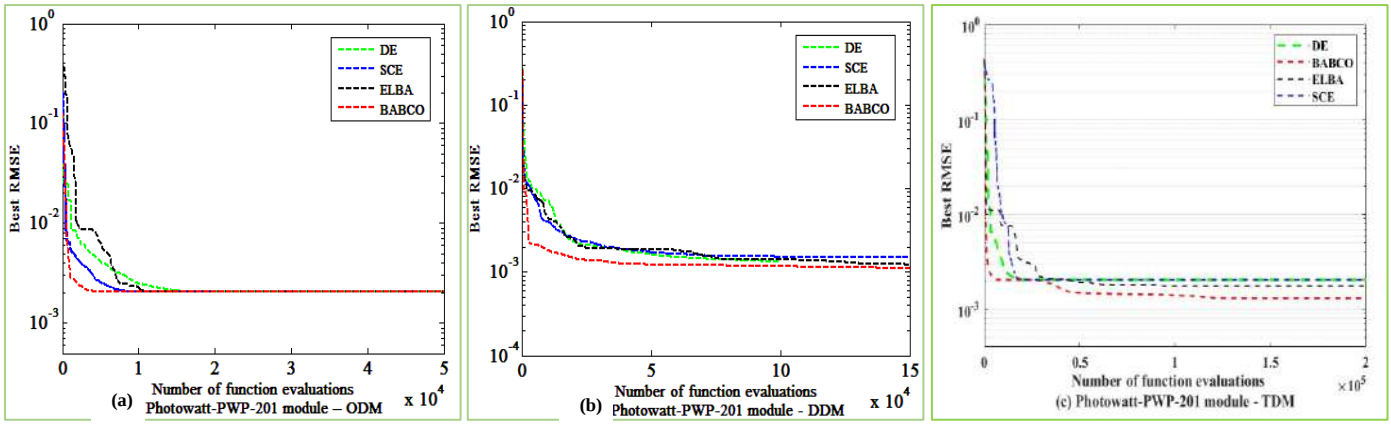

Fig. 3.11 Convergence curves of BABCO and competing optimizers for the Photowatt-PWP-201 module: **(a)** SDM, **(b)** DDM, **(c)** TDM.

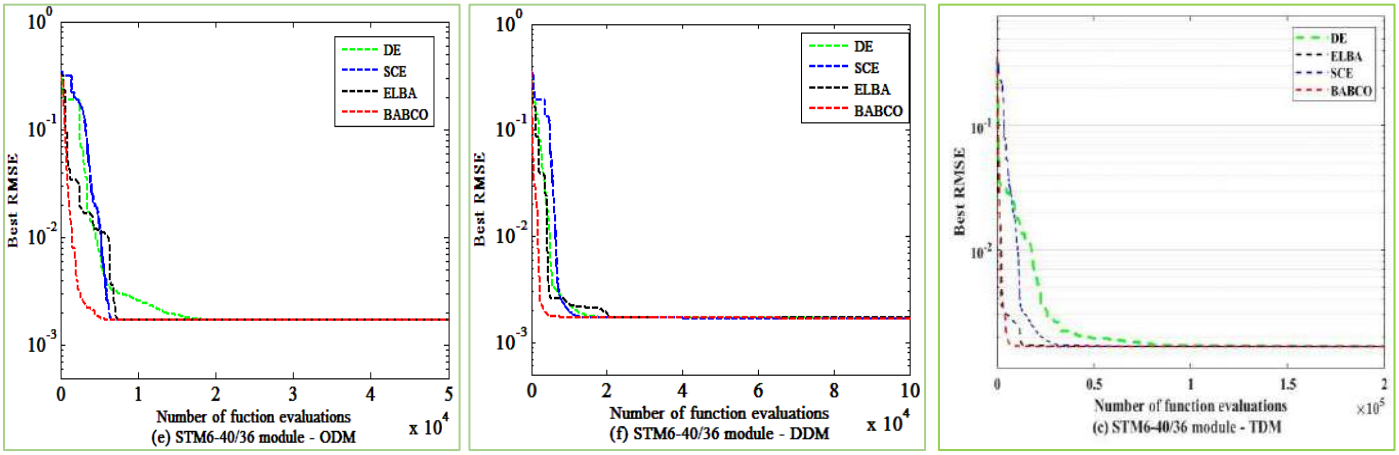

Fig. 3.12 Convergence curves of BABCO and competing optimizers for the STM6-40/36 module: **(a)** SDM, **(b)** DDM, **(c)** TDM.

3.6.6. Validation of the proposed methods using experimental testing

Experimental testing was conducted to validate the effectiveness of NLBBODE and BABCO, on the commercial PV CLS-220P module and CLP-220P string using SDM.

The parameter identification was carried out by measuring I-V experimental data at various levels of irradiance and cells' temperature in the power system laboratory at the DIEEI department of the University of Catania in Italy.

The experimental setup included the PV module/string, the data acquisition board, the control components, and the electronic load. Irradiance was measured using a SPECTRON 210 sensor, and temperature was measured with a sensor type PT100. A program developed in the LabVIEW environment was used to control a DC electronic load to extract the I-V data, spanning the voltage in a specified range with a time step of about 30 seconds.

Using the I-V curves obtained, several tests were carried out to validate the proposed optimizers. The working conditions of temperature and irradiance for the CLP-220P module/string are provided in Table 3.1, and the identified parameters of the CLS-220P module using the BABCO optimizer in four cases are provided in Table 3.7. The I-V curves of the measured data and the estimated data for each case are presented in Fig. 3.13.

The NLBBODE optimizer is used to identify the model parameters of the CLS-220P string in four cases, and the results are provided in Table 3.8. The I-V curves of the measured data and the estimated data are shown in Fig. 3.14.

As can be clearly observed, the optimized values using the NLBBODE and BABCO methods are in thorough agreement with the measured ones, as illustrated in the figures and tables.

Table 3.7 Results of modeling of the CLS-220P module using the BABCO method [68]

Parameter	**Case n° 1**	**Case n° 2**	**Case n° 3**	**Case n° 4**
	G=810 (W/m²) *T=322.645(K)*	*G=661.897(W/m²)* *T=321.470 (K)*	*G=523.444 (W/m²)* *T=315.909 (K)*	*G=149 (W/m²)* *T=313 (K)*
I_{ph} *(A)*	7.737922	6.144189	4.662543	3.363097
n	1.142963	1.149615	1.077737	1.103166
R_s *(Ω)*	0.694400	0.670193	0.714373	0.677725
R_{sh} *(Ω)*	1953.310	5000	5000	672.269132
I_{sd} *(μA)*	0.352886	0.324803	0.046295	0.036799
RMSE	8.145668E-03	6.526124E-03	7.532402E-03	3.015816E-03
Min	8.145668E-03	6.526124E-03	7.532402E-03	3.015816E-03
Mean	8.145668E-03	6.526124E-03	7.532402E-03	3.015816E-03
Max	8.145668E-03	6.526124E-03	7.532402E-03	3.015816E-03
StD	6.608792E-16	2.224589E-16	7.940896E-14	3.919476E-14
CPU time (s)	4.317	5.897	6.25	5.867
NFE	12825	12765	16873	18183

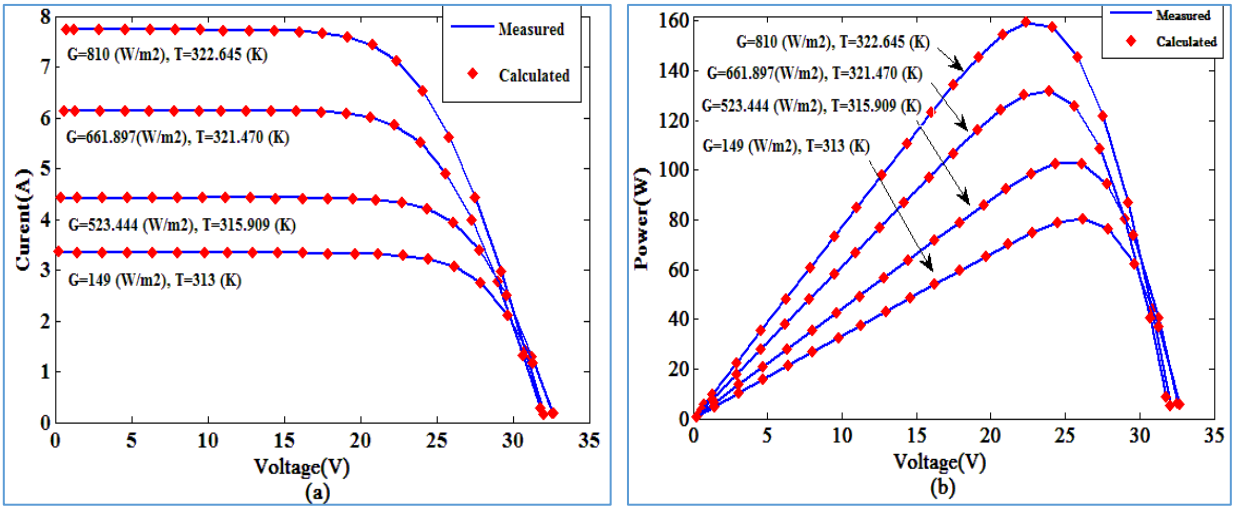

Figure 3.13. Measured and estimated data based on the parameters identified by BABCO on CLS-220P module model: **(a)** I-V characteristic curve, **(b)** P-V characteristic curve.

Table 3.8 Results of modeling of the PV mono CLS-220P string using NLBBODE method [83]

Parameter	***Case* n° *1***	***Case* n° *2***	***Case* n° *3***	***Case* n° *4***
	G=952.36(W/m²) T=322.86 (K)	*G=879.21(W/m²) T=323.34(K)*	*G=661.9587 (W/m²) T=319.532(K)*	*G=474.0594 (W/m²) T=317.022(K)*
I_{ph} (A)	8.5209544	7.917167	5.902533	4.099844
n	1.2884684	1.261452	1.260257	1.299100
R_s (Ω)	1.7168982	1.732561	1.645193	1.572744
R_{sh} (Ω)	575.71839	475.948	989.078	316.656
I_{sd} (μA)	0.0000017	1.2028860	0.689010	0.775763
RMSE	7.167909E-03	8.274260E-03	3.667190E-03	6.168046E-03
Min	7.167909E-03	8.274260E-03	3.667190E-03	6.168046E-03
Mean	7.167909E-03	8.274260E-03	3.667190E-03	6.168046E-03
Max	7.167909E-03	8.274260E-03	3.667190E-03	6.168046E-03
StD	2.05145E-17	5.910058E-17	1.025875E-16	6.584745E-17
CPU time (s)	8.954	8.554	9.658	10.215
NFE	24600	24500	26540	30581

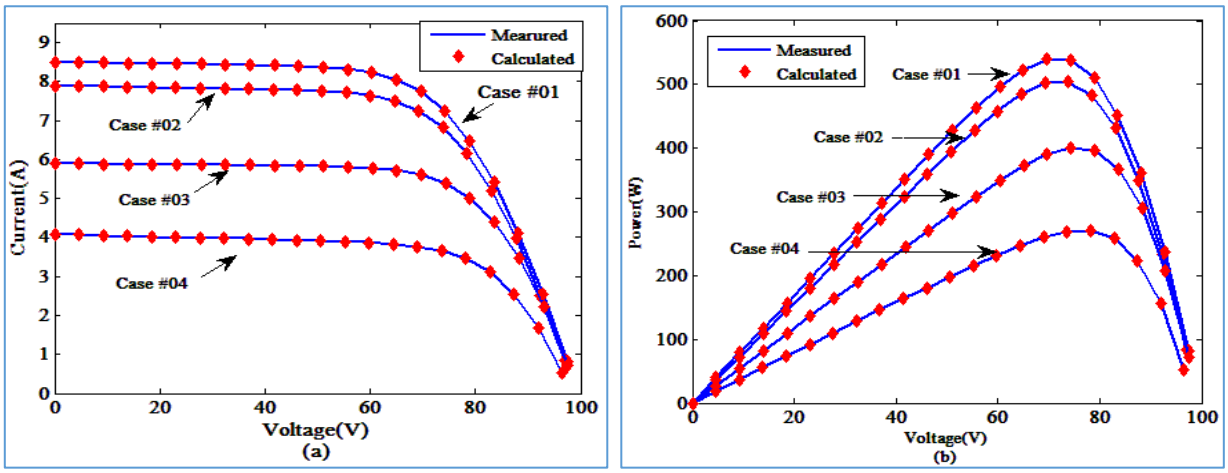

Fig 3.14. Measured and estimated data based on the parameters identified by NLBBODE on the CLS-220P string model: **(a)** I-V characteristic curve, **(b)** P-V characteristic curve.

3.7. Conclusion

In this chapter, the problem of the PV generator modeling was presented, and two methods have been proposed to solve it. These methods are named Bat - Artificial Bee Colony Optimizer (BABCO), and Nested Loop Biogeography-based Optimization - Differential Evolution referred to as (NLBBODE). The two proposed methods have proved their quick and accurate performance in identifying the parameters for different PV generator models.

The two methods have been employed to solve five problems of PV generator modeling, or parameter extraction of PV generator models. The equivalent electrical circuit used in the modeling are the single-diode model (SDM), double-diode model (DDM), and three-diode model (TDM).

The two proposed methods have been evaluated and compared with many cited approaches in the literature. The results and metrics used to compare the performances of the proposed methods are the RMSE values, STD, NFE, and CPU time, where it is clearly demonstrated that they achieve more accuracy, reliability, and quick convergence compared to other approaches.

Thus, the proposed optimizer shows promise in identifying parameters for solar photovoltaic cell and module models, making it a powerful tool for PV generator simulation under normal and abnormal conditions for fault diagnosis purposes based on the I-V curve parameters.

The PV generator modeling (parameter extraction) issues have been addressed using two methods. These two methods utilize equivalent electrical circuits, the single-diode model (SDM), double-diode model (DDM), and three-diode model (TDM).

Extensive evaluation and comparison with various approaches cited in the literature have been conducted to assess the effectiveness of these methods. The metrics used were RMSE values, standard deviation (StD), number of function evaluations (NFE), and CPU run time. The obtained results clearly demonstrate that the proposed methods outperform other approaches in terms of accuracy, reliability, and quick convergence.

It is clear that the proposed methods are very effective means of identifying parameters for models of solar PV generators. In the following chapters, these modeling methods will be applied to simulate PV generators in both normal and abnormal conditions. This will aid in diagnosing faults based on I-V curve parameters.

Chapter 04:

Photovoltaic generator simulator in normal and faulty conditions

4.1. Introduction

In the literature, it has been found that some researchers use the words simulation and modeling interchangeably, but in reality, they are not synonymous [86]. As mentioned in Chapter 02, a model of the PV generator is an informative representation that describes it and illustrates the relations between its inputs and outputs. However, in the context of the present thesis, simulation of the PV generator is the conception of a software tool to imitate the behavior of the real PV generator in different conditions by the use of its model.

Simulation of the PV generator in both healthy and faulty conditions provide numerous advantages that contribute to the advancement and optimization of solar energy systems. This approach allows for a better understanding of system behavior, reduces troubleshooting costs and production interruption, and aids in decision-making and management [31, 87].

To ensure that a PV generator functions accurately, it is important to verify its performance by simulating healthy operating conditions and comparing predicted results to real-world measurements. This process confirms that the model effectively captures the expected behavior of the system. Moreover, engineers and designers can use simulations of optimal performance to adjust component specifications, layout configurations, and energy management strategies. This iterative process results in more efficient and productive PV systems.

On the other hand, identifying potential issues and malfunctions within a PV system can be done by simulating faulty conditions [31]. This analysis helps operators and maintenance teams quickly diagnose problems and take corrective actions. By understanding how the PV system behaves under faulty conditions, proactive maintenance plans and strategies can be developed to reduce downtime, prevent system failures, and minimize the risk of costly repairs. Assessing the impact of various faults on energy production and system efficiency aids in prioritizing maintenance efforts. Evaluating how individual components respond to faults provides insights into their resilience and performance during adverse conditions, which guides component selection and contributes to the overall system's reliability. Simulating faulty conditions helps ensure that the PV system complies with safety regulations and standards, as well as grid codes, which is crucial for maintaining system integrity and avoiding penalties.

By integrating both healthy and faulty condition simulations, stakeholders can make informed decisions that optimize energy production, enhance system reliability, and improve financial outcomes. This approach to simulating both scenarios provide a complete picture of the system's capabilities and limitations, enabling continuous improvement and innovation in the field of

solar energy. Incorporating the benefits of simulating PV generators in both healthy and faulty conditions into the broader context of photovoltaic technology drives progress toward more efficient, reliable, and sustainable energy solutions.

Nevertheless, identifying performance discrepancies in a PV system can be challenging, as some malfunctions may go unnoticed for extended periods [31]. Therefore, it is crucial to establish a proactive monitoring mechanism to detect any anomalies early. By closely observing the system's patterns, fluctuations, and responses to changing environmental conditions, valuable insights can be gained to identify potential issues and facilitate timely maintenance and intervention [87].

The PV generator, which is the most important element of the PV system, is an outdoor component that can be affected by various internal and external factors and anomalies, potentially leading to decreased efficiency or complete system failure. Detecting and diagnosing these issues early is essential to ensure consistent and optimal functioning [21].

In the field of modeling, simulating, and analyzing PV systems, there are several software packages available, such as Solar Pro, PV-Design Pro, PV-Spice, and PV CAD. However, these packages have some drawbacks such as their high cost, limited commercial availability, difficulty interfacing with electronic power systems, and proprietary nature [88]. Thus, the MATLAB/Simulink tool is a good alternative to overcome the aforementioned limitations. Since it can help improve comprehension and simulation of I-V characteristics and P-V power output for standalone PV systems, fulfilling desired essential features [89].

4.2. Description of the physical PV generator and the experimental setup

The PV generator that needs to be simulated comprises a PV string consisting of three polycrystalline (C-Si) modules of the CLS-220P type. Each module has three sub-strings, with each sub-string having 20 series cells and a bypass diode. Overall, each module contains 60 cells, making a total of 180 cells in the PV string.

The entire experimental setup utilized for conducting experiments and performing measurements is situated in the Power System Laboratory at the DIEEI Department of the University of Catania in Italy. In addition to the PV string, the setup also incorporates the data acquisition board, control components, and electronic load. The SPECTRON210 sensor measures irradiance while the PT100 sensor measures temperature. A program developed under the LabVIEW environment is employed to extract I-V, which controls a DC electronic load to span the voltage within a specified range with a time step of about 30 seconds.

The entire setup is depicted in Fig. 4.1.

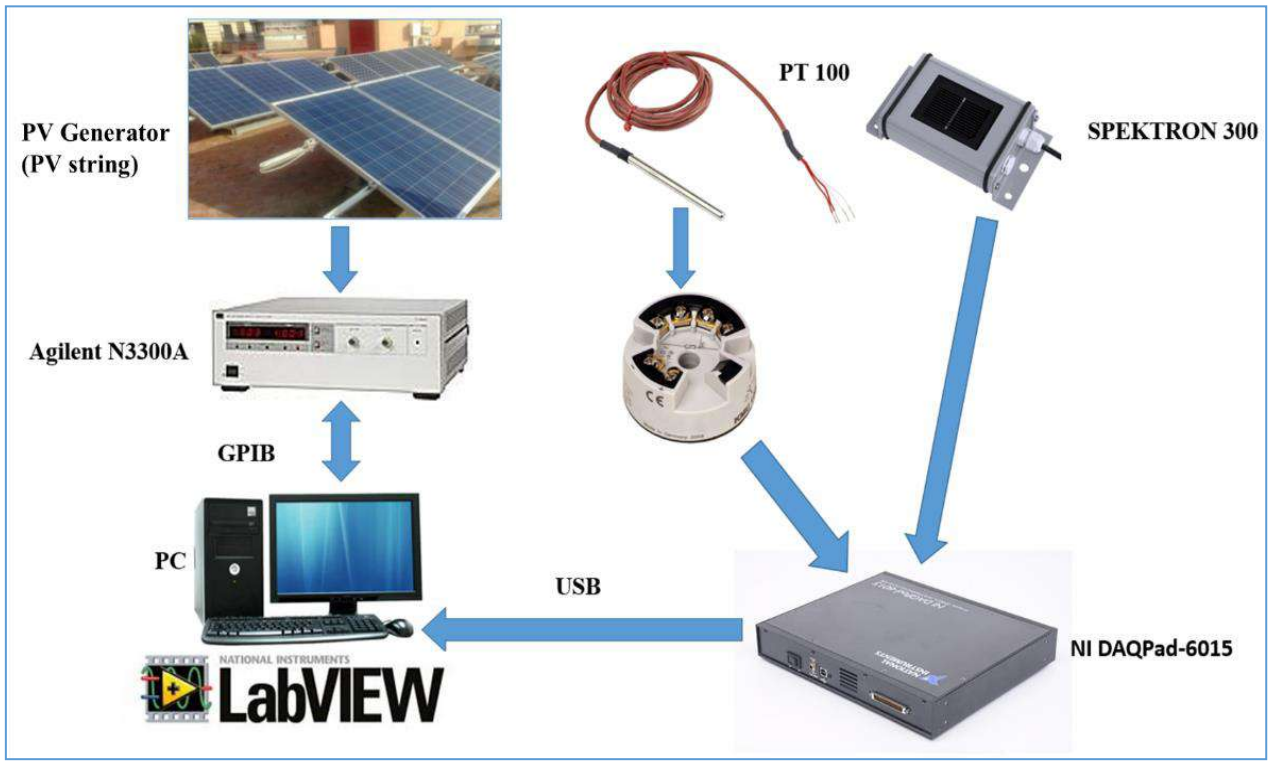

Fig. 4.1 Experimental setup of the PV generator and accessories.

4.3. MATLAB/Simulink simulator of the PV generators

The Matlab/Simulink simulator for PV generators can be a solution for exploring, analyzing, and simulating PV systems. This simulation platform offers a unique blend of versatility and safety, empowering researchers and engineers to conduct operations and experiments that surpass the limitations of physical laboratories, all while avoiding potential damage to sensitive hardware.

Traditional research methods for photovoltaic (PV) systems rely heavily on physical experimentation in laboratory settings. While these setups provide valuable insights, they are limited by practical constraints that can restrict the scope of experimentation. For example, certain operations like intentionally inducing faults, such as short-circuiting modules or strings, can be risky and lead to irreversible damage to expensive components. Additionally, replicating various environmental conditions accurately can be difficult, which can hinder the accuracy of results obtained from physical experimentation.

This simulator leverages computational modeling and simulation to create a virtual representation of the PV generator, allowing for unprecedented experimentation without the associated risks.

4.4. Simulator design procedure

During the design process of the PV generator simulator, the chosen equivalent electrical circuit model to be simulated is the SDM due to its simplicity and rapidity.

The output current is calculated using the Lambert W function formula, which provides high accuracy. Although the DDM and TDM equivalent circuit models are more precise, their difference is barely noticeable except at low levels of irradiance, typically below G = 150 W/m². Additionally, the SDM is valuable due to its faster execution time compared to DDM and TDM, as presented in Chapter 02. This faster response time is especially valuable when simulating fault scenarios that require quick detection procedures [72].

Fig. 4.2 illustrates the equivalent electrical circuit of the PV generator (PV string) and its related parameters. The output current is formulated as follows:

$$I_{out} = I_{ph} - I_d.\left[exp\left(\frac{V_{out}+R_S.I_{out}N_S}{n.V_{th}}\right) - 1\right] - \left(\frac{V_{out}+R_S.I_{out}N_S}{R_{sh}.N_S}\right) \quad (4.1)$$

where, N_s is number of series PV cells that forming the module/string (All cells are connected in series, i.e., N_p = 1). V_{th} is the thermal voltage expressed as follows:

$$V_{th} = T.N_s.k/q \quad (4.2)$$

- T is the cell's temperature in Kelvin;
- q = 1.60217646 ×10^{-19} C is the electron charge;
- k = 1.380653×10^{-23} J/K is the Boltzmann's constant and

As demonstrated in Chapter 02, this PV string model has five unknown parameters:

- I_{ph}: The photo-generated current.
- I_d: The reverse-bias saturation current
- R_s: The series resistor that represents current leakage to the ground
- R_{sh}: The shunt resistor that represents internal loss caused by
- n: The ideality factor.

The PV string simulator uses Eq. 4.1 and the identified PV string parameters to generate the I-V and P-V characteristics at the given conditions of irradiance and temperature. The identification process of the five parameters is already discussed in Chapter 02, where two metaheuristic techniques were proposed and validated as reliable approaches.

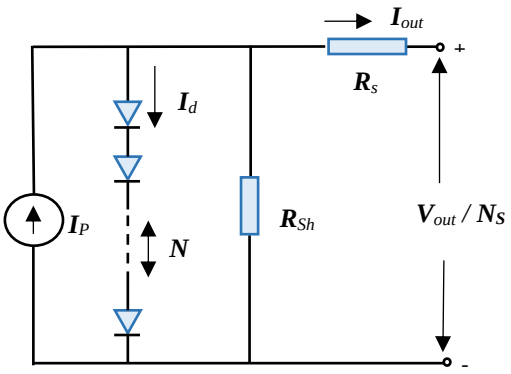

Fig. 4.2. SDM of PV module/string.

To validate the PV generator (PV sub-string/module/string) simulator, it is essential to ensure that certain requirements are met:

- Firstly, the simulator should be able to provide the I-V and P-V characteristics that are in acceptable agreement with the physical PV generator under healthy conditions.
- Secondly, the simulator should be able to provide the I-V and P-V characteristics that are in acceptable agreement with the physical PV generator under faulty circumstances, such as partial shading, open circuits, and so on.

To achieve this, many tests of actual measurements should be conducted and compared to the outputs of the simulator in the same healthy and faulty conditions. The success of the simulator in these tests means that it is able to accurately and reliably predict the real PV generator performance at the studied conditions.

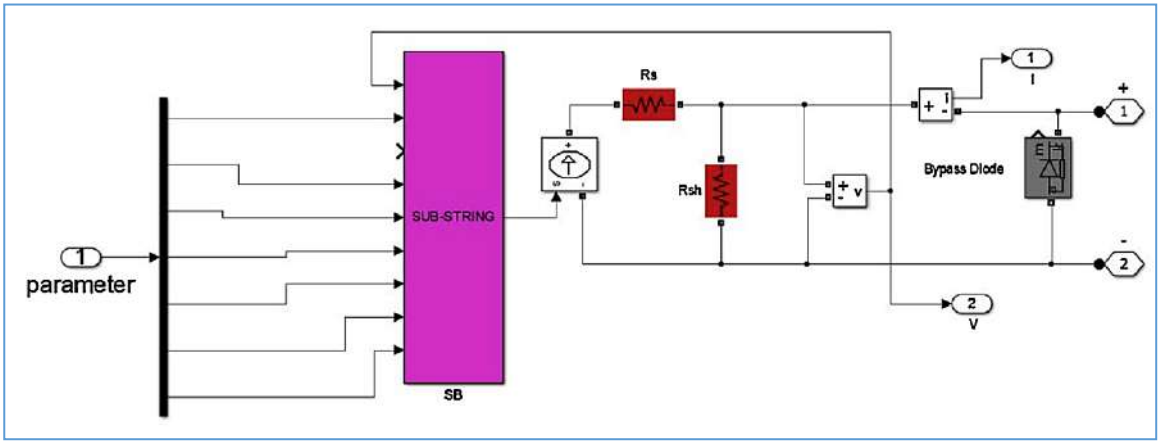

Fig. 4.3. Matlab-Simulink emulator of one PV sub-string.

Fig 4.3 depicts the Matlab/Simulink simulator or emulator of a single PV sub-string, which serves as the fundamental model of the proposed PV simulator. Each PV module comprises three substrings, with each substring being bypassed by a bypass diode. In case of partial shading of a

substring, the corresponding bypass diode is activated to bypass only that particular substring, thereby preventing the entire module from deactivating.

Fig 4.4 illustrates the entire PV string simulator formed by three modules (pointed in dashed red lines) and nine substrings. To model the defects of the connection cables, resistors have been introduced among the substrings.

It is worth noting that the simulation model is primarily based on the difference between the measured and estimated absolute errors (AE) values of current short circuit (I_{sc}) and voltage open circuit (V_{oc}).

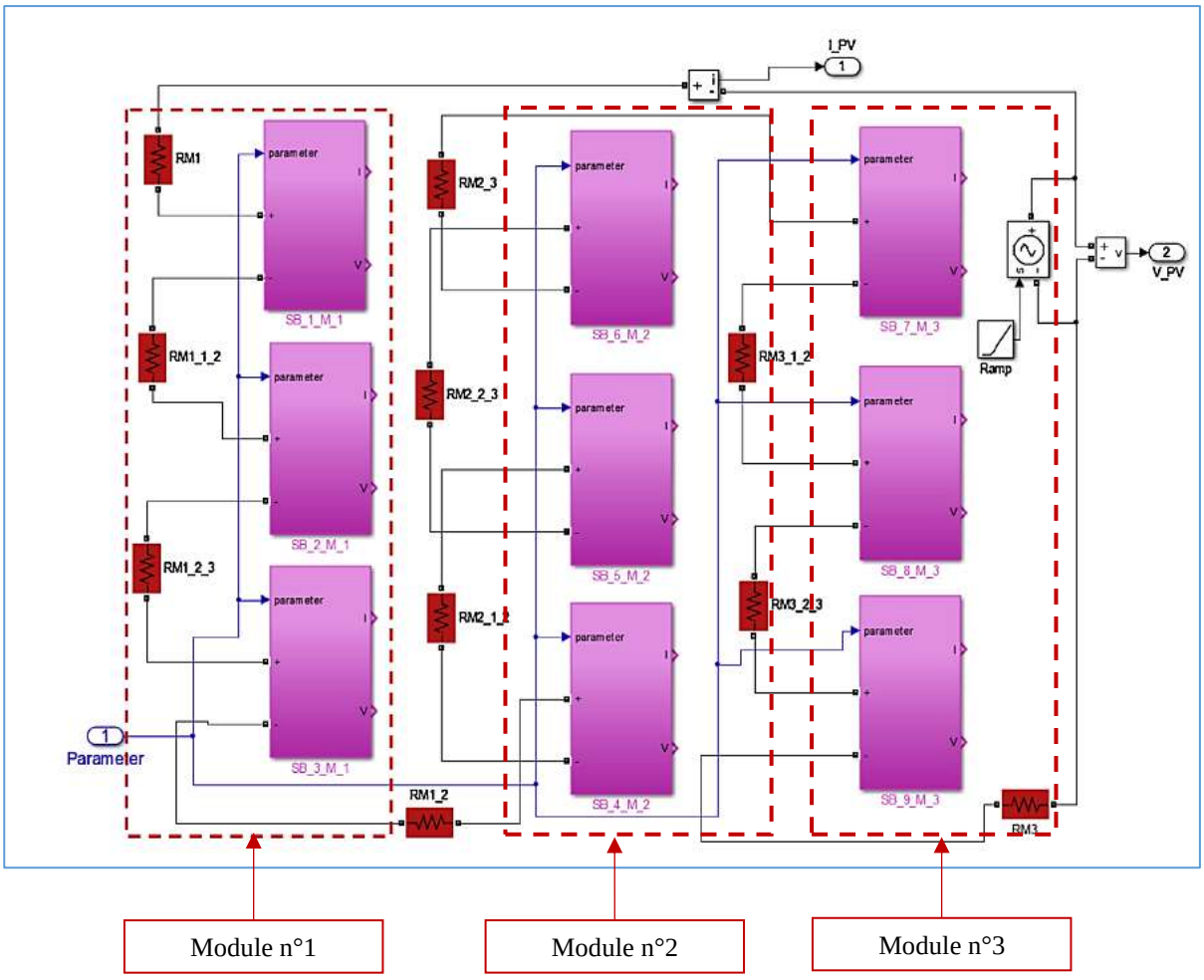

Fig. 4.4. Matlab-Simulink emulator of the entire PV string.

In addition, the proposed PV string simulation procedure refers to the lookup table, previously established as database reference. This lookup table containing 1080 reference rows containing parameters extracted from measured I-V curves at normal operating conditions. The algorithm developed to run along with the Simulink simulator will select the closest values of irradiance

and temperature from the lookup table based on the measured values of these two input parameters.

Table 4.1 presents some samples taken from the lookup table comprising the estimated parameters among 1080 others representing I-V curves at varying operating conditions [72].

The appropriate five parameters for each PV sub-string can be chosen from the lookup table. The threshold up which the minimum absolute error (AE) should not exceed for each PV sub-string is 0.4% for the I_{sc}, and 0.8% for V_{oc}. The AE should be reduced under normal operating conditions if it exceeds these thresholds.

Table 4.1 Lookup table for CLS 220P PV string (extracted from 1080 I-V curves at varying operating conditions).

$G\ (W/m^2)$	$T\ (K)$	$I_{ph}\ (A)$	n	$R_s\ (\Omega)$	$R_{sh}\ (\Omega)$	$I_{sat}\ (\mu A)$	*RMSE*	*StD*	*CPU Time (s)*
965.79	322	8.57450	1.29660	1.71487	1432.04	1.59660	9.85950 E-03	1.28392 E-16	1.95
961.82	322	8.62869	1.29763	1.70157	473.850	1.65817	1.20136 E-02	2.30198 E-16	2.16
957.18	323.11	8.59383	1.30824	1.67325	540.952	2.13568	1.46038 E-02	3.38129 E-16	2.27
952.36	322.86	8.52321	1.28486	1.72408	563.339	1.60657	1.16416 E-02	1.94389 E-16	2.31
947.55	322.85	8.49591	1.23891	1.75031	435.658	0.86026	1.53370 E-02	3.93817 E-16	2.17
945.36	323.40	8.47621	1.27494	1.73312	514.607	1.49849	1.37685 E-02	1.23892 E-16	1.89
918.72	324.24	8.26700	1.25735	1.78024	432.375	1.29248	1.07025 E-02	2.91823 E-16	1.96
908.02	323.77	8.16386	1.26451	1.73666	466.347	1.38424	1.32812 E-02	188392 E -16	2.44
889.50	323.22	8.00628	1.25376	1.74777	485.215	1.12742	1.17525 E-02	2.03918 E-16	2.18
879.21	323.34	7.91596	1.26495	1.73102	484.240	1.27120	1.18125 E-02	3.82732 E-16	2.02
867.72	323.49	7.81825	1.25182	1.74996	503.644	1.10307	1.25386 E-02	3.21738 E-16	1.98
863.83	322.01	7.70197	1.21604	1.77036	809.801	0.53142	1.09742 E-02	3.28482 E-16	2.49
855.52	323.28	7.73169	1.24673	1.75290	426.043	1.00572	1.01612 E-02	4.23487 E-16	2.35
849.63	324.34	7.60754	1.25861	1.71773	880.283	1.31916	1.07828 E-02	4.73772 E-16	2.16
848.74	325.16	7.60593	1.25256	1.72972	832.559	1.31595	1.07453 E-02	2.38242 E-16	2.22
848.54	324.39	7.59851	1.26478	1.71481	852.023	1.38953	8.77790 E-03	3.27482 E-16	2.37
. . .	. . .	. . .	. . .	. . .	. . .	. . .	. . .	. . .	. . .
210.77	307.20	1.34092	1.20806	1.7238	1216.78	1.6235	1.15919 E-03	9.03840 E-17	1.22
206.29	307.05	1.29188	1.21181	1.7129	1341.56	1.2176	1.05159 E-03	1.38849 E-16	1.42
203.81	308.27	1.29157	1.21005	1.7324	769.850	1.2246	8.94160 E-04	1.29372 E-16	2.45
202.60	306.95	1.25145	1.21759	1.7109	1456.27	0.7769	1.11370 E-03	3.48293 E-16	1.84
199.02	306.68	1.21685	1.22551	1.7783	1396.48	1.1656	1.26751 E-03	4.53849 E-16	1.92
194.90	306.53	1.17713	1.21998	1.7238	1292.79	1.3465	1.29752 E-03	7.32840 E-17	2.06
194.36	306.10	1.25490	1.24226	1.7827	580.424	1.3419	3.14148 E-03	8.02300 E-17	2.43
190.43	306.47	1.13146	1.20696	1.7928	1227.91	0.9283	1.41636 E-03	1.34399 E-16	2.23
186.49	306.25	1.08719	1.19490	1.7028	1309.50	1.2324	1.46564 E-03	3.88272 E-16	2.03
180.60	301.23	1.06255	1.20894	1.7031	1149.37	1.4337	7.64540 E-04	2.39883 E-16	1.81

Although the V_{oc} of one PV sub-string is nine (09) times that of a single PV string, the I_{sc} is the same as the sub-strings are connected in series. A more detailed model description can be found in [40].

Outdoor I-V curve measurements can be disrupted by factors such as transient shadings or clouds. Hence, the above-mentioned 1080 data needs to be cleaned from corrupted data to ensure accuracy during the tests. This process involves considering only those curves which have a

descending shape. Any curve that does not meet this criterion is deemed corrupted and discarded. As a result of this filtering process, only 690 I-V curves with negative current gradients have been considered valid and stored for future use as illustrated in Fig 4.5. The following condition was applied to the 1080 IV curves to get validity:

$$\frac{\partial I}{\partial V} < 0 \qquad (4.3)$$

Therefore, 690 irradiance and temperature values of valid curves are considered for the PV string test.

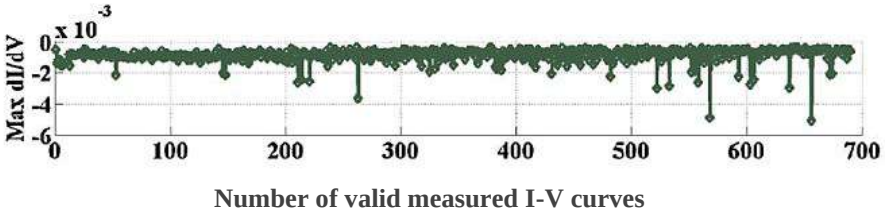

Fig. 4.5. Set of the I-V curves satisfying negative gradient condition.

To ensure the accuracy and reliability of the PV simulator, a simulation of all 690 I-V curves is performed by incorporating the five parameters mentioned in Eq. 4.1. This was done to produce simulated I-V curves that cover various irradiance and temperature conditions. The ultimate aim was to confirm that the absolute error (AE) between the simulated and measured curves is negligible. Fig 4.6 illustrates the absolute errors (AE) between measured and simulated values of the key electrical parameters of the PV string which are the short-circuit current I_{sc}, current at the maximum power point I_{mpp}, voltage at the maximum power point V_{mpp}, and the maximum power point P_{mpp}.

As can be noticed, the AE of the short-circuit current I_{sc} is below 0.06 (A), the AE of the current at the maximum power point I_{mpp} is below 0.08 (A), the AE of the voltage at the maximum power point V_{mpp}, is less than 0.9 (V), and the AE of the maximum power point P_{mpp} is less than 0.7 (W).

4.5. PV Simulator outputs in healthy conditions

For the validation of the PV string simulator, seven (07) cases of healthy conditions were tested under various irradiance and temperature conditions. The values of these conditions are provided in Table 4.2.

These conditions were chosen to cover a range of irradiance levels, from high to medium to relatively low values.

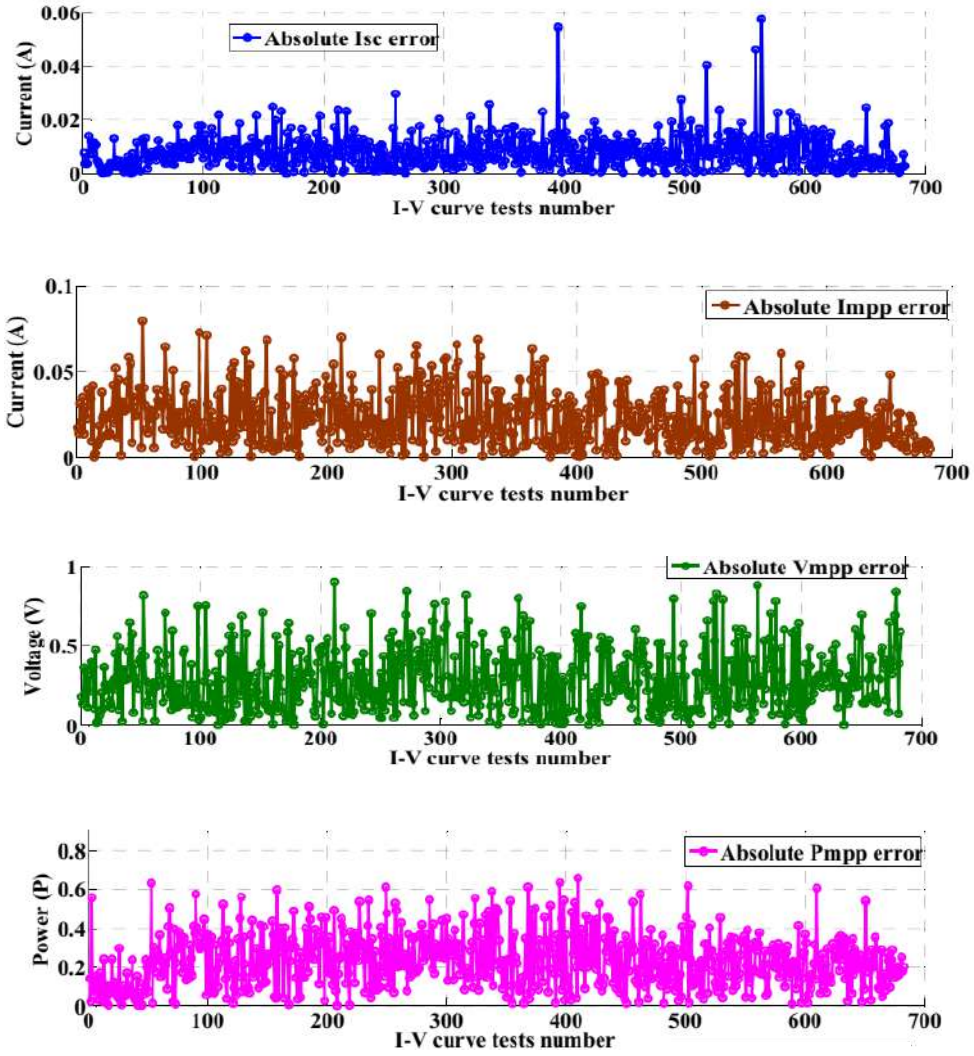

Fig. 4.6. AE between measured and simulated values of key electrical parameters of the PV string.

Table 4.2. PV string in healthy working conditions

Case number	*Solar incident irradiance (W/m^2)*	*PV temperature (Kelvin)*
01	965.7909	322.0030
02	826.5600	323.340
03	748.4342	321.0250
04	618.2313	314.0200
05	508.4862	317.1500
06	296.7585	314.7560
07	180.6090	301.2390

The simulation test results of the PV string simulator are compared to real measured data as illustrated in Fig. 4.7. The figure shows (a) the I-V characteristic curves, and (b) the P-V characteristic curves.

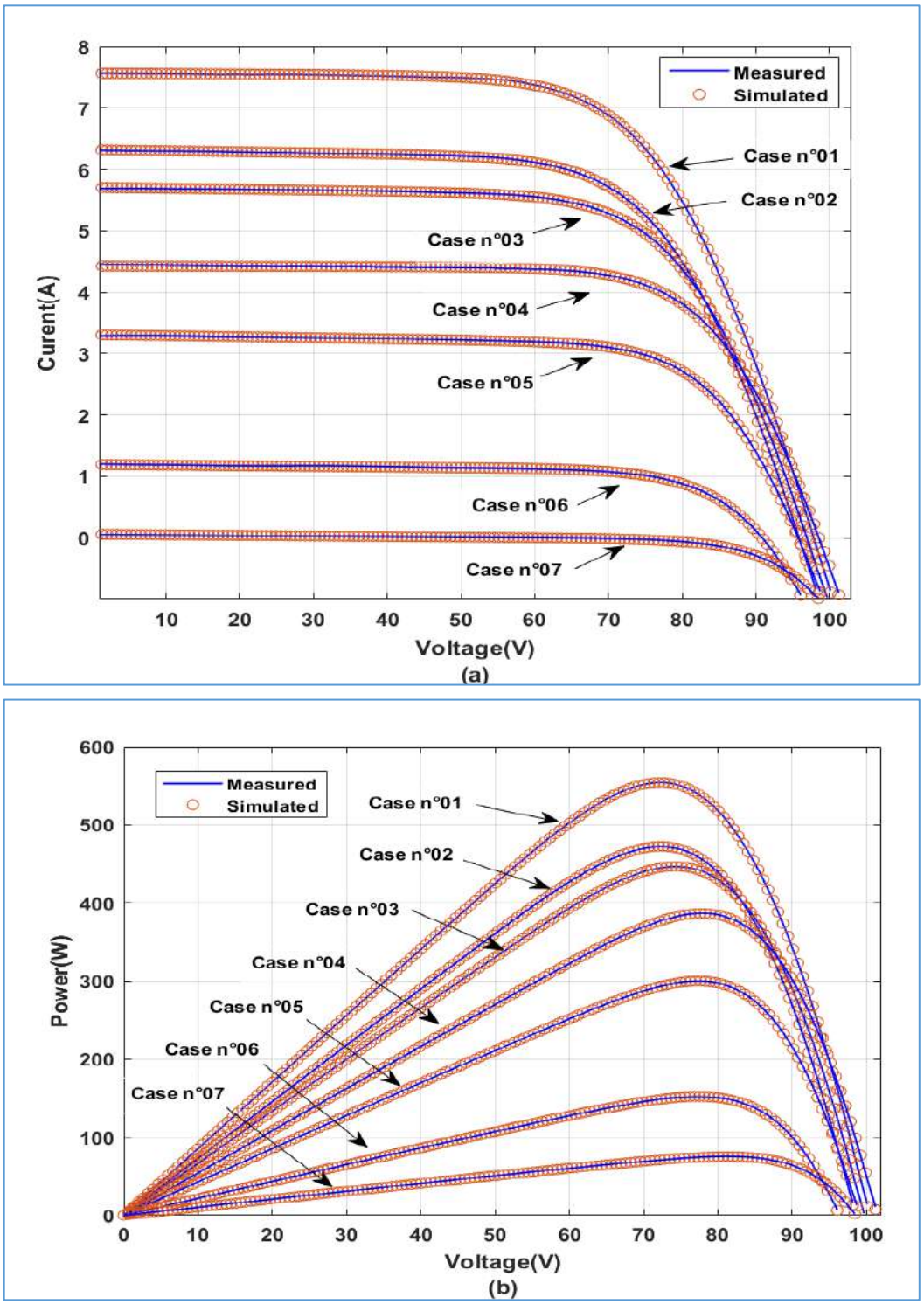

Fig 4.7. PV string simulator results compared to real measured data: (a) I-V curves, (b) P-V curves

As can be seen, the simulated data corresponds perfectly to the measured ones. This proves that variations in irradiance and temperature values do not affect the accuracy of the adopted SDM in the simulation design process and the performance of the proposed PV simulator.

4.6. PV Simulator outputs in faulty conditions

Once the PV string has been tested and proven to be functional under normal working conditions, it is important to perform additional tests that simulate faulty scenarios. Comparing the results of the PV string simulator with real-life faulty situations gives a better understanding of its accuracy and reliability in replicating those scenarios.

Nonetheless, it can be challenging to conduct a thorough experimental study by provoking real faults in the PV generator. This is due to a variety of factors that can adversely affect the results.

For example, performing artificial shading tests on a PV module can cause significant temperatures to rise in the shaded portions, resulting in cell burnout. It is therefore crucial to avoid obtaining incorrect measurement data or destroying the PV cells. Short-circuit real test is another example of faults to avoid performing on a PV generator without taking special precautions.

Therefore, a limited number of real faulty conditions can be considered for comparison with simulated ones, due to the above-mentioned constraints and for safety concerns.

4.6.1. Partial shading scenarios

Partial shading is one of the most common faulty conditions on solar PV generators that has been extensively studied by researchers in the last few years. Furthermore, multiple partial shading scenarios have been diagnosed using different methods in the literature where a variety of hardware and software solutions have been proposed [90].

Maximum power point tracking (MPPT) algorithms are among the most popular proposed techniques [91, 92, 93], which are developed to maximize the efficiency of PV generators. The reason for this is that partially shaded PV generators exhibit multiple local power points on their power-voltage (P-V) characteristics.

To validate the ability of the PV string emulator in simulation partial shading scenarios, five (05) cases of partial shad conditions were tested under various irradiance and temperature conditions as described in Table 4.3.

As shown in Table 4.3 and Fig 4.8, scenario n°01 can be achieved by obstructing a single cell in each module, causing its complete shading. This occurs when the irradiance is at G = 839.5390 W/m^2 and the temperature is T = 324.142 K.

Table 4.3. Partial shading scenarios

Scenario number	*Solar incident irradiance (W/m^2)*	*PV temperature (Kelvin)*	*Description of the shading scenarios*
01	839.5390	324.142	One cell of each module is shaded
02	781.1890	321.3120	Vertical half of module n°2 is shaded (30 cells are shaded)
03	621.3710	314.3180	Vertical half of module n°3 is shaded (30 cells are shaded) and a partial portion of module n°2 is shaded
04	501.7000	312.0340	Horizontal row of cells of module n°1 and module n°2 is shaded.
05	400.3190	312.6170	Small rows are causing random shading on module n°1 and module n°2

On the other hand, scenario n°2 is realized by shading 30 cells on the vertical half of the second module as illustrated in Fig 4.9. This occurs when the solar irradiance is G = 781.1890 W/m2 and the temperature is T = 321.312 K.

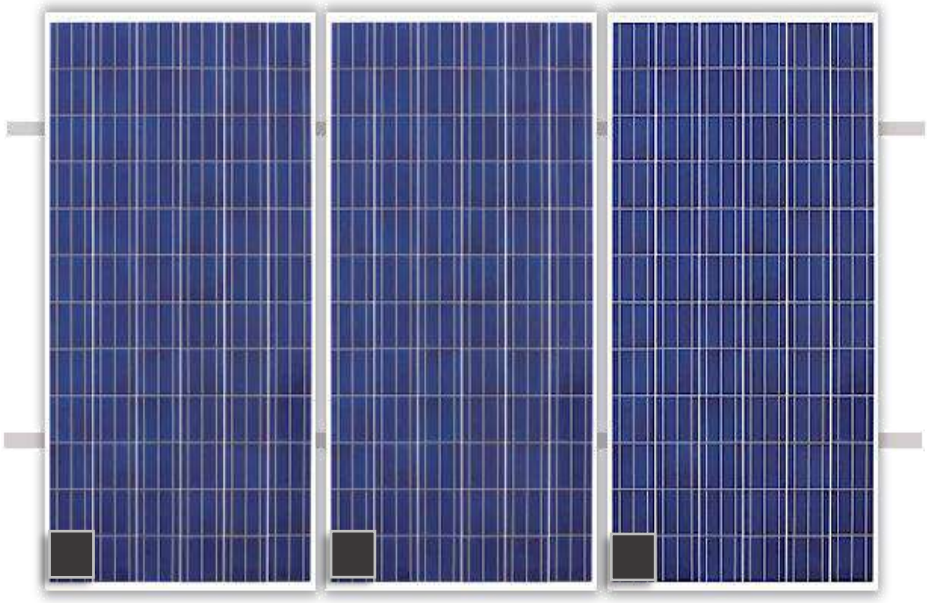

Fig 4.8. Scenario # 01 :One cell of each module is shaded

In scenario n° 3, the vertical half of module n° 3 is obstructed to create a shade on 30 cells of the module. At the same time, a small part of module n°2 is also shaded, as shown in Figure 4.10. This test is done under irradiance of G = 621.3710 W/m^2 and T = 314.3180 K.

Scenario n° 04 is achieved under the irradiance conditions of G = 501.7000 W/m² and a temperature of T = 312.0340 K. As illustrated in Figure 4.11, this scenario was achieved by creating a shade simultaneously on the horizontal row of cells of module n° 1 and module n° 2.

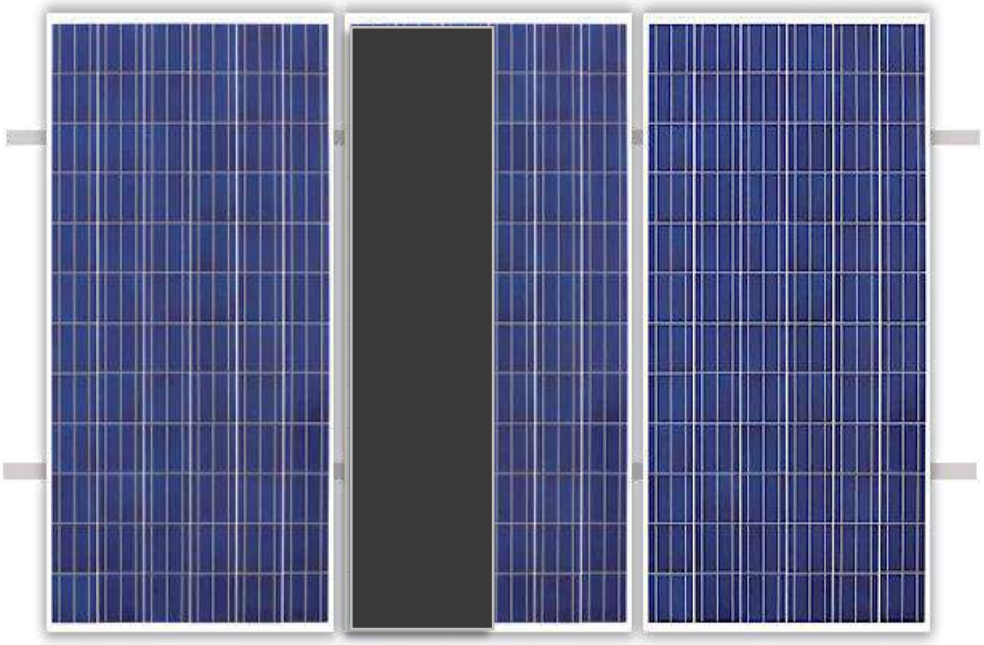

Fig 4.9. Scenario # 02 :Vertical half of module n°2 is shaded

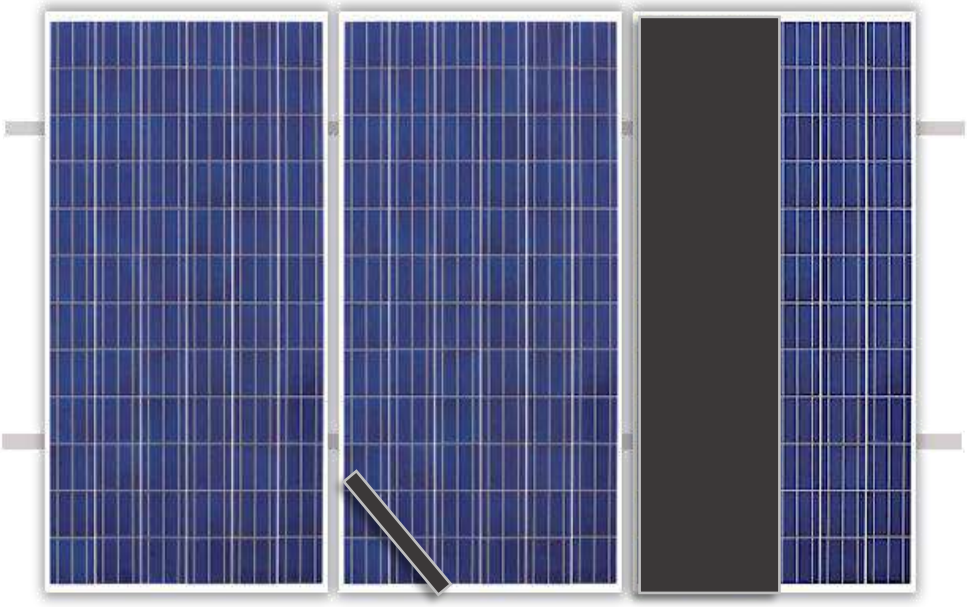

Fig 4.10. Scenario # 03 :Vertical half of module n°3 is shaded (30 cells are shaded) and a narrow diagonal portion of module n°2 is shaded

In the last scenario n°05, a random pattern of shade is realized as illustrated in Fig. 4.12, where two small rows shade modules n°1 and n°2. The measurement of the irradiance at that time was G = 400.3190, and the temperature was = T 312.6170.K

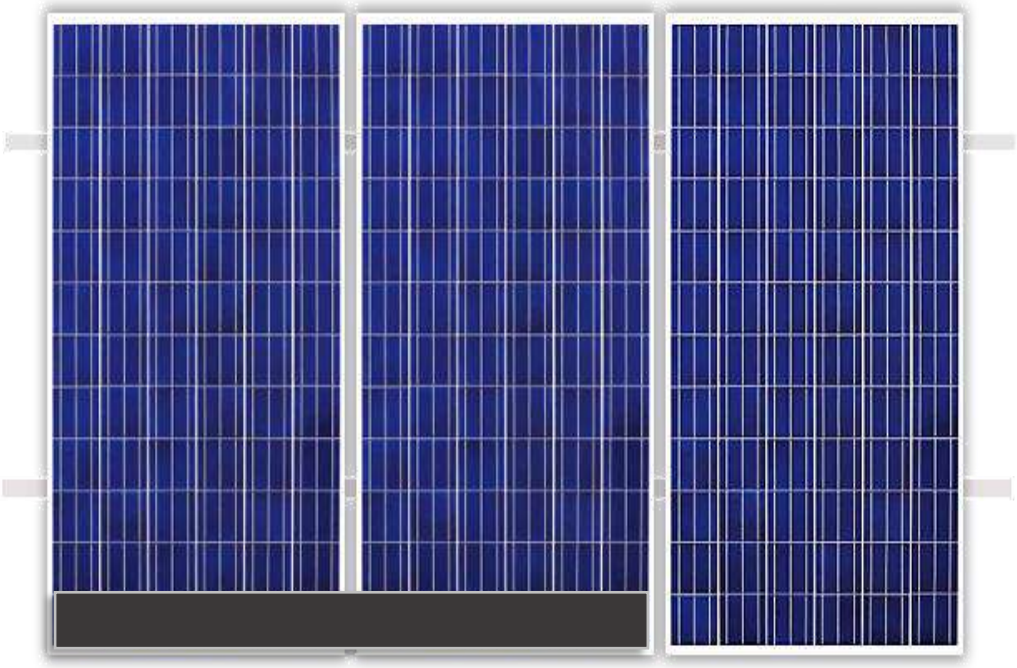

Fig 4.11. Scenario # 04 :The horizontal row of cells of module n°1 and module n°2 is shaded

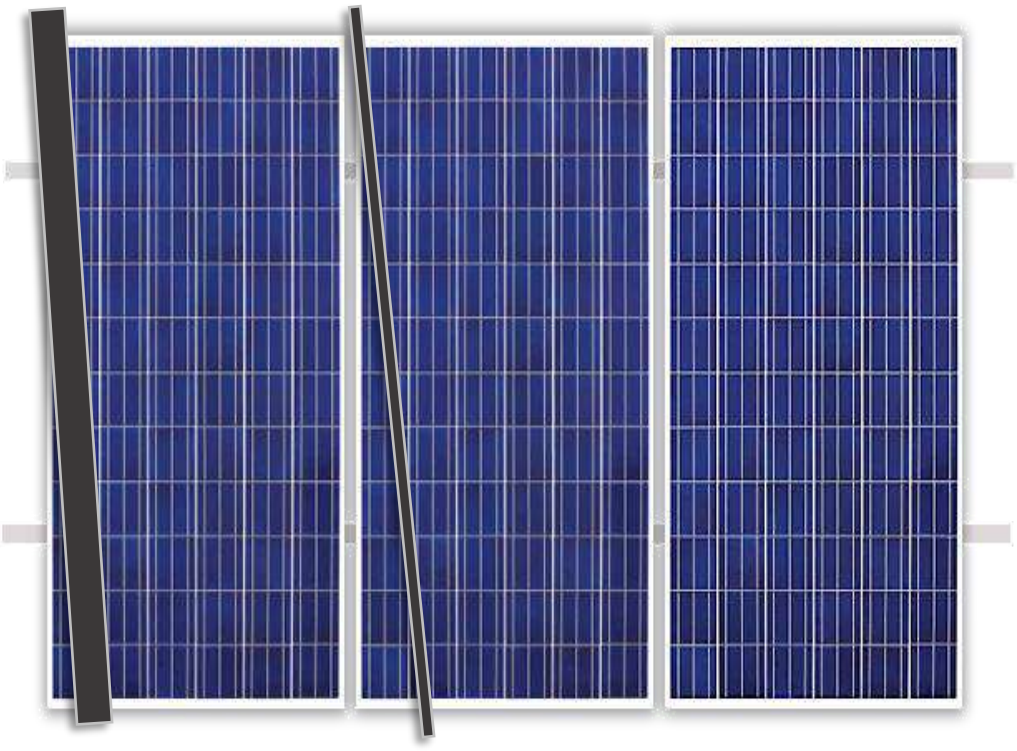

Fig 4.12. Scenario # 05 :Small rows are causing random shading on module n°1 and module n°2.

Table 4.4. Results of simulation of the partial shading scenarios

Scenario n°	*Irradiance (W/m^2)*	*Temperature (K)*	*Result*	*Isc*	*Voc*	*Mpp*	*Impp*	*Vmpp*
01	839.5390	324.142	*Measured*	7.6907	96.999	319.0834	6.8273	46.7358
			Simulated	7.7080	97.003	319.9614	6.8461	46.7358
02	781.1890	321.3120	*Measured*	7.0744	94.6728	343.2504	6.2154	55.2258
			Simulated	7.0885	94.6728	343.140	6.2134	55.2258
03	621.3710	314.3180	*Measured*	5.4548	99.9100	270.2484	3.6733	73.5700
			Simulated	5.4733	99.9100	270.8559	3.7276	72.6618
04	501.7000	312.0340	*Measured*	4.4479	93.4200	88.8909	4.0836	21.7677
			Simulated	4.4634	93.4200	89.29384	4.1021	21.7677
05	400.3190	312.6170	*Measured*	3.2518	96.5628	189.4173	2.7161	69.7398
			Simulated	3.2681	96.5628	190.2766	2.7284	69.7398

The results of the key points of the measured and simulated data are presented in Table 4.4. These key points include the short circuit current (Isc), the voltage of the open circuit (Voc), the maximum power point (Mpp), the current at the maximum power point (Impp), and the voltage at the maximum power point (Vmpp). It is worth noting that the measured and simulated data are in excellent agreement.

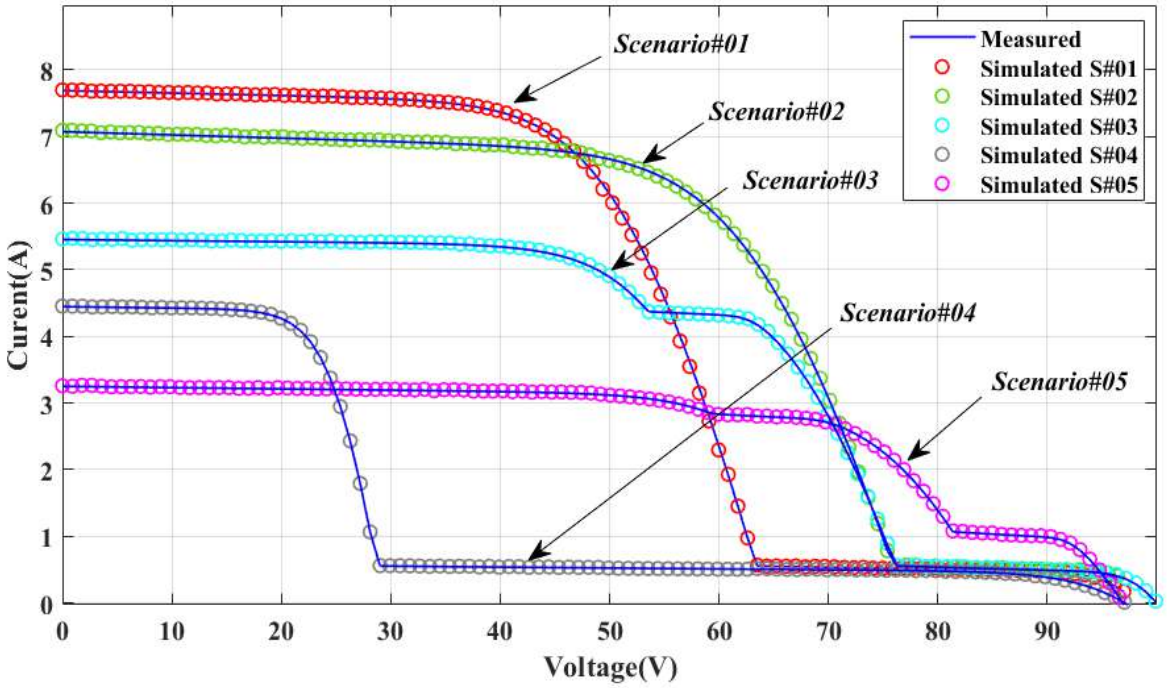

Fig 4.13. I-V curves of measured and simulated data of different scenarios.

Likewise, Fig 4.13 and Fig 4.14 illustrate the I-V and the P-V curves respectively of measured and simulated data of the five (05) scenarios. The blue data represent the measured data while

the other colors represent the simulated ones. Each color for one scenario is described in the agenda rectangle.

As can be noticed, the outputs of the PV string emulator fit thoroughly the physical PV string measurements that represent the different partial shading patterns. The error between the two types of data is very low, which proves its efficiency and reliability in describing the real behavior of the PV string generator.

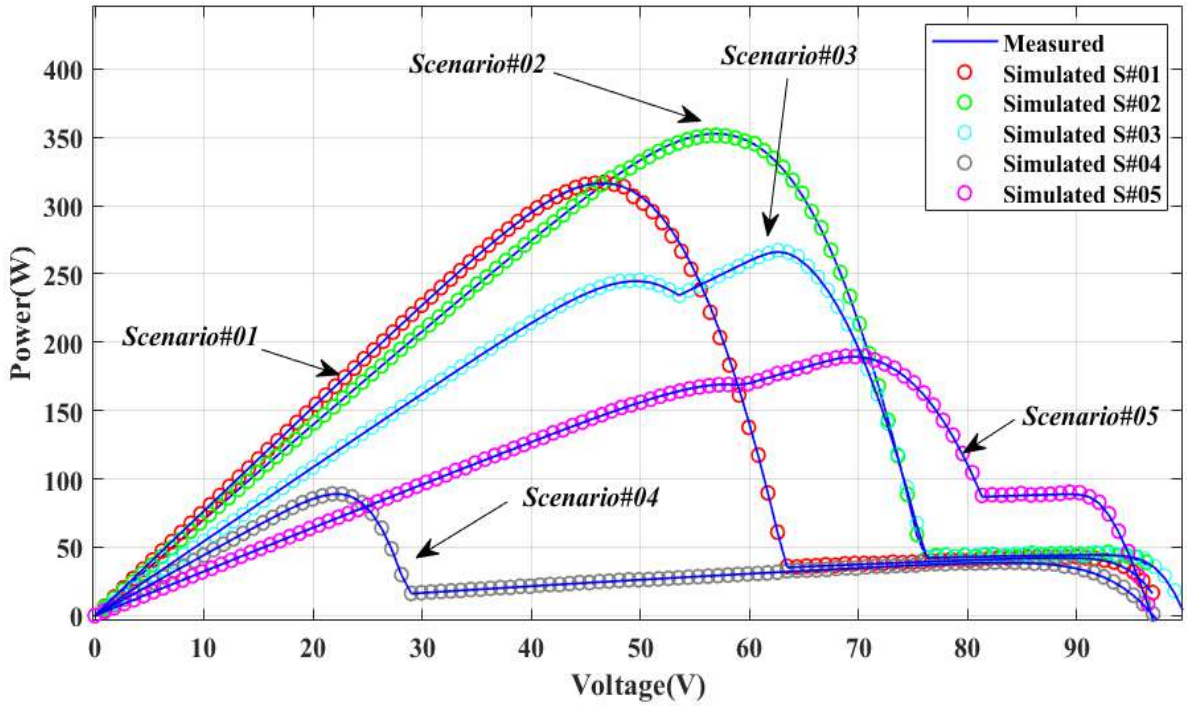

Fig 4.14. P-V curves of measured and simulated data of different scenarios.

4.6.2. Scenarios of other types of faults

Other types of faults must be simulated to validate the PV string emulator. By-pass diode faults, cable disconnection faults, module short-circuited default, among others, may affect the PV generator, in addition to the multiple faults that may occur simultaneously.

As discussed previously, intentionally causing certain types of faults on a real PV generator is not practical due to concerns related to safety and installation integrity. For instance, short-circuiting a PV module or reversing a bypass diode can result in irreversible damage or even cause a fire. Moreover, since there is a lack of experimental data on some types of faults, it is preferred to simulate the scenarios under consideration instead of attempting to replicate them on an actual PV generator.

Five (05) scenarios are considered for the simulation study, and they are described as follows:

1) *S 2.1: Connection resistance fault:*

The cables that connect modules, substrings, or junction boxes can be affected by various kinds of defaults which can result in energy loss. This may occur due to poor connection, overheating, external damage, and other causes. As a result, the cable might generate internal resistivity which can cause problems. Through experimentation, it was discovered that a connection resistance fault can take place when the cable resistance exceeds 1 Ohm. Therefore, this fault can be intentionally provoked by installing a variable resistance between 1 and 10 ohms. Similarly, in the simulator, a cable that is free from faults has a resistance of 1.0E-06, while a faulty cable presents a resistance of 5 Ohms. As illustrated in Fig 4.4 of the Matlab-Simulink emulator, this fault can be simulated by adjusting the targeted cable resistance to 5 Ohms.

2) S 2.2: Bypass diode of substring n°1 inverted and the same substring is shaded

This scenario presents two faults: the bypass diode of substring n°1 is (because of human error after a maintenance operation or due to manufacturing default), and the same substring is subject to partial shading.

3) S 2.3: Module n° 2 short-circuited

This scenario describes a short circuit in module n°2, which occurs when an electrical conductor falls and accidentally connects the cables of the module.

4) S 2.4: One substring is shaded, other bypass diode is inverted, and one connection resistance fault is present

In this scenario, one substring is shaded, a bypass of another substring is inverted mistakenly, and the module n°2 is short-circuited. All these events happen at the same time.

5) S 2.5: A connection resistance fault is present, and one substring is shaded

This scenario describes two simultaneous faults: one substring is shaded, and the bypass of another substring is inverted mistakenly.

The working conditions of the five scenarios are provided in Table 4.5.

The results of comparison between simulated and measured data are presented in Fig 4.15 (a) for the I-V curves, and in Fig 4.15 (b) for the P-V characteristics.

Table 4.5. Scenarios of other types and simultaneous faults

Scenario	*Solar incident irradiance (W/m^2)*	*PV temperature (K)*	*Description of the faulty scenarios*
S 2.1	835.542	324.061	Connection resistance fault
S 2.2	709.084	317.465	Bypass diode of substring n°1 inverted and the same substring is shaded
S 2.3	619.091	316.550	Module n° 2 short-circuited
S 2.4	530.134	312.456	One substring is shaded, other bypass diode is inverted, and one connection resistance fault is present
S 2.5	408.058	315.763	A connection resistance fault is present, and one substring is shaded

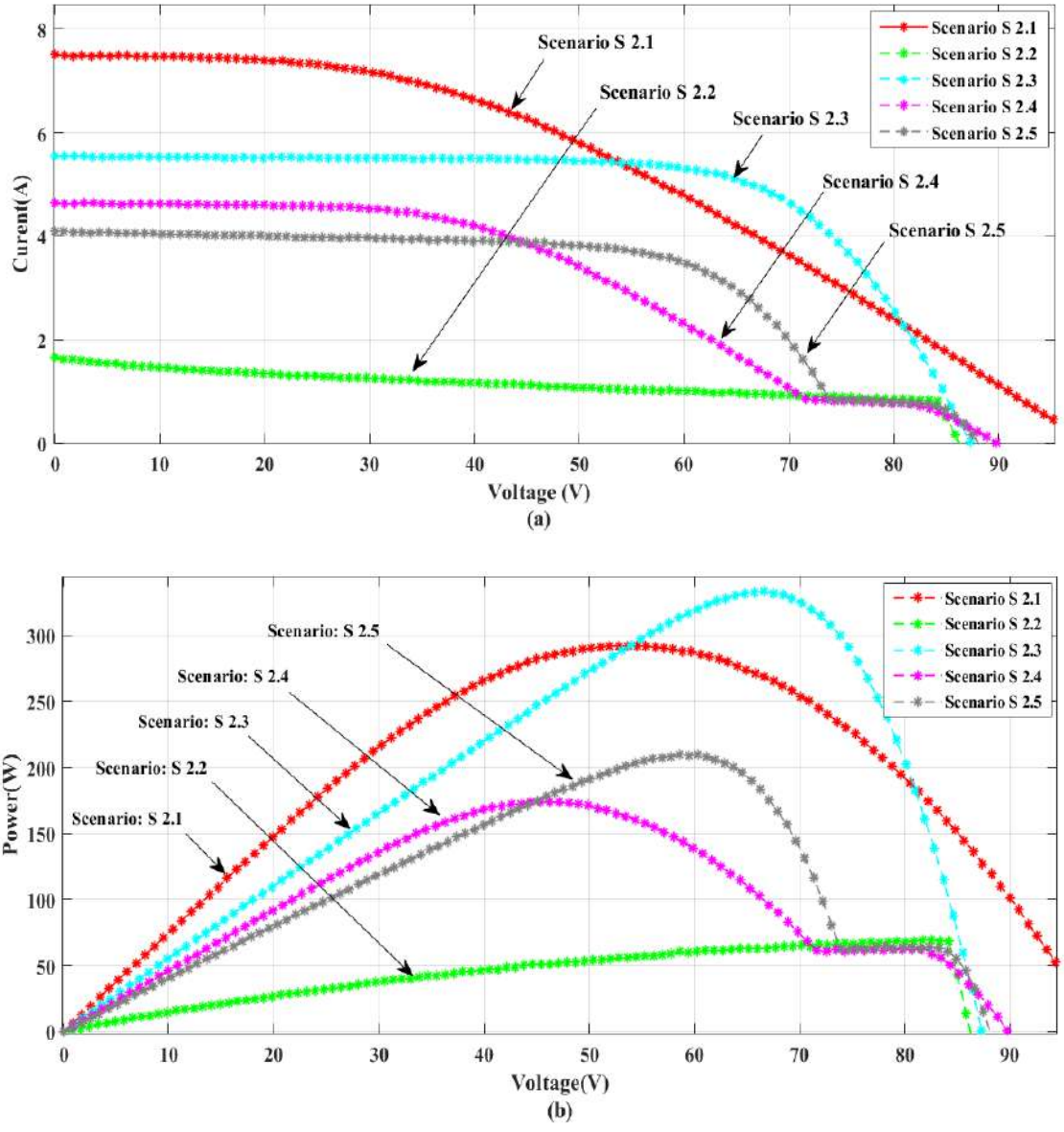

Fig 4.15. Results of other types and simultaneous faults scenarios: **(a):** I-V curves. **(b):** P-V: curves

In addition, the resulting key electrical values (*Isc*, *Voc*, *Mpp*, *Impp*, and *Vmpp*) of the five studied scenarios are presented in the following table:

Table 4.6. Results of simulation of scenarios (S 2.1, …, S 2.5)

Scenario	*Irradiance (W/m^2)*	*Temperature (K)*	*Isc*	*Voc*	*Mpp*	*Impp*	*Vmpp*
S 2.1	835.542	324.061	7.4861	95.1890	296.1353	5.4319	54.5170
S 2.2	709.084	317.465	1.6404	85.8321	68.1003	0.8090	84.1815
S 2.3	619.091	316.55	5.5336	86.4070	331.5088	4.9772	66.6054
S 2.4	530.134	312.456	4.6208	89.7480	173.3184	3.7487	46.2338
S 2.5	408.058	315.763	4.0757	87.4732	209.0357	3.5163	59.4478

When comparing the I-V and P-V curves of the partial shading scenarios to these of the five scenarios of other types of faults, it is clear that the shading curves have their own unique shapes with multiple maximum power points. For the other types of faults, each scenario presents a distinct shape that indicates the presence of the corresponding fault signatures. For instance, the curves in scenario S 2.2 indicate a significant energy loss due to the bypass diode inversion and shading on the same substring. This means that the shaded substring is consuming the energy produced by the remaining PV string because its bypass diode is unable to prevent the current from flowing in the opposite direction.

The simulated results of the five scenarios have demonstrated satisfactory outcomes, as they perfectly match reality. Thus, the PV string emulator has proven to be efficient in simulating the studied scenarios and replicating the actual behavior of the PV generator under study.

4.7. Conclusion

In this chapter, a PV generator emulator is presented for both healthy and faulty situations. The proposed simulator is designed using MATLAB/Simulink software to mimic the real behavior of the physical PV generator according to a predefined procedure.

Simulating both healthy and faulty conditions play a pivotal role in advancing the field of solar energy, principally in modeling and assessing PV systems performances.

The process of simulating optimal performance not only validates the accuracy of PV generator models but also helps manufacturers, operators, and managers improve component specifications, layout configurations, and energy management strategies.

Equally important, simulating faulty conditions is to identify potential issues and malfunctions, help operators and maintenance teams quickly diagnose problems, formulate preventive maintenance plans, and implement corrective actions.

The proposed emulator addresses the challenges of conducting risky experiments on the physical PV generator. For instance, overheated cells during artificial partial shading tests and short-circuiting a PV module in real tests without taking special precautions. The majority of tests can be safely and reliably performed on the soft PV emulator rather than the real one, with confidence to obtain accurate results.

The results obtained from the outputs of the proposed emulator show how the simulated data corresponds perfectly to the measured ones in both healthy and faulty conditions. Also, the weather condition variations (irradiance, temperature...) do not affect the accuracy of the adopted PV simulator.

Chapter 05:

Contribution to the PV generator fault diagnosis: Proposed method

5.1 Introduction

Solar photovoltaic is the most widespread renewable energy due to its availability and durability. Therefore, the global PV market is increasingly growing, together with its related technologies that are also in continuous progress. Nevertheless, this progress is always generating complexities during the lifecycle of PV systems. Especially, photovoltaic generators can encounter faults that reduce their efficiency and performance [94].

These faults must be detected and diagnosed promptly to ensure the reliability and safety of the PV generator as well as the entire PV installation [95]. Analytical methods that were frequently used in classic fault detection and diagnostic methods may not be practical or effective in real-time situations. In recent years, advanced methods such as artificial intelligence and metaheuristic approaches have become worthwhile methods for detecting and diagnosing faults in various engineering fields, including PV generator [21].

Even though several research works have been achieved on PV fault detection and diagnosis using different methods, but still lot of effort has to be deployed to solve many problems still taking place in this field. This is because the related works can only forecast limited types of faults, or one type at once [94, 96]. Detection and diagnosis of multiple and simultaneous PV defaults is still a challenge for researchers around the world, and only a few works dealing with this problem are published in the literature.

The objective of this chapter is to present a real-time fault diagnosis algorithm, which means that this algorithm can be used as a tool for monitoring and supervising the PV generator. The idea here is to use the I-V characteristics to extract the PV generator model in the faulty situation similarly to using them for healthy situations. For this purpose, the proposed algorithm uses the I-Vs characteristics that represent the real-time operation of a PV generator, measured under various solar irradiance and temperature conditions.

In the first stage, the data of I-V curves, representing considered scenarios, are obtained from the PV string simulator for different levels of irradiance and temperature. The algorithm then inputs this I-V data to extract the parameters of the PV string model during the modeling process.

As seen in Chapter 04, the emulator creates data that accurately represents both healthy and faulty situations. In Chapter 04, we saw that the emulator creates data that accurately represents both healthy and faulty situations. In this chapter, the data generated by the PV string emulator is considered as measured data since the emulator is known to be highly accurate and reliable in

mimicking the real behavior of the physical PV string. On the other hand, estimated data is the result of the metaheuristic algorithm proposed for fault detection and diagnosis.

5.2 Hypothesis

In a PV generator, each level of radiation and temperature corresponds to specific I-V characteristics. Using a metaheuristic technique and the corresponding I-V data, the parameters of a healthy PV generator model can be easily determined. Healthy PV generator cases are assumed to produce correct parameters during the optimization process. Similarly, in faulty situations, the corresponding I-V characteristics produce erroneous parameters. In other words, analysis of the parameters extracted from the I-V curves representing faulty situations can lead to different patterns with different signs of fault. Simultaneous faults are simulated and submitted to the algorithm to detect signs of these faults.

5.3 Proposed PV generator fault diagnosis technique "DSCE"

The proposed PV generator fault detection and diagnosis method is based on the analysis of the extracted PV generator model parameters. The proposed technique is named "Differential Shuffled Complex Evolution", denoted DSCE.

DSCE is a hybrid technique developed using a modified version of differential evolution (DE) and the original version of the Shuffled Complex Evolution (SCE) algorithm.

SCE was introduced by Duan et al in 1993, its architecture is based on four concepts: [97] a) the combination of deterministic and probabilistic methods. b) Clustering. c) Systematic evolution of a complex of points spanning the search space, and d) Competitive evolution.

The SCE algorithm starts by generating the initial population from a random sample of points spanning the search space. These initial points are divided into "p" complexes. Each complex, which contains "m" points, is involved independently using the Competitive Complex Evolution (CCE), which is a sub-routine of SCE, to update the worst vertex of simplex and drive the search toward enhancement direction [98]. The number of sampled points is $s = p \times m$ constitutes the population. After a certain number of generations, the complexes are forced to mix, and through shuffling, new complexes are resulting. This is to ensure information sharing among different complexes.

The CCE strategy is the core of the SCE algorithm. It comprises two phases: reflection and inside it, a contraction which is a phase of the Nelder-Mead algorithm [98, 99]. It is applied to generate the most offspring that are used to replace the worst vortex of simplex. The simplex is then driven

towards the local optimum. Triangular probability distribution is used to guarantee that the evolution is competitive and to select the better parents to form the simplex according the following equation:

$$P_i = \frac{2(m+1-i)}{[m\,(m+1)]}\ ,\ i = 1, \dots, m. \tag{5.1}$$

The original version of SCE has proved its efficiency in solving global optimization problems in many engineering fields. However, it suffers from shortcomings, such as parameter identifiability, lack of balance between exploration and exploitation processes, and the large number of function evaluations (NFE). The more random the offspring-generating process, the lower the probability of generating qualified offspring [98].

To deal will these issues, one can combine a modified (DE) with the original version of the SCE. The hybrid optimizer DSCE starts with random initialization of the population on the search space, evaluation of each candidate solution, and sorting them. The modified DE mutation process is then applied on each target vector X_i using the following equation:

$$V_i = X_{best} + F.(X_{r_1} - X_{r_2}) + F.(X_{r_3} - X_{r_4}) \tag{5.2}$$

where "*F*" is the mutation factor and X_{r_1}, X_{r_2}, X_{r_3} and X_{r_4} are four vectors randomly chosen from the current population, ($i \neq r_1 \neq r_2 \neq r_3 \neq r_4$) The result population is then sorted from the best to the worst, where it will be divided to "*p*" complexes. Each complex, which contains "*m*" individual, is involved independently using the CCE subroutine to update the worst vertex of simplex and drive the search toward enhancement direction. The crossover process of DE is then performed on the best candidate solution using the following equation:

$$U_{i,j} = \begin{cases} V_{i,j} & \text{if } r_4 < Cr \text{ or } j = j_{rand} \\ X_{i,j} & \text{otherwise} \end{cases} \tag{5.3}$$

where, *j* is the index of dimension, from 1 to D, j_{rand} is a random number from 1 to D, while D is the number of decision variables. C_r is the crossover rate, and r_4 is a random number from [0, 1].

Finally, the selection process of DE is performed to keep either the target vector or the trial vector into the next generation using the following equation:

$$X_{i+1} = \begin{cases} U_i & \text{if } Ob\,(U_i) \leq Ob\,(X_i) \\ X_i & \text{otherwise} \end{cases} \tag{5.4}$$

where $Ob\,(X_i)$ is the fitness function that drives the optimization problem.

Flowchart and pseudo code of DSCE is given in appendix B.3.

5.4 Modeling of the PV generator using "DSCE"

5.4.1 PV generator model parameter extraction in healthy conditions

The DSCE algorithm is used to address the problem of PV generator modeling in healthy conditions. Initially, it employs SDM, DDM, and TDM for PV cell modeling. However, since DDM and TDM require high computational effort and the use of the *W* Lambert function, only SDM is considered appropriate for PV modules and strings due to its simplicity and acceptable precision. To assess the performance of DSCE, its results are compared to those of recent competitors.

The PV generators model identified in this study include the RTC France PV cell, the poly-crystalline Photowatt-PWP201, the mono-crystalline STM6-40/36, the CLS-220P modules, and the PV CLS-220P string.

Table 5.1 presents results of the outcomes of the DCSE technique compared to competitor techniques. This test is presented through 06 metrics: the minimum (min) value of the RMSE, the maximum (max) value of the RMSE, the mean (mean) value of the RMSE, and the standard deviation (STD) of the RMSE is the that reflects the precision of the extracted parameters and the reliability of the algorithm in general. NFE denotes the number of function evaluation, which is the number of times that the algorithm calls the objective function. Finally, the CPU execution time which represents the amount of time needed by the algorithm to reach the corresponding minimum value of the RMSE. As can be noticed, DSCE performance is better than other algorithms in terms of the over mentioned metrics. The best results are presented is bold font.

N.B: The references of the competing techniques are reported in the references provided in front of title of the table.

Table 5.2 presents results of the outcomes of the DCSE technique when extracting the parameters of the CLS-220P PV module model. The resulted NFE is varying from 7600 to 9600, and the CPU execution time is varying from 1.85s to 2.91s. These results prove the rapidity of the proposed technique when extracting the module model parameter as well as the less CPU resources consumption. The Standard deviation is in the range of 2.76E-16 to 9.00E-17, which reflect the good reliability of the proposed DSCE technique.

Figures 5.1 illustrates the perfect matching of the measured and estimated I-V and P-V curves respectively for different levels of irradiance and cell temperature on CLS-220P module model.

Table 5.1 Statistical results obtained by DSCE method and compared to recent methods: [68, 83]:

PV generator	*Model*	*Algorithm*	*Min*	*Mean*	*Max*	*StD*	*CPU time (s)*	*NFE*
RTC France solar cell	SDM	GWOCS	9.8607E-04	9.8874E-04	9.9095E-04	2.4696E-06	-	-
		TLBO	1.0293371E-03	6.8166220E-03	3.76453111E-02	8.48143E-03	-	-
		LCJAYA	9.8602E-04	9.8602E-04	9.8602E-04	5.6997E-16	-	-
		AEO	7.7301E-04	-	-	1.6402E-05	40.523 3	-
		EPSO	8.0621E-04	-	-	4.3109E-04	13.670	-
		FC-EPSO1	7.7301E-04	-	-	1:5688E-10	11.519	-
		ELPSO	7.7301E-04	7.7314E-4	7.7455E-4	3.4508E-07	-	-
		TVACPSO	7.7301E-04	7.7301E-04	7.7301E-04	5.5805E-10	-	-
		DSCE	7.730062E-04	7.730062E-04	7.730062E-04	**9.294465E-18**	**0.859**	**3100**
	DDM	GWOCS	9.8334E-04	9.9411E-04	1.0017E-03	9.5937E-06	-	-
		TLBO	1.355232E-03	8.8698208E-03	6.606815E-02	1.387828E-02	-	-
		LCJAYA	9.8250E-04	9.8308E-04	9.8602E-04	1.3118E-06	-	-
		AEO	7.6068E-04	-	-	1.4844E-04	**10.413**	-
		EPSO	7.6312E-04	-	-	1.5424E-04	15.485	-
		FC-EPSO1	7.4489E-04	-	-	**2.1153E-10**	12.036	-
		ELPSO	7.4240E-04	7.5904E-04	7.9208E-04	9.4291E-06	-	-
		TVCPSO	7.4365E-04	7.5883E-04	7.8476E-04	1.1044E-05	-	-
		DSCE	6.7451339E-04	6.967355E-04	7.300686E-04	2.721610E-05	15.520	**26500**
	TDM	EPSO	7.5440E-04	-	-	-2.6967E-04	43.014 7	-
		FC-EPSO1	7.4300E-04	-	-	**9.1140E-11**	39.521 2	-
		DSCE	**6.2853937E-04**	6.5725960E-04	6.7379416E-04	5.54877E-06	**21.252**	**170000**
Photowatt-PWP-201 module	SDM	GWOCS	2.4251E−03	2.4261E−03	2.4275E−03	1.196700E-06	-	-
		TLBO	5.212918E-03	7.0276795E-02	8.247839E-01	1.454545E-01	-	-
		LCJAYA	2.425075E-03	2.425075E-03	2.425075E-03	**2.415229E-16**	-	-
		CPSO	2.0530E-03	2.0531E-03	2.0576E-03	8.6188E-07	-	-
		TVACPSO	2.0530E-03	2.0530E-03	2.0537E-03	1.3400E-07	-	-
		DSCE	2.052960E-03	2.052960E-03	2.052960E-03	**9.918879E-18**	**1.850**	**7800**
STM6-40/36 module	SDM	GWOCS	1.7337E-03	1.7457E-03	1.7528E-03	1.0447E-05	-	-
		TLBO	1.7298184E-03	2.9262854E-03	3.3684813E-03	4.952945E-04	-	-
		EPSO	2.6358E-03	-	-	4.7034E-03	4.171	-
		FC-EPSO1	1.7889E-03	-	-	7.3391E-10	**3.944**	-
		ELPSO	2.1803E-03	2.2503E-03	3.7160E-03	2.9211E-04	-	-
		SDO	1.7298E-03	1.7703E-03	1.9500E-03	4.5108E-05	-	-
		DSCE	1.7219215E-03	1.7219215E-03	1.7219215E-03	**4.997376E-18**	**1.540**	**7900**

Table 5.2 Extracted parameters of the CLS-220P module using DSCE technique

	Case 1	***Case 2***	***Case 3***	***Case 4***
Parameter	*G=810 (W/m²) T=322.645(K)*	*G=661.897(W/m²) T=321.470 (K)*	*G=523.444 (W/m²) T=315.909 (K)*	*G=149 (W/m²) T=313 (K)*
I_{ph} *(A)*	7.735408	6.145556	4.662543	3.363097
n	1.174950	1.145283	1.077720	1.103166
R_s *(Ω)*	0.673634	0.689372	0.714373	0.677725
R_{sh} *(Ω)*	4999.999999	4999.999999	5000	672.269079
I_{sd} *(μA)*	5.725569E-07	2.670263E-07	0.046295	0.036799
RMSE	5.310634E-03	7.700110E-03	4.982573E-03	3.015816E-03
Min	5.310634E-03	7.700110E-03	4.982573E-03	3.015816E-03
Mean	5.310634E-03	7.700110E-03	4.982573E-03	3.015816E-03
Max	5.310634E-03	7.700110E-03	4.982573E-03	3.015816E-03
STD	2.766149E-16	9.007856E-17	4.2193679-17	2.463775E-17
CPU time (s)	2.210	2.919	2.169	1.854
NFE	7600	8300	9400	9600

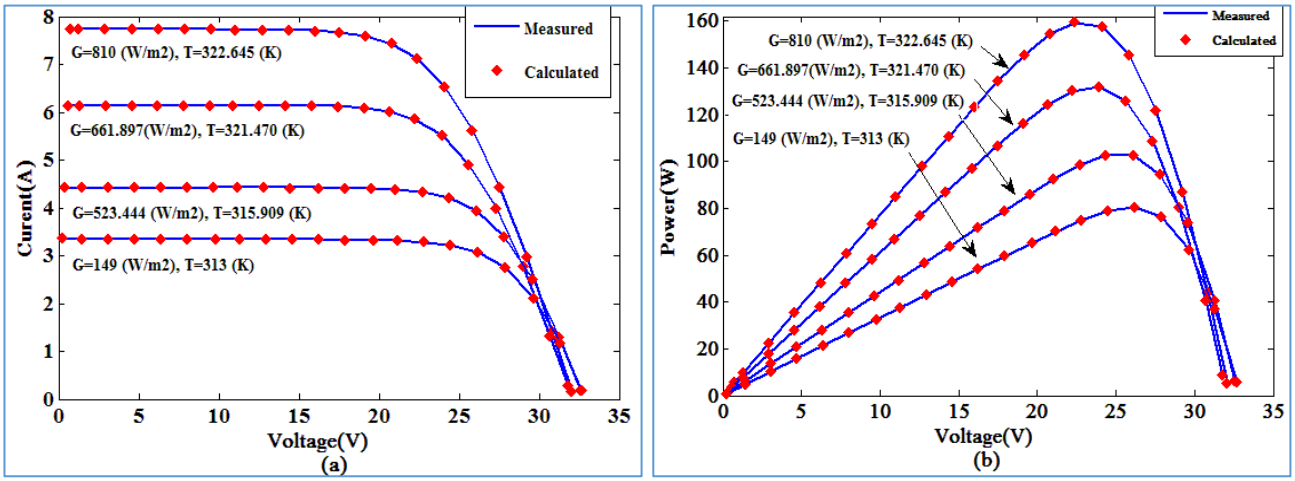

Figure 5.1. Results of the parameters extracted by DSCE on CLS-220P module model:
(a) I-V characteristic curve, **(b)** P-V characteristic curve.

Likewise, table 5.3 presents the outcomes of the DCSE technique when modeling the CLS-220P PV string. As can be noticed, the resulted NFE is varying from 6500 to 10700, and the CPU execution time is varying from 1.65 s to 2.33 s. These results validate the fast operation of the proposed technique when extracting the string model parameter as well as the less CPU resources consumption. The Standard deviation is in the range of 5.59E-18 to 3.54E-17, which validate in its turn, the good reliability of the proposed DSCE technique.

Figures 5.2 illustrates the unified matching of the measured and estimated I-V and PV curves respectively for different levels of irradiance and cell temperature of the CLS-220P string model.

Consequently, DSCE demonstrates high qualifications for the CLS-220P PV module/string modeling in the healthy conditions.

Table 5.3 Extracted parameters of the CLS-220P string using DSCE technique

	Case 1	***Case 2***	***Case 3***	***Case 4***
Parameter	*G=952.3687 (W/m²) T=322.862(K)*	*G=661.9587(W/m²) T=319.5320(K)*	*G=474.0594 (W/m²) T=317.0220 (K)*	*G=210.7716 (W/m²) T=307.205 (K)*
I_{ph} *(A)*	8.520954	5.902532	4.099844	1.340319
n	1.288468	1.260257	1.299099	1.233646
R_s *(Ω)*	1.716898	1.645193	1.572743	1.512666
R_{sh} *(Ω)*	575.718380	989.078412	316.655564	1239.569111
I_{sd} *(μA)*	1.661378E-06	6.890101E-07	7.757631E-07	8.809222E-08
RMSE	7.167909E-03	3.667190E-03	6.168046E-03	9.130975E-04
Min	7.167909E-03	3.667190E-03	6.168046E-03	9.130975E-04
Mean	7.167909E-03	3.667190E-03	6.168046E-03	9.130975E-04
Max	7.167909E-03	3.667190E-03	6.168046E-03	9.130975E-04
STD	9.140527E-17	3.546995E-17	4.2193679-17	5.594735E-18
CPU time (s)	1.650	1.890	1.678	2.335
NFE	6500	8300	7300	10700

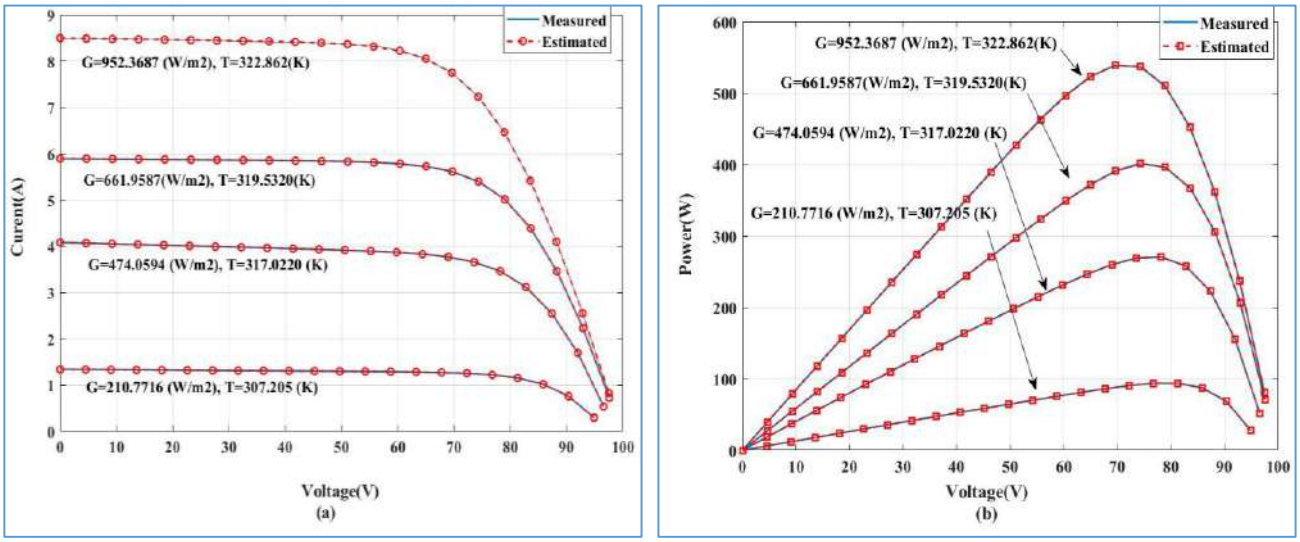

Figure 5.2 Results of the parameters extracted by DSCE on the CLS-220P string model:

(a) I-V characteristic curve, **(b)** P-V characteristic curve.

5.4.2 Fault detection and diagnosis of the PV string using "DSCE"

After testing and validating the performances of the proposed DCSE technique on modeling accurately, rapidly, and reliably the healthy PV generator models, DSCE is used for the CLS-220P PV string fault detection and diagnosis.

In faulty situations, the DSCE uses the faulty I-V data to extract the PV string model parameters in the same way as mentioned for healthy situations. The produced parameters, as well as any resulting parameters and functions (MPP, Voc, Isc, 1st and 2nd current/voltage derivatives…etc.), are analyzed and investigated in the detection and diagnosis process.

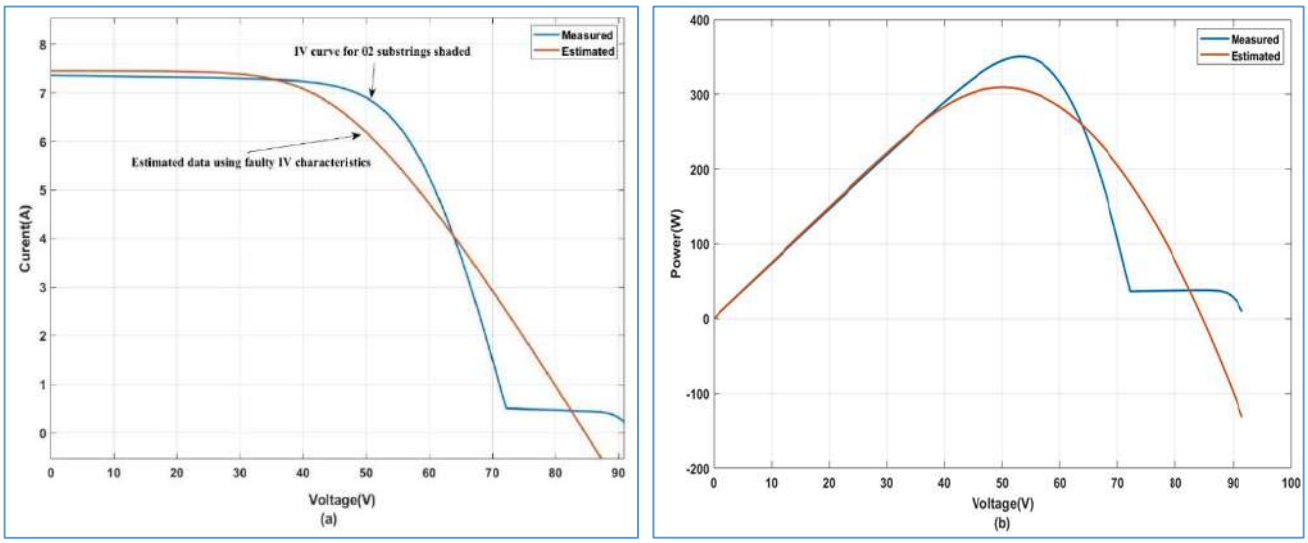

Figure 5.3 Estimated data (red curves) and measured data (blue curves) in a scenario of 02 shaded substrings:
(a) I-V characteristics, **(b)** P-V characteristics.

Figure 5.3 (a) illustrates an example of a scenario of shading on two (02) substrings. The faulty I-V data (blue curve) is used by the DSCE technique to extract PV string model parameters in modeling process. This faulty condition is taken under a level of radiation G = 813.0920 W/m^2 and a temperature of T = 322.889 K. After extraction of the parameters, the estimated curve is represented in (red curve).

In Figure 5.3 (b), the measured P-V curve presents two maximum power points (MPP) due to the shading effect. However, on the estimated curve, only one MPP appears. The reason for this is that during the modeling process, the DSCE uses the measured I-V data to optimize and find the vector representing the five model parameters, leading to a minimum value of the RMSE. The DSCE then attempts to fit the estimated I-V data with the measured ones, according to the RMSE value. However, this is not possible due to the deforming shape of the measured I-V curve.

In this scerario, some mesured and estimated data could be compared to understand the fault pattern. For instance, the measured Isc = 7.32 A, and the estimated Isc = 7.39 A. The measured Voc = 92.87 V, while the estimated Voc = 85.52 V. The measured MPP = 345.23 W, but the estimated MPP = 315.23 W.

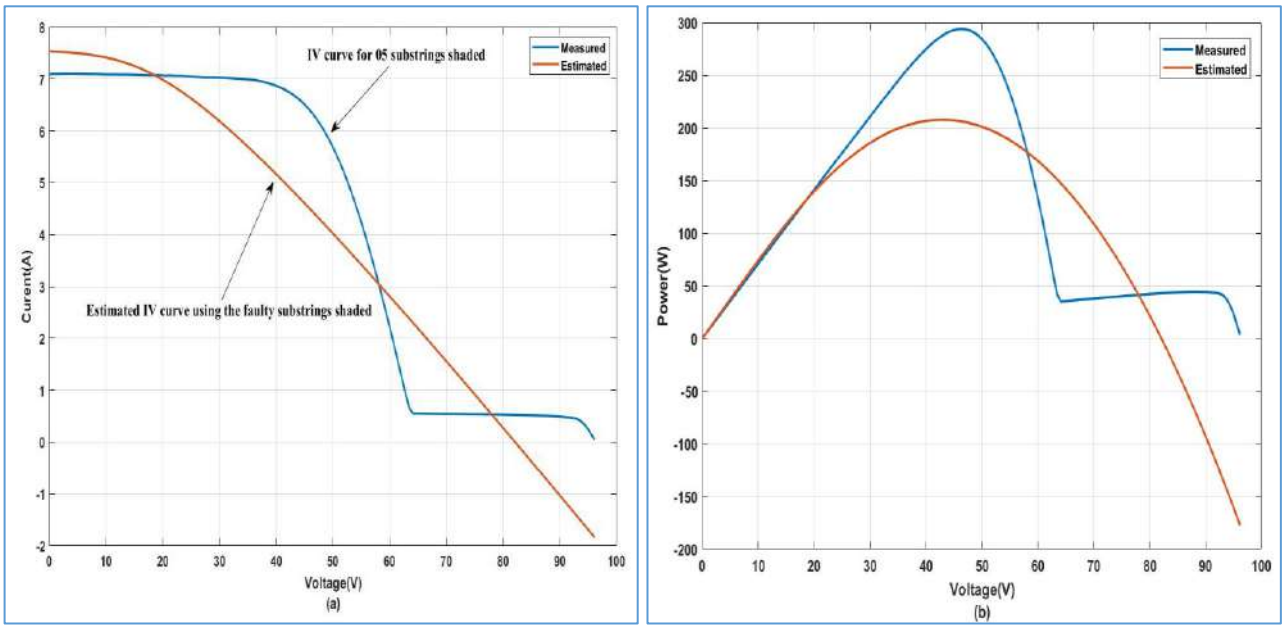

Figure 5.4 Measured and estimated data of 05 shaded substrings: **(a)** I-V characteristics, **(b)** P-V characteristics

Another example of 05 substrings shaded is given in Figure 5.4, where G = 784.103 W/m^2 and a temperature of T = 301.2390 K. Similar observations can be formulated in the estimated and measured I-V and P-V curves as in the previous example. However, in this case, the match between the estimated and measured curves is worse due to the increase in the shape distortion of the measured I-V curve compared to the previous scenario. In addition, the difference between

the produced parameters and the estimated ones (Isc, the Voc, and the MPP) is increased compared to the previous scenario. Numerically:

- Measured Isc = 7.08 A, and estimated Isc = 7.54 A.
- Measured Voc = 97.24 V, and estimated Voc = 83.54 V.
- Measured MPP = 345.23 W, but estimated MPP = 295.78 W.

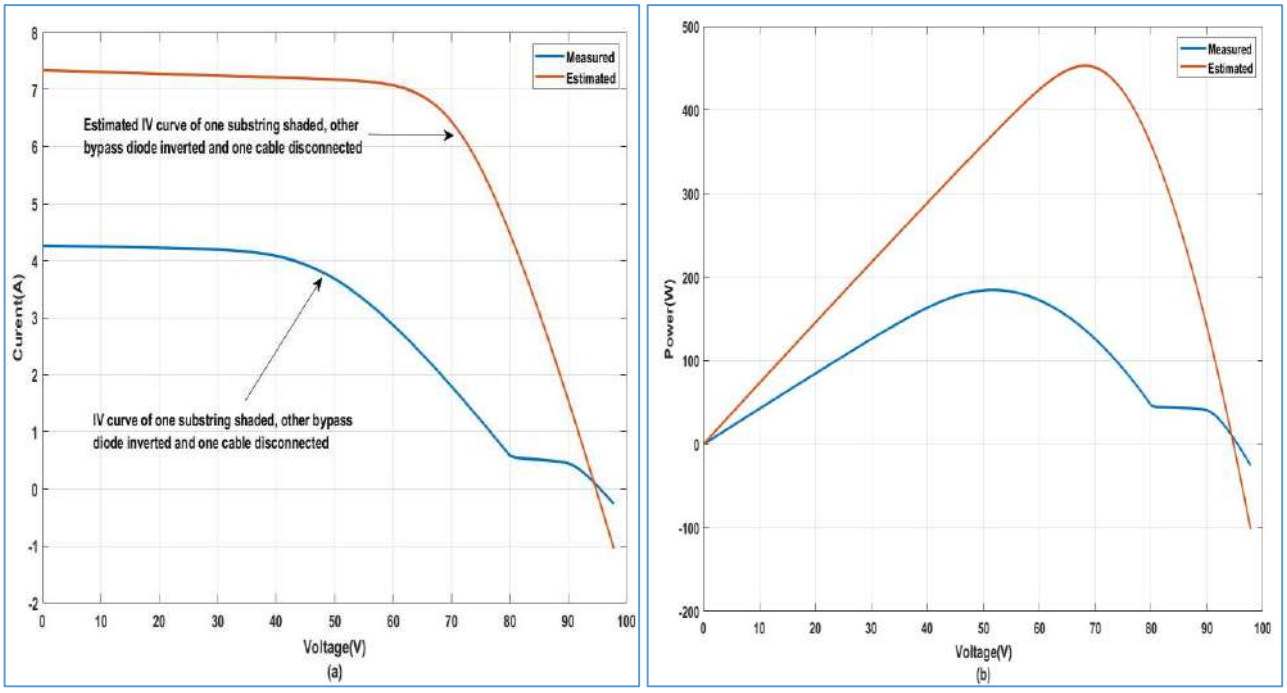

Figure 5.5 Measured and estimated data of scenario of one substring shaded, a bypass diode inverted, and connection resistance fault: **(a)** I-V characteristics, **(b)** P-V characteristics.

A third example is illustrated in Figure 5.5, where multiple faults are occurring on the PV string simultaneously. This scenario is a combination of three faults: one substring is shaded, one bypass diode is inverted, and a cable resistance is faulty. Due to the impact of these simultaneous faults, the matching between the measured curves and the estimated ones is even worse compared to the previous examples. The produced parameters, such as RMSE, Iph, Rs, Isc, Voc, MPP, etc., are also different from the previous scenarios.

From the above-mentioned examples, it can be concluded that every fault has an impact on the resulting model parameters and the other estimated electrical values. This means that any inherent fault in the I-V input data will produce a trace of its signature in the resulting estimated data after the modeling process.

To understand the various fault signatures and their patterns in the estimated parameters, it is essential to conduct an in-depth investigation study of different faulty conditions.

5.5 Considered faulty scenarios

5.5.1 Partial shading scenarios

Several shading scenarios are considered in this study at different levels of irradiance and temperature. The considering scenarios are chosen as follows:

Case n° 01:

- Case 1.1: The total surface (100%) of faulty substring is shaded in condition of G= 826.560 W/m^2 and T= 324.865 K. Nine (09) scenarios are considered in this case and are referred to as (S 1.1.1, S 1.1.2…, S 1.1.9).
- Case 1.2: The same description, as in case 1.1, but in the condition of G= 662.2860 W/m2, T= 319.251 K. Likewise, nine (09) scenarios are considered in this case and are referred to as (S 1.2.1, S 1.2.2…, S 1.2.9).
- Case 1.3: The same description, as in previous cases, but in the condition of G= 482.754 W/m^2, T= 311.127 K. Similarly, the nine (09) considered scenarios are referred to as (S 1.3.1, S 13.2…, S 1.3.9).

Case n° 02:

In this case, one module (03 substrings) is shaded at different percentages under the conditions of irradiance G = 783.809 W/m2 and temperature T = 322.957 K. Six (06) scenarios are considered in this case and are described as follows:

- S 2.1: 10% of the faulty module is shaded.
- S 2.2: 20% of the faulty module is shaded.
- S 2.3: 40% of the faulty module is shaded.
- S 2.4: 60% of the faulty module is shaded.
- S 2.5: 80% of the faulty module is shaded.
- S 2.6: 90% of the faulty module is shaded.

5.5.2 Other types of faults and simultaneous faults scenarios

In this case, referred to as case n°03, different types of faults and simultaneous faults are studied under irradiance of G = 826.560 W/m^2 and temperature T = 301.239 K. Ten (10) scenarios are considered in this case, and are described as follows:

- S 3.1: One substring is shaded.
- :S 3.2One connection resistance fault is present.

- :S 3.3One substring is shaded and one connection resistance fault is present simultaneously.
- S 3.4: Bypass diode n°1 is inverted. (This could happen after an erroneous maintenance operation).
- S 3.5: Bypass diode n°1 is inverted and substring n°1 is shaded simultaneously.
- :S 3.6Bypass diode n°1 is inverted and another substring is shaded.
- S 3.7: Bypass diode n°1 is inverted, another substring is shaded, and one connection resistance fault is present simultaneously.
- S 3.8: Module n° 2 is short-circuited.
- S 3.9: Module n°2 is open-circuited.
- S 3.10: Module n°2 is open-circuited and one substring is shaded.

5.6 Results, discussion and interpretation

The results of fault detection and diagnosis using DSCE technique for the scenarios studied in case n° 01, case n° 02, and case n° 03 are presented as follows:

- Table 5.4 displays the estimated parameters for scenarios of case 1.1, while Fig. 5.6 shows the corresponding graphs.
- Table 5.5 presents the estimated parameters for scenarios of case 1.2, and Fig 5.7 illustrates the corresponding graphs.
- Table 5.6 presents the estimated parameters for scenarios of case 1.3, and Fig 5.8 demonstrates the corresponding graphs.
- Table 5.7 presents the results of the estimated parameters for scenarios of the case n° 02, and Fig 5.9 demonstrates the corresponding graphs.
- Table 5.8 reports the numerical estimated parameters for scenarios of the case n° 03, and Fig 5.10 shows the corresponding graphs.

The first row in all five (05) tables is highlighted in light green, and it represents the results of the healthy PV string for each of the studied cases. The estimated parameters mentioned in this row are to be considered as reference parameters to compare against the estimated parameters of other faulty scenarios. Likewise, in all graphs, the first value of each estimated parameter corresponds to the healthy parameter of the PV string.

Upon analyzing the data obtained through the PV string modeling process using the DSCE technique, it has turned out that the following parameters are the most significant ones to retain:

- The RMSE, which is the minimum value of the objective function that drives the optimization process.
- The vector of the optimal solution, which contains the five parameters extracted of the model: (Iph, I0, Rs, Rsh, and n).
- The estimated values of the following parameters: short circuit current (Isc), open circuit voltage (Voc), maximum power point (Pmp), current at the maximum power point (Imp), voltage at the maximum power point (Vmp), and fill factor (FF).

5.7 Design of the PV string fault tree algorithm

After analyzing the data presented in the tables and graphs mentioned above, a fault tree algorithm can be designed to represent the faulty scenarios studied. The following observations can guide the design:

1) *RMSE* < 3E-4 in the following scenarios:
   - Healthy PV string.
   - S 1.1.9, S 1.2.9, and S 1.3.9: Fully shaded PV strings.
   - S 3.2: One connection resistance fault.
   - S 3.4: One bypass diode is inverted.
   - S 3.8: One module is short-circuited.
   - S 3.9: One module is open-circuited or a module cable is disconnected.

2) 1.0E-02 < *RMSE* < 3.5E-02 in the following scenario:
   - S 3.5: One bypass diode is inverted and the same substring is shaded (or when I_{ph} < 2 at this level of irradiance).

3) 1.9E-01 < *RMSE* < 3.5E-01 in the following scenarios:
   - S 1.1.1, S 1.2.1, S 1.3.1, One PV substring is shaded (when 0.10 < n < 0.13).
   - S 2.2: 20% of one module shaded (when 0.50 < n < 0.60).
   - S 3.3: One PV substring is shaded and a connection resistance fault is present simultaneously (when R_{sh} > 4000 or n > 0.19).

4) 0.68 < *FF* < 0.72 in the following scenarios:
   - Healthy string (when I_{ph} > 1).
   - S 1.1.9, S 1.2.9, and S 1.3.9: Fully shaded string (when I_{ph} < 0.5).

5) 0.60 < *FF* < 0.67 in the following scenarios:

- S 3.1: One substring is shaded.
- S 2.1: 10% of a module is shaded.
- S 3.4: One bypass diode is inverted
- S 3.6: One bypass diode is inverted and another substring is shaded.
- S 3.7: One substring is shaded; another bypass diode is inverted and one connection resistance fault is present.
- S 3.8: One module is short-circuited.

6) $0.50 < FF < 0.59$ in the following scenarios:
   - S 1.1.2, S 1.2.2, S 1.3.2, Two (02) substrings are shaded.
   - S 2.2: 20% of a module is shaded.

7) $0.39 < FF < 0.49$ in the following scenarios:
   - S 1.1.3, S 1.2.3, and S 1.3.3: Three (03) substrings are shaded.
   - S 2.3: 40% of a module is shaded (when 4.0E-01 < *RMSE* < 4.5E-01, or $n > 0.9$).
   - S 2.4: 60% of a module is shaded (when 6.0E-01 < *RMSE* < 6.5E-01, or $n < 0.2$).
   - S 2.6: 90% of a module is shaded (when 9.0E-01 < *RMSE* < 9.5E-01, or $n < 0.05$).
   - S 3.5: One bypass diode inverted with the same substring shaded (when 1.0E-02 < *RMSE* < 3.5E-02).
   - S 3.9: One module is open-circuited or a module cable is disconnected (when *RMSE* < 2E-04).

8) 7.0E-01 < *RMSE* < 8.5E-01 in the following scenarios:
   - S 2.5: 80% of a module is shaded (when $0.37 < FF < 0.38$).
   - 03 substrings shaded when (when $0.40 < FF < 0.45$).
   - 04 substrings shaded when (when $0.30 < FF < 0.35$).

After analyzing and comparing all the estimated parameters provided in the aforementioned tables and graphs, the studied faulty scenarios can be classified using a fault tree algorithm illustrated by its flowchart given in Fig 5.11.

The algorithm first reads the input data, which includes Irradiance G, temperature T, and I-V characteristics. Then, it uses the DSCE technique to extract the model parameters of the PV string and calculates other estimated electrical values such as Isc, Imp, Pmp, Voc, and FF. Several tests are then conducted to define the range of the RMSE,

In the next phase, the algorithm tests the five model parameters (Iph, I0, Rs, Rsh, and n) as well as the FF value. At the end of this phase, some alert messages begin to appear flagging the appropriate faulty scenario. The remaining alerts are processed in the next phases where tests are made on the rest of the estimated values.

For example, if the RMSE is in the range of 2.0E-04 to 3.0E-4, FF is in the range of 0.68 to 0.72, and Iph is greater than 1, the algorithm indicates that the PV string is healthy with no faults detected. However, if Iph is less than 1, the PV string is declared fully shaded, as mentioned in Fig 5.11.

Although the algorithm identifies and categorizes a restricted number of faults, since the study is limited to the faulty scenarios that were considered, however, in future works, the study can be extended to other types of faults.

As can be observed, the algorithm is highly robust as it can precisely detect and classify several types of faults as well as multiple and simultaneous faults, irrespective of the weather conditions.

5.8 Conclusion

In this chapter, the main contribution part of the thesis is described, which is a new approach to diagnosing faults in PV generators. The proposed approach involves using the PV generator modeling process to supervise it in real-time. The initial idea is that in faulty circumstances, the I-V characteristics will contain fault signatures that will appear in the estimated model parameters. However, in healthy situations, the I-V characteristics are clear from any fault signature.

The PV generator modeling process is performed using a newly proposed metaheuristic technique called Differential Shuffled Complex Evolution (DSCE). The DSCE is a hybrid algorithm developed based on two other algorithms, the Shuffled Complex Evolution (SCE) algorithm and the Differential Evolution (DE) algorithm. The DSCE is tested and compared to state-of-the-art techniques and has proven its accuracy and reliability in performing the parameter identification of different PV generator models under different working conditions. The most significant advantage of the DSCE is its speed and computational efficiency when optimizing the model parameters. For instance, it takes less than 2.5 seconds to model the CLS-220P string, making it a typical real-time fault diagnosis tool for this PV string.

Several faulty scenarios have been studied in this chapter, and a fault tree algorithm was designed to detect and classify their corresponding faults. This algorithm has proven its efficiency and robustness according to the results obtained when diagnosing numerous types of faults and multiple and simultaneous faults under different conditions.

Table 5.4 Estimated parameters using the DSCE technique for scenarios of case 1.1 (G = 826.560 W/m^2, T = 324.865 K)

Scenarios	*Description*	*RMSE*	I_{ph}	I_0	R_s	R_{sh}	*n*	*Isc*	*Voc*	*Pmp*	*Imp*	*Vmp*	*FF*
Healthy PV string	0 substring shaded	2.3956461E-04	7.3346079	1.371284175E-06	1.706201	656.464706	1.3753831	7.3155860	95.107000	477.291849	6.571809	72.6271636	0.685997
S 1.1.1	1 substring shaded	3.4261500E-01	7.5178775	2.911986441E-78	4.380125	206.404996	0.1077106	7.3616557	90.783955	405.750503	7.004296	57.9288091	0.607120
S 1.1.2	2 substrings shaded	6.2003846E-01	7.3341695	2.070672708E-118	5.274034	1007.836307	0.0686846	7.2959894	87.325518	347.316779	7.04744	49.2827182	0.545130
S 1.1.3	3 substrings shaded	9.4408719E-01	7.4954225	1.220884521E-160	6.742785	4917.504905	0.0483275	7.4851590	83.002473	256.737168	6.060003	42.3658455	0.413235
S 1.1.4	4 substrings shaded	1.2194309E+00	7.3559714	6.978546092E-159	8.121131	2259.645422	0.0465220	7.3296288	79.544036	193.860074	4.874283	39.772018	0.332505
S 1.1.5	5 substrings shaded	1.4632351E+00	9.9999999	2.335727249E-121	9.999999	4999.230959	0.0587113	7.6433605	76.085600	147.051996	3.865436	38.042800	0.252862
S 1.1.6	6 substrings shaded	1.7256678E+00	9.9999999	1.000000000E-04	10	5000	1.3248654	6.4787290	70.897945	118.059483	3.251111	36.313582	0.257026
S 1.1.7	7 substrings shaded	1.6900849E+00	8.7027090	4.338883168E-19	9.772837	8.493474	1.9999179	4.0465880	73.491773	74.774486	2.011246	37.178191	0.251435
S 1.1.8	8 substrings shaded	1.0572433E+00	1.9436930	7.477942875E-20	9.999821	44.178384	1.9572869	1.5849399	85.596300	34.022763	0.787009	43.230455	0.250785
S 1.1.9	9 substrings shaded	2.8717227E-04	0.5488580	1.733530395E-08	2.016755	1103.740202	1.1395626	0.5478572	90.783955	33.984822	0.451800	75.220991	0.683295

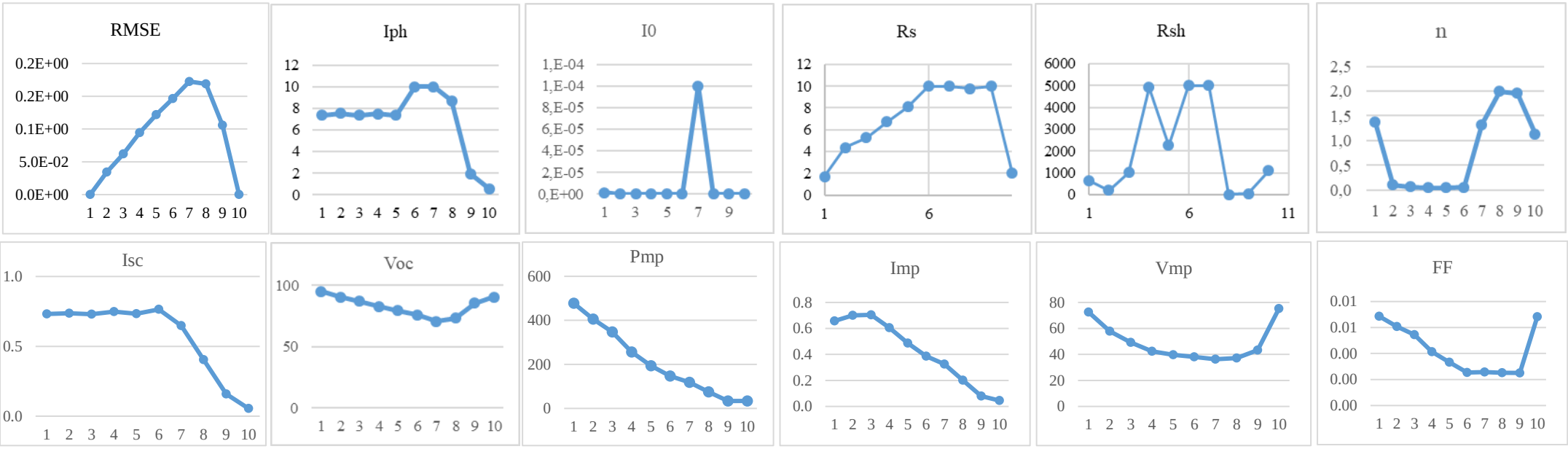

Figure 5.6 Graphs of the estimated parameters using the DSCE technique in the different scenarios of case 1.1

Table 5.5 Estimated parameters using the DSCE technique for scenarios of case 1.2: G = 662.2860 W/m^2, T = 319.251 K)

Scenarios	*Description*	*RMSE*	I_{ph}	I_0	R_s	R_{sh}	*n*	*Isc*	*Voc*	*Pmp*	*Imp*	*Vmp*	*FF*
Healthy PV string	0 substring shaded	2.6089417E-04	5.9375764	7.0821798E-07	1.661131	1175.904	1.353642	5.9291979	99.13000	409.14534	5.341291	76.60045	0.6961079
S 1.2.1	1 substring shaded	2.7306172E-01	6.0440526	1.341603E-68	5.066544	356.38347	0.129596	5.9593315	95.52527	365.98506	5.719955	63.98391	0.6429061
S 1.2.2	2 substrings shaded	5.4526675E-01	5.9321931	2.684390E-115	6.599390	4945.35760	0.073007	5.9242874	90.11818	295.73980	5.757348	51.36736	0.5539381
S 1.2.3	3 substrings shaded	7.7373350E-01	6.1225973	3.157528E-167	8.836902	348.11197	0.048593	5.9710216	87.41464	214.34221	4.853994	44.15791	0.4106529
S 1.2.4	4 substrings shaded	9.9611811E-01	5.9685129	9.121850E-150	9.987502	4989.00844	0.050930	5.9565884	82.00755	167.55112	4.041821	41.45436	0.3430014
S 1.2.5	5 substrings shaded	1.2343590E+00	10.0000000	1.000000E-04	10.000000	20.22842	1.511525	6.2352150	77.50164	132.05837	3.330434	39.65200	0.2732773
S 1.2.6	6 substrings shaded	1.3243195E+00	9.9999899	3.980501E-20	7.787346	7.74578	1.996884	4.9866164	76.60045	96.56301	2.491896	38.75082	0.2527979
S 1.2.7	7 substrings shaded	1.3399937E+00	5.9809547	8.016537E-20	9.597699	12.81745	1.986072	3.4200352	76.60045	65.53761	1.691257	38.75082	0.2501662
S 1.2.8	8 substrings shaded	8.6966605E-01	1.5589975	1.863715E-53	4.553290	57.47586	0.167634	1.4445583	89.21700	32.35874	0.718140	45.05909	0.2510782
S 1.2.9	9 substrings shaded	2.9862890E-04	0.5487915	1.819845E-08	1.979005	1103.65168	1.142835	0.5478092	91.01936	33.96744	0.454122	74.79809	0.6812390

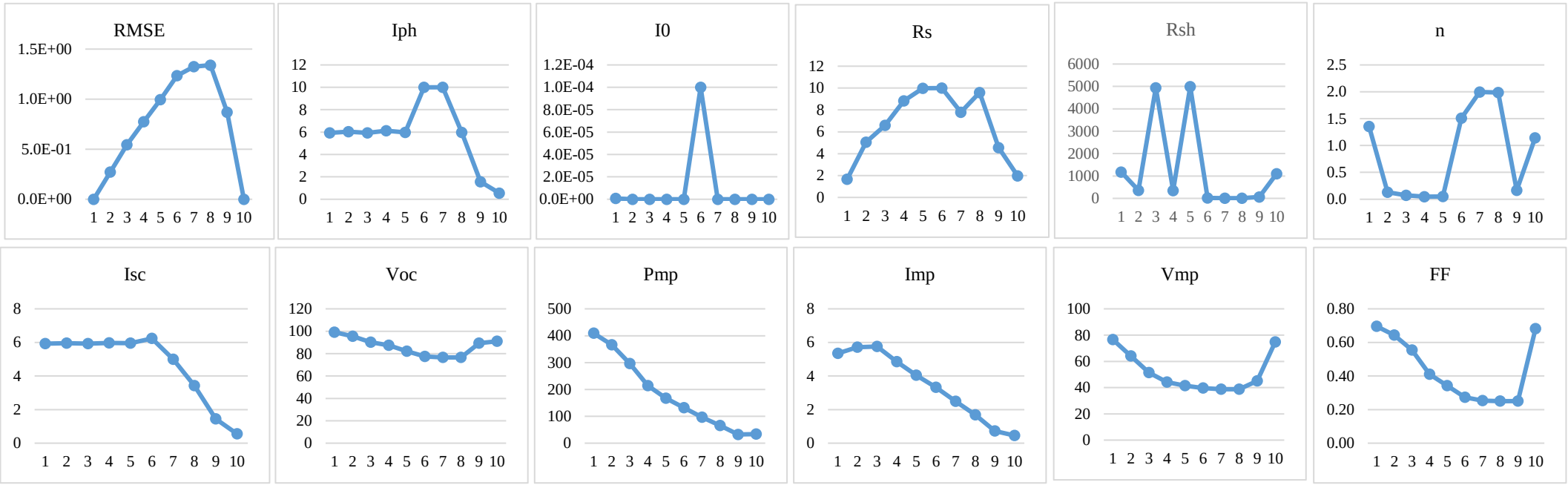

Figure 5.7 Graphs of the estimated parameters using the DSCE technique for scenarios of case 1.2

Table 5.6 Estimated parameters using the DSCE technique for scenarios of case 1.3: (G = 482.754 W/m^2, T = 311.127 K)

Scenarios	*Description*	*RMSE*	I_{ph}	I_0	R_s	R_{sh}	*n*	*Isc*	*Voc*	*Pmp*	*Imp*	*Vmp*	*FF*
Healthy PV string	0 substring shaded	2.7514370E-04	4.3209542	1.182355E-07	1.750925	599.815	1.231647	4.30837723	97.79300	302.883352	3.871486	78.234400	0.7188759
S 1.3.1	1 substring shaded	1.9512707E-01	4.4114012	4.979756E-85	6.580169	336.448	0.104587	4.32677918	95.12592	271.636060	4.073907	66.677045	0.6599694
S 1.3.2	2 substrings shaded	3.8518297E-01	4.3126280	2.09597E-128	8.932653	916.704	0.065955	4.27100990	90.68078	218.555030	4.097269	53.34164	0.5643064
S 1.3.3	3 substrings shaded	5.7961909E-01	4.3240229	2.807105E-11	10	5000	0.721506	4.31538198	86.23565	161.793344	3.433758	47.118445	0.4347650
S 1.3.4	4 substrings shaded	7.2342564E-01	9.9989361	1.049087E-19	8.425969	8.749870	1.999549	5.09374783	87.12467	111.410298	2.557491	43.562336	0.3310422
S 1.3.5	5 substrings shaded	8.0558632E-01	10	4.553367E-20	10	8.224478	1.958541	4.51287448	81.79051	92.787265	2.268901	40.895255	0.2513809
S 1.3.6	6 substrings shaded	9.1474172E-01	6.8744727	1.377779E-21	9.998850	11.541164	2.000000	3.68335017	79.12343	73.053454	1.826052	40.006227	0.2506644
S 1.3.7	7 substrings shaded	9.3048170E-01	3.8375312	1.199535E-20	9.994505	20.708992	1.999992	2.58835020	79.12342	51.422571	1.285364	40.006227	0.2510878
S 1.3.8	8 substrings shaded	6.1275698E-01	1.2790022	4.132407E-54	5.7869349	77.465506	0.163774	1.190098	91.56980	29.477565	0.592091	49.785527	0.2704934
S 1.3.9	9 substrings shaded	2.9498327E-04	0.5488108	1.796886E-08	1.9871380	1103.71777	1.141977	0.547825	90.68078	33.967843	0.454856	74.678291	0.6837720

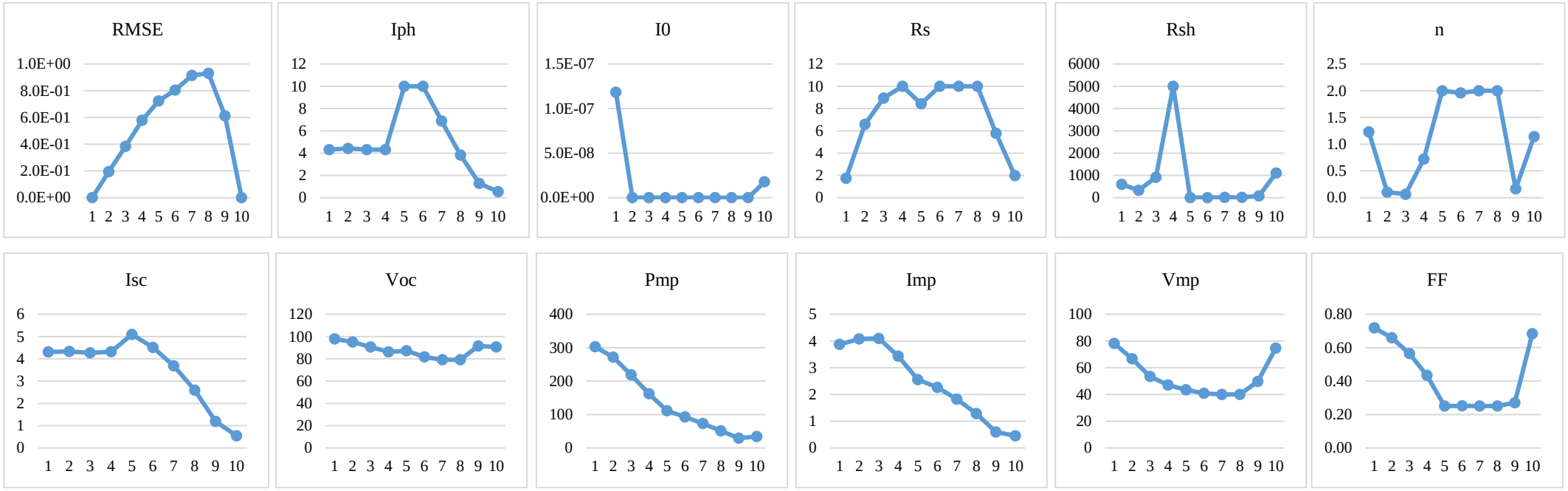

Figure 5.8 Graphs of the estimated parameters using the DSCE technique for scenarios of case 1.3.

Table 5.7 Estimated parameters using the DSCE technique in scenarios of case n° 02 (G = 783.809 W/m^2, T = 322.957 K)

Scenarios	*Percentage of shading*	*RMSE*	I_{ph}	I_0	R_s	R_{sh}	*n*	*Isc*	*Voc*	*Pmp*	*Imp*	*Vmp*	*FF*
Healthy PV string	0%	2.425754E-04	7.115097	1.511478E-06	1.686145	1014.091628	1.3918370	7.103277	96.1550	469.690083	6.396655	73.427455	0.6876710
S 2.1	10%	1.115227E-01	7.528500	2.460214E-11	2.159581	66.999	0.7994536	7.293412	96.1550	438.698509	5.904295	74.301591	0.6255522
S 2.2	20%	2.417826E-01	8.042520	3.971835E-18	2.438333	34.800	0.5043711	7.515905	96.1550	408.802325	5.314366	76.924000	0.5656661
S 2.3	40%	4.532893E-01	7.149254	2.571714E-11	10	5000	0.9435862	7.134710	96.1550	304.173540	5.04305	60.31541	0.4433770
S 2.4	60%	6.384751E-01	7.267606	1.747475E-80	10	466.695822	0.1214989	7.115148	96.1550	273.575109	5.130593	53.322318	0.3998718
S 2.5	80%	8.329192E-01	7.416227	1.67081E-158	8.254880	3985.732544	0.0536076	7.400898	90.9101	251.657424	5.431937	46.329227	0.3740355
S 2.6	90%	9.072673E-01	7.236507	5.67438E-176	7.236490	746.983375	0.045276	7.167074	85.66536	252.027463	5.883999	42.832681	0.4104881

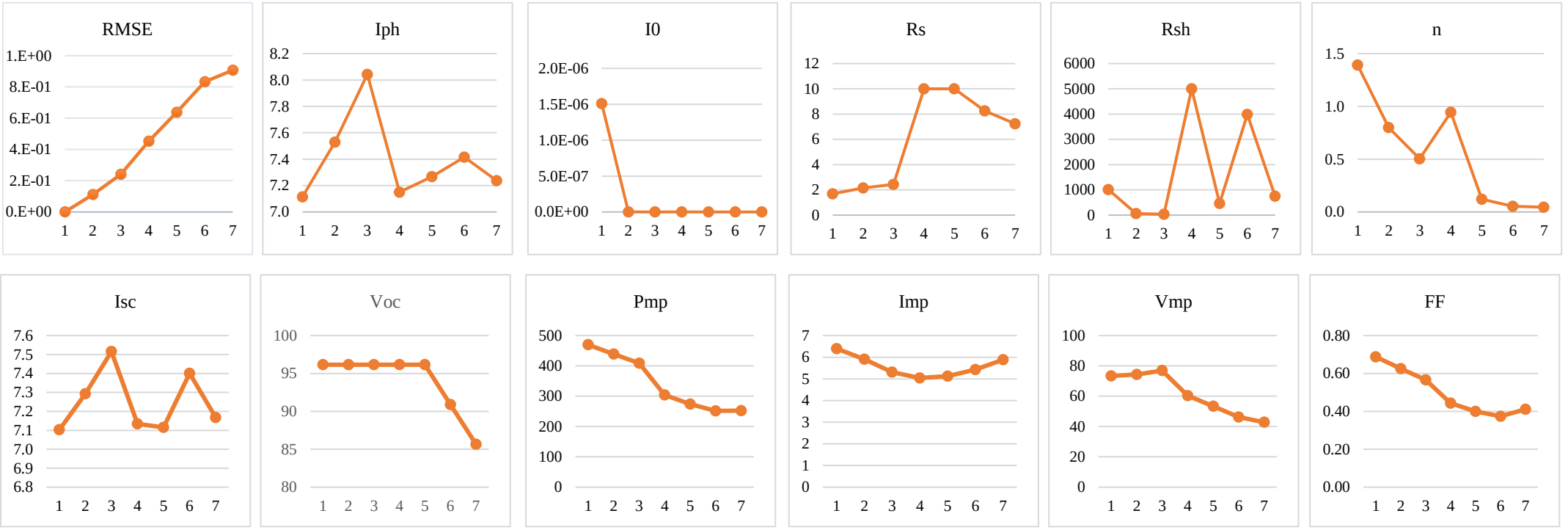

Figure 5.9 Graphs of the estimated parameters using the DSCE technique for scenarios of case n° 02.

Table 5.8 Estimated parameters using the DSCE technique for scenarios of case n° 03 (G = 826.560 W/m^2, T = 324.865 K)

Scenarios	*Description*	*RMSE*	I_{ph}	I_0	R_s	R_{sh}	*n*	*Isc*	*Voc*	*Pmp*	*Imp*	*Vmp*	*FF*
Healthy PV string	No faults	2.3956461E-04	7.3346079	1.371284175E-06	1.706201	656.464706	1.3753831	7.3155860	95.107000	477.291849	6.571809	72.6271636	0.685997
S 3.1	1 substring is shaded	3.4255651E-01	7.5247481	1.958613E-79	4.383285	203.382451	0.1061324	7.3659967	90.783955	405.863402	7.0062445	57.9288091	0.606930
S 3.2	1 connection resistance fault	2.2174214E-04	7.3176006	1.509450E-06	6.697572	785.490573	1.4705431	7.2539738	95.107000	323.907609	5.5092495	58.7934182	0.469496
S 3.3	1 substring shaded and 1 Connection resistance fault	2.2439003E-01	7.1612433	1.267660E-43	9.045779	4999.99999	0.1909733	7.1483109	89.054736	218.288068	4.8551970	44.9596727	0.342901
S 3.4	Bypass diode n°1 inverted	1.502216E-04	7.335461	1.21176045E-06	1.5166396	586.285956	1.2999297	7.3165277	94.242391	459.715439	6.564237	70.0333364	0.666711
S 3.5	Bypass diode n°1 inverted and substring n°1 shaded	3.207941E-02	1.316929	3.06693369E-62	0.3812089	115.213721	0.1440105	1.3125865	94.242391	49.788719	0.654378	76.0856000	0.402492
S 3.6	Bypass Diode n°1 inverted and other substring is shaded	3.718281E-01	7.277334	4.28144906E-89	4.2992986	927.274069	0.0931605	7.2437486	89.054736	404.539178	7.089194	57.0642000	0.627105
S 3.7	01 substring is shaded, other bypass diode is inverted and 1 connection resistance fault	1.039937E-01	7.397845	1.91326597E-10	2.4264949	310.7655775	0.83308633	7.340529099	94.242391	452.773450	6.628787	68.3041182	0.654496
S 3.8	Module n° 2 short-circuited	2.647170E-04	7.334965	1.37366398E-06	1.1368480	430.2198144	0.85276373	7.315623466	61.387245	292.827174	6.513107	44.9596727	0.652051
S 3.9	Module n° 2 open-circuited	1.515033E-04	7.314818	1.48502931E-06	6.7003752	819.1130443	1.32823987	7.251768786	95.107000	274.481967	5.291061	51.8765455	0.397976
S 3.10	Module n°2 open circuited and 1 substring shaded	2.196232E-01	8.107874	2.08535362E-69	9.0721994	76.82351975	0.12005049	7.251530621	89.054736	218.852673	4.867755	44.9596727	0.338895

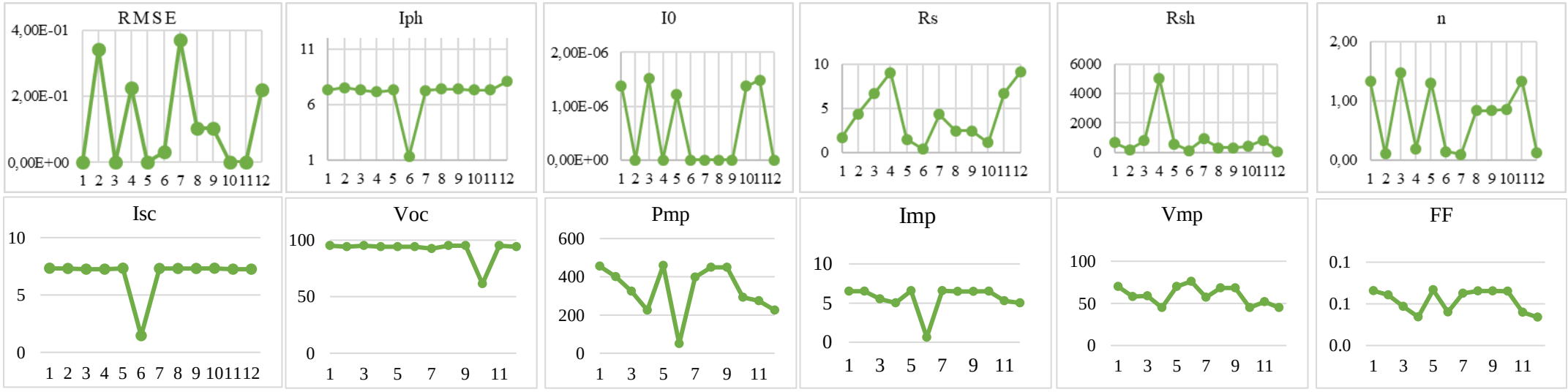

Figure 5.10 Graphs of the estimated parameters using the DSCE technique for scenarios of case n° 03

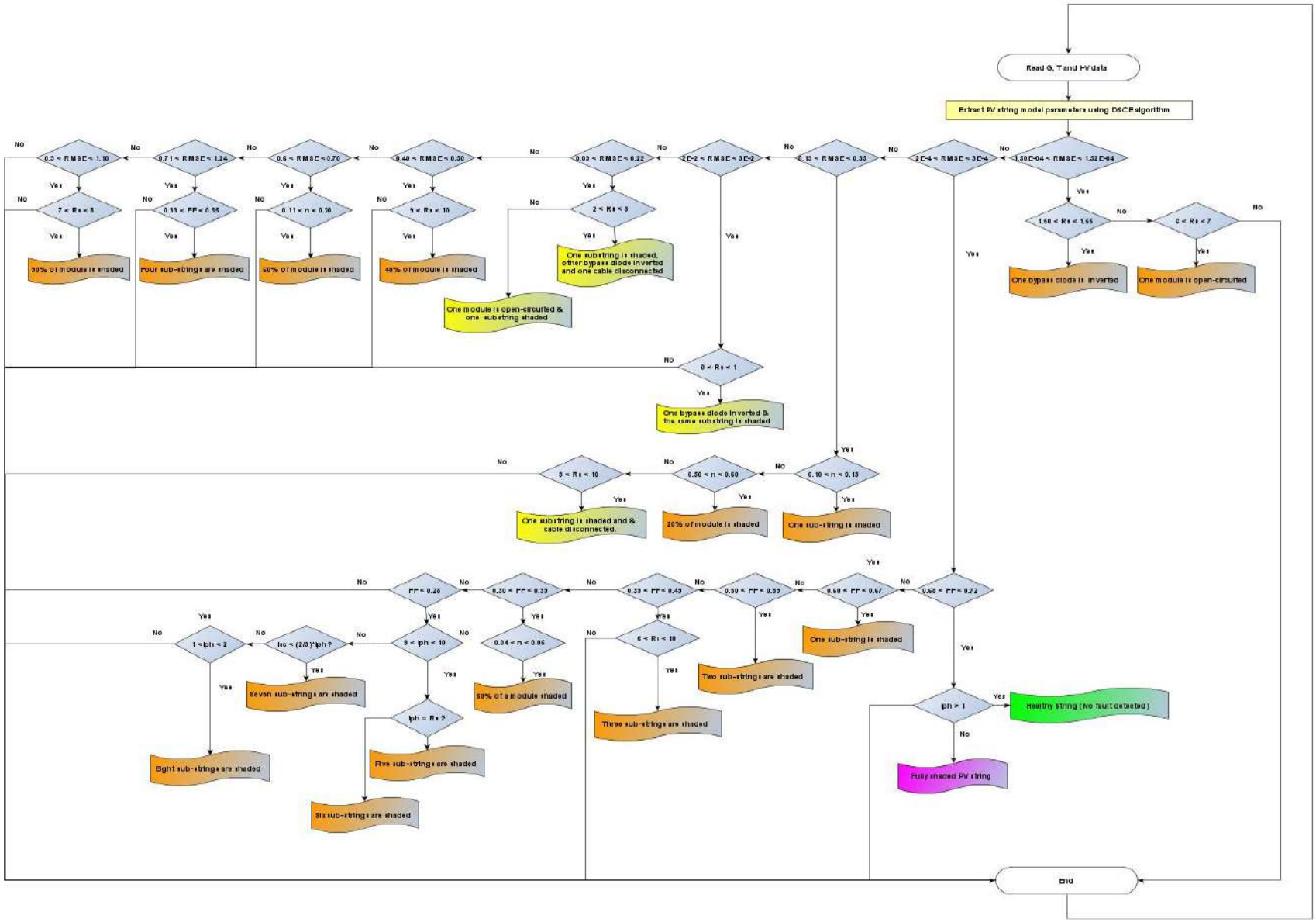

Figure 5.11 Flowchart of the fault tree algorithm using the DSCE technique

General conclusion

General conclusion (thesis conclusion)

The work presented as part of this thesis focuses on PV generator modeling and fault diagnosis using the process of modeling itself. As the PV generator is the most important part of the entire PV system, the research presented here focuses on it and offers specialized insights into this field of science.

The thesis provides a structured examination of key aspects, including understanding fault types and detection methods, and delving into the fundamental principles of the photovoltaic effect as well as the various PV generator technologies available in the market and laboratories, including technology generations.

The thesis also focuses on the problem of parameter identification in the PV generator model, which is still the subject of progressing research. To address this issue, innovative metaheuristic techniques have been introduced. These optimizers contribute significantly to enhancing the accuracy of the PV generator modeling process while consuming a minimum execution time and optimal computational resources to perform the optimization process.

The three proposed techniques are named the Bat-Artificial Bee Colony Optimizer (BABCO), the Nested Loop Biogeography-based Optimization-Differential Evolution (NLBBODE), and the Differential Shuffled Complex Evolution (DSCE). The first two methods have been used to solve the problem of PV generator modeling, while the third one was also used in fault diagnosis. All three algorithms have proven their reliability and accuracy.

Due to constraints of feasibility and safety when testing some types of faults on the real PV generator, the development of a simulator that can replicate the behavior of the PV generator was considered an important contribution to the field. The thesis presents, therefore, a PV generator simulator that has undergone rigorous testing under both normal and faulty conditions, including partial shading in different scenarios, connection resistance faults, bypass diode faults, module short-circuited, multiple simultaneous faults…etc. The majority of faults may be simulated accurately.

When identifying the PV generator model parameters using the proposed techniques, according to the electrical circuit-based models, accuracy and computational effort need to be balanced. To achieve this, the three models, SDM, DDM, and TDM, were studied, tested, and validated in the PV generator modeling phase. Meanwhile, the SDM model was chosen in the simulation and fault diagnosis processes due to its simplicity and proven accuracy.

The DSCE technique was utilized to detect and diagnose faults in PV generators based on a well-defined hypothesis. This hypothesis states that correct model parameters are produced by the input data of a healthy PV generator therefore incorrect model parameters are produced by the input data of a faulty PV generator. The analysis of the extracted parameters of faulty situations leads to patterns that indicate signs of fault.

The results presented conclusively demonstrate the effectiveness of the proposed technique in modeling PV generators under healthy conditions and diagnosing faults in various faulty scenarios. Hence, this contribution adds a practical and resolute dimension to the theoretical frameworks discussed throughout the thesis.

This research project has yielded notable achievements, including:

- The deepening of the understanding of PV generator modeling using different electrical circuit-based models via modern optimization techniques. It was proven that the merging of metaheuristic techniques and numerical methods in PV generator modeling improves model precision.
- The successful implementation and validation of several metaheuristic techniques that precisely model PV generators while consuming optimal computational resources.
- The comprehension enhancement of the metaheuristic algorithms' working mechanism to solve the problem of PV generator modeling in particular and to solve real-world problems in general.
- The development and experimental validation of a highly effective PV generator simulator that accurately replicates its real-world behavior.
- The classification and simulation of various types of faults with high accuracy.
- The pioneering of a novel fault diagnosis method through the modeling process itself.
- The strengthening of knowledge of solar PV energy applications in general.

Perspectives and Future Works

As with any research project, the work presented in this thesis is not finished yet. There are several possible directions to explore in future works, including:

- The development of novel metaheuristic algorithms to solve the problem of PV generators with more precision and low effort. These algorithms can have applications in other domains of engineering.
- Testing and verifying the proposed fault diagnosis technique using different types of faults at the PV generator level.

- Experimentally validating the proposed technique by using the modeling process, since the simulation process has already been validated.
- Expanding the fault detection method to be applied to the entire PV system.

Appendices

Appendix A: *Extracts of the published journal and conference papers*

Energy Conversion and Management 248 (2021) 114667

Contents lists available at ScienceDirect

Energy Conversion and Management

journal homepage: www.elsevier.com/locate/enconman

Photovoltaic mono and bifacial module/string electrical model parameters identification and validation based on a new differential evolution bee colony optimizer

Oussama Hachana [a,*], Belkacem Aoufi [b], Giuseppe Marco Tina [c], Mohamed Amine Sid [d]

[a] Department of Drilling and Rig Mechanics, Faculty of Hydrocarbons, Renewable Energies, and Earth, and Universe Sciences, University of Ouargla, 30000, Algeria
[b] Department of Electronics and Communications, Faculty of New Information Technologies and Communication, University of Ouargla, 30000 Algeria
[c] Department of Electric, Electronic and Computer Engineering (DIEEI), University of Catania, 95125, Italy
[d] Mechatronics Laboratory (LMETR) E1764200 Optics and Precision Mechanics Institute, Setif1 University, Setif 19000, Algeria

ARTICLE INFO

Keyword:
Hybrid meta-heuristic algorithm
Bifacial PV module
Lambert W function
Online PV parameters extraction
Partial shading

ABSTRACT

Well estimating the electrical model parameters of the photovoltaic (PV) module/string serves to develop an accurate simulator and a fault diagnosis tool. Several based evolutionary techniques were proposed to identify the unknown circuit equivalent PV generator (PVG) parameters. Whereas most of them have not been examined to various real operating conditions of solar irradiance and PV cells temperature. That requires larger search range than the adopted one in the literature. Enlarging the search range imposes more computational time and high exploration and exploitation features. Hence, a novel hybrid differential evolution and artificial bee colony intelligence (nDEBCO) approach is proposed. In terms of convergence quality, CPU execution time, number of function evaluations (NFE), and error standard deviation (StD). The newly developed approach permits to accurately identify the PV module/string unknown parameters with suitable implementation complexity. Monofacial CLS 220P PV string has been utilized employing an adequate experimental setup with online implementation. 1080 I-V curves have been measured and estimated, where the overall RMSE ± StD is below 0.02 ± 1e−16. The nDEBCO outperforms the present-day published works, for common case studies in the literature with two based root mean square error (RMSE) objective functions namely Lambert W function (LWF) and classic. It yields 7.73006268e− 4 of RMSE, 7.8785e− 18 of StD, and 2150 NFE under ODM with LWF for RTC France PV cell. Bifacial PV module has been evaluated and the electrical parameters have been extracted within less than 1.36 s of CPU run time and not>8.0299631e− 3 ± 6.9096e− 16 of RMSE ± StD for front and rear faces. Additionally, the parameter identification procedure has been well validated to simulate the real partial shading scenarios of the studied PV string with a RMSE less than 0.045 and 0.397% of power maximum point absolute error.

1. Introduction

Renewable electricity is the world's fastest-growing source of commercialized energy. It is expected that by 2050, photovoltaic and wind power generation will be the main part of several developed countries' energy resources [1]. The task of replacing fossil fuels can be met by solar energy technology, not only because of their prices continue to decrease while the cost of fossil fuels continues to increase. But also because of the advantage of limitless resources, lightweight, no emissions, preservation, and long-term maintenance required [2].

To examine and evaluate the PV generator (PVG) behavior under different operating conditions, it is necessary to select a significant synoptic model and a robust method to identify the unknown electrical parameters. Several models in the literature express the physical behavior of the PV modules to emulate the estimated I-V curves [3]. The most common and used of which is the one diode-based circuit model (ODM). It is verified that this model provides an accurate prediction in outdoor measurements of the annual energy yield, especially for mono-c-Si and multi-c-Si technologies [4]. The double diode model (DDM) and the triple diode model (TDM) are still prevalent, by taking into account the recombination effects of the charge carriers, however they require more computational time [5].

Due to the transcendental aspect of the PV module's characteristic

* Corresponding author.
E-mail address: oussamahachana@yahoo.fr (O. Hachana).

https://doi.org/10.1016/j.enconman.2021.114667
Received 2 June 2021; Accepted 17 August 2021
Available online 13 October 2021

Journal of Computational Electronics
https://doi.org/10.1007/s10825-022-01870-4

Precise and fast parameter identification of mono-crystalline, poly-crystalline, and mono-facial photovoltaic modules using a new Bat Artificial Bee Colony optimizer

Belkacem Aoufi[1] · Oussama Hachana[2] · Mohamed Amine Sid[3] · Giuseppe Marco Tina[4]

Received: 22 October 2021 / Accepted: 3 February 2022

Abstract
Precise and fast identification of the photovoltaic model parameters plays a crucial role in many model-based design issues. It is the cornerstone of PV system simulation, control, and fault diagnosis. In this paper, a new optimizer is proposed to deal successfully with the difficulties of the PV modeling with considerable accuracy, reliability, and minimum execution time, especially for online applications. This new optimizer is named "Bat Artificial Bee Colony Optimizer" (BABCO), boosted with evolutionary strategies. It provides an accurate scheme to identify the unknown parameters of the different photovoltaic models based on the experimental current–voltage data. The performance of this optimizer was evaluated and compared to many recently published techniques and is tested by solving four problems of parameter estimation: PV cell model, mono-crystalline, poly-crystalline, and mono-facial photovoltaic modules model. The four problems were solved utilizing one diode model and double diode model-based circuit, and using, as the fitness function, the root mean square error (RMSE) with the employment of the Lambert *W* function to calculate the output current. The results and the performance metrics demonstrate the advantage of the proposed optimizer over several most cited methods in the literature.

Keywords Parameter identification · Photovoltaic model · Bat algorithm · Mono-facial · Artificial bee colony optimizer

1 Introduction

Solar photovoltaic energy is one of the promising alternative energy sources in the world, due to the health and environmental problems caused by fossil energy. In addition, photovoltaic energy could be transformed into electricity without polluting the atmosphere or emitting greenhouse gases. In addition, it is low cost and available almost all over the world. Nevertheless, operations like control, monitoring, or fault diagnosis of photovoltaic systems come with high complications due to the ever-changing weather conditions. Consequently, precise measurement of the climate parameters, such as solar irradiance and ambient temperature, is crucial for the photovoltaic system performance [1–4].

To deal with the above-mentioned difficulties, modeling the photovoltaic power generation system is a high-priority step. For this reason, the parameter identification of photovoltaic systems is a very attractive domain for many researchers nowadays. The modeling can be achieved by formulating a photovoltaic parameter model starting from the initial principles of physics and then estimating the characteristic parameters of this system using experimental data and appropriate optimization algorithms. The most popular equivalent circuit models are the one diode model (ODM) and the double diode model (DDM) [5–7]. In PV modeling, the curves obtained by the designed model must thoroughly represent the nonlinear *I*–*V* curve of solar PV [8].

Both ODM and DDM models are given by only one equation relating the measured current and voltage with five and seven unknown parameters to be identified, respectively. This fact makes the parameter estimation issue

✉ Belkacem Aoufi
belkacem2015.ka@gmail.com

[1] Department of Electronics and Communications, Faculty of New Technologies of Information and Communications, University of Ouargla, 30000 Ouargla, Algeria

[2] Department of Drilling and Rig Mechanics, Faculty of Hydrocarbons, Renewable Energy, Science, Earth and Universe, University of Ouargla, 30000 Ouargla, Algeria

[3] Department of Electrical Engineering, Faculty of Technology, University of Setif, 19000 Sétif, Algeria

[4] DIEEI: Department of Electric, Electronic and Computer Engineering, University of Catania, 95125 Catania, Italy

Published online: 17 March 2022

Applied Soft Computing 145 (2023) 110597

Contents lists available at ScienceDirect

Applied Soft Computing

journal homepage: www.elsevier.com/locate/asoc

NLBBODE optimizer for accurate and fast modeling of photovoltaic module/string generator and its application to solve real-world constrained optimization problems

Belkacem Aoufi [a,*], Oussama Hachana [b], Mohamed Amine Sid [c], Giuseppe Marco Tina [d]

[a] Department of Electronics and Communications, Faculty of New Information Technologies and Communication, University of Ouargla, 30000, Algeria
[b] Department of Drilling and Rig Mechanics, Faculty of Hydrocarbons, Renewable Energies, and Earth and Universe Sciences, University of Ouargla, 30000, Algeria
[c] Department of Electrical Engineering, Faculty of Technology, University of Setif, 19000, Algeria
[d] Department of Electric, Electronic and Computer Engineering (DIEEI), University of Catania, 95125, Italy

ARTICLE INFO

Article history:
Received 2 March 2022
Received in revised form 28 April 2023
Accepted 23 June 2023
Available online 5 July 2023

Keywords:
Parameter identification
Engineering design problems
Photovoltaic module
Biogeography-based optimization
Hybrid algorithm
Differential Evolution

ABSTRACT

In this paper, a new optimizer is presented to quickly and accurately identify parameters of the photovoltaic (PV) module/string models. This optimizer is named Nested Loop Biogeography-based Optimization - Differential Evolution referred to as (NLBBODE). It has been developed to identify the PV parameters with reasonable computational effort and minimum execution time, despite the nonlinearity of the PV system dynamics and the insufficiency of data. In addition, the NLBBODE optimizer is used to solve some engineering design problems known as highly constrained, nonlinear, and non-convex. The weaknesses of the original versions of BBO and DE approaches have been overpassed. Furthermore, the proposed optimizer is compared to the state-of-the-art metaheuristic methods using performance evaluation metrics. The computational resources needed to obtain the optimum solution using NLBBODE are significantly reduced due to the nested loop design. The results obtained prove that the NLBBODE optimizer is a suitable candidate to solve the problem of the PV modeling as well as to solve various real-world constrained optimization problems, with high accuracy and low processor runtime, which is a necessary condition for online applications. For instance, the well-known Photowatt-PWP-201 module model represented in the single diode model, NLBBODE registers a standard deviation value of 1.4682E-17 within a time of 13.9 s. For the STM6-40/36 module model represented in the single diode model, the NLBBODE optimizer records a standard deviation value of 6.191583E-18 within an execution time of 6 s. For the speed reducer design problem, the standard deviation obtained by the NLBBODE is 1.515824E-13 and needs a time of less than 1 s to obtain the optimum solution.

1. Introduction

Solar photovoltaic energy is the most promising alternative energy resource in the world due to global warming and economic issues related to fossil energy. This is due to its non-polluting electrical energy generation and worldwide availability [1]. As compared to other energy sources, operation and maintenance in solar photovoltaic (PV) facilities are relatively low cost [2]. However, because weather conditions are continuously changing, producing electricity using PV generators involves a high level of complexity [3]. Thus, accurate PV modeling is necessary to manage, monitor, simulate, and diagnose defaults in photovoltaic facilities. PV modeling may be achieved by the design of the PV parametric model from the basic principles of physics and simplifying assumptions, and then, estimate the unknown parameters using experimental data and dedicated optimization techniques. The optimization approaches use the experimental current–voltage (I–V) data to produce the estimated ones. Unfortunately, the experimental (measured) I–V data is characterized by its nonlinearity and its sensitivity to the weather conditions changing, that is to say, the solar irradiance and cells temperature [4]. The PV model is represented in equivalent electrical circuits, and the most popular models are the single diode model (SDM) and the double diode model (DDM) [5–7]. The curves generated by the optimization method must thoroughly match the measured I–V curves of a solar PV generator [8].

The problem of the PV parameter identification using classic methods is not successful, since both the SDM and DDM models are represented by a single equation that relates the measured

* Corresponding author.
E-mail address: belkacem2015.ka@gmail.com (B. Aoufi).

https://doi.org/10.1016/j.asoc.2023.110597
1568-4946/

A New Mutated-Firefly Algorithm for Parameters Extraction of Solar Photovoltaic Cell Model

B. Aoufi[1(✉)] and O. Hachana[2]

[1] Department of Electronics and Communications, Faculty of New Information Technologies and Communication, Kasdi Merbah University, Ouargla, Algeria
belkacem2015.ka@gmail.com

[2] Department of Drilling and Rig Mechanics, Faculty of Hydrocarbons, Renewable Energies and Earth and Universe Sciences, Kasdi Merbah University, Ouargla, Algeria
oussamahachana@yahoo.fr

Abstract. Based on experimental data and metaheuristic algorithms, the extraction of the solar photovoltaic (PV) model remains an active research domain during the past few years. However, it is still a challenge to estimate those parameters accurately using metaheuristic algorithms. In this paper, a new hybridized approach is presented to extract the photovoltaic model parameters called Mutated Firefly (Mu-FA). This new algorithm is used to identify both the single-diode and double-diode PV model, while the estimation is based on the experimental data of the nonlinear I-V curve of the (PV) cell. The fitness function used to perform the optimization is the Root Mean Square Error (RMSE), which is a function of estimated and experimental data. In order to assess this new approach, a comparison study with the latest published meta-heuristic methods has been presented. Results have shown the efficiency, robustness, and reliability of the (Mu-FA), thus it is concluded that it is a promising optimization technique for PV model parameters estimation.

Keywords: Metaheuristic · Photovoltaic · Optimization · Firefly algorithm · Differential Evolution

1 Introduction

Solar energy is the principal type among the renewable sources in the world, because of environmental and economic considerations such as cleanliness in production facilities (no CO_2 emission) and low cost in installation and maintenance operations. Algeria, being the largest country in Africa, in the Mediterranean and in the Arab world, has one of the highest solar irradiance in the world, estimated to exceed 5 billion GWh/year. The annual sunshine duration is estimated to be around 2.500 h average, and could exceed 3.600 h in some parts of the country [1]. In both industrial and academic research projects related to solar energy, an important effort has been conducted to identify the photovoltaic (PV) model parameters. In that context, theoretical studies are required, and it is obvious that this kind of study is a very attractive area for

M. Hatti (Ed.): ICAIRES 2020, LNNS 174, pp. 551–561, 2021.
https://doi.org/10.1007/978-3-030-63846-7_52

Appendix B

B.1: Pseudo code of the BABCO algorithm

Set the BABCO parameters: *NP*, *A0*; *A∞*; *Fmin*; *Fmax*; *SF*; *NFE_Max*

Randomly Initialize the *NP* population using Eq. (3.40).

Evaluate fitness of each bat and define the best location X_i

NFE=NP

Initialize loudness: A_0

While *NFE* ≤ *NFE_Max* **do**

Adjust frequency using Eq. (3.41)

Update solution using Eq. (3.42)

Evaluate fitness of the new bat location

NFE= FNE+1

if *rand* <A_i and *Ob* (X_i+1) < *Ob* (X_i) then

Accept the new solutions: $X_i = X_i^{new}$ using Eq. (3.42)

Increase A_i using Eq. (3.43)

end if

SumPi= SumPi +*Ob*(X_i)

for *i*=1 to *NP* **do**

Pi(*i*)= *Ob*(*Xi*) / SumPi (Eq. 3.44)

end

Sort(Pi)

for *j*= 1 to (*NP/f*) **do**

indxf= indexPi (*j*)

indexl=indexPi (*NP-j+1*)

end for

Select randomly *04 indices* (h_1, h_2, h_3 and h_4) and perform crossover process using Eq. (3.45)

for *i*= 1 to *NP* **do**

Select randomly 04 bats (X_{r1}, X_{r2}, X_{r3} and X_{r4}) that will interact with each other to generate a new solution X_{i+1} using Eq. (3.46) (*i≠r1≠r2≠r3≠r4*)

Evaluate fitness of the bat location: *Ob*(X_{i+1})

NFE =NFE+ 1

Update the best solution: X_{best}

end for

Return the best points X_{1best} as the best vector of PV parameters model

end while

B. 2: Pseudo code and flowchart of the NLBBODE algorithm

Define problem aspects: *Ob(x)*, *Dim*; *LB*, *UB*; NFE_Max

Set algorithm parameters: *NP*; *Kr* (Keep Rate); Migration Rates μ; α; and scaling factor of DE: β_{min} and β_{max};

Generate a random set of habitats (islands)

for each habitat, calculate the corresponding HSI value

NFE = NP

Sort the habitats from the best to the worst

While *NFE* < *NFE_Max* **do**

for *i*= 1 to *NP* **do *(outer loop)***

for *k*: 1 to *Dim* **do**

if rand ≤ λ_i **then**

Assign the immigration rate λ_i and the emigration rate μ_i to each candidate X_i using Eq. (3.47) and Eq.(3.48)

end if

for *i*=1 to *NP* **do *(inner loop)***

Mutation: choose randomly 3 vectors with different indices r_1, r_2 and r_3 to generate donor vector V_i using Eq. (3.49).

Evaluate the fitness of the new solution

NFE = FNE +1

Selection: **if** *Ob* (V_i) < *Ob* (X_i) **then**

$X_i^{new} = V_i$

else $X_i^{new} = X_i$ (Using Eq. (3.50)

end if

end for

end for

Evaluate the fitness of the new solution X_i^{new}

NFE = FNE +1

Sort the new solutions

Elitism: keep the best old population and add them to the new population using Eq. (3.51)

Return the best solution X_1^{best} as the optimum solution

End while

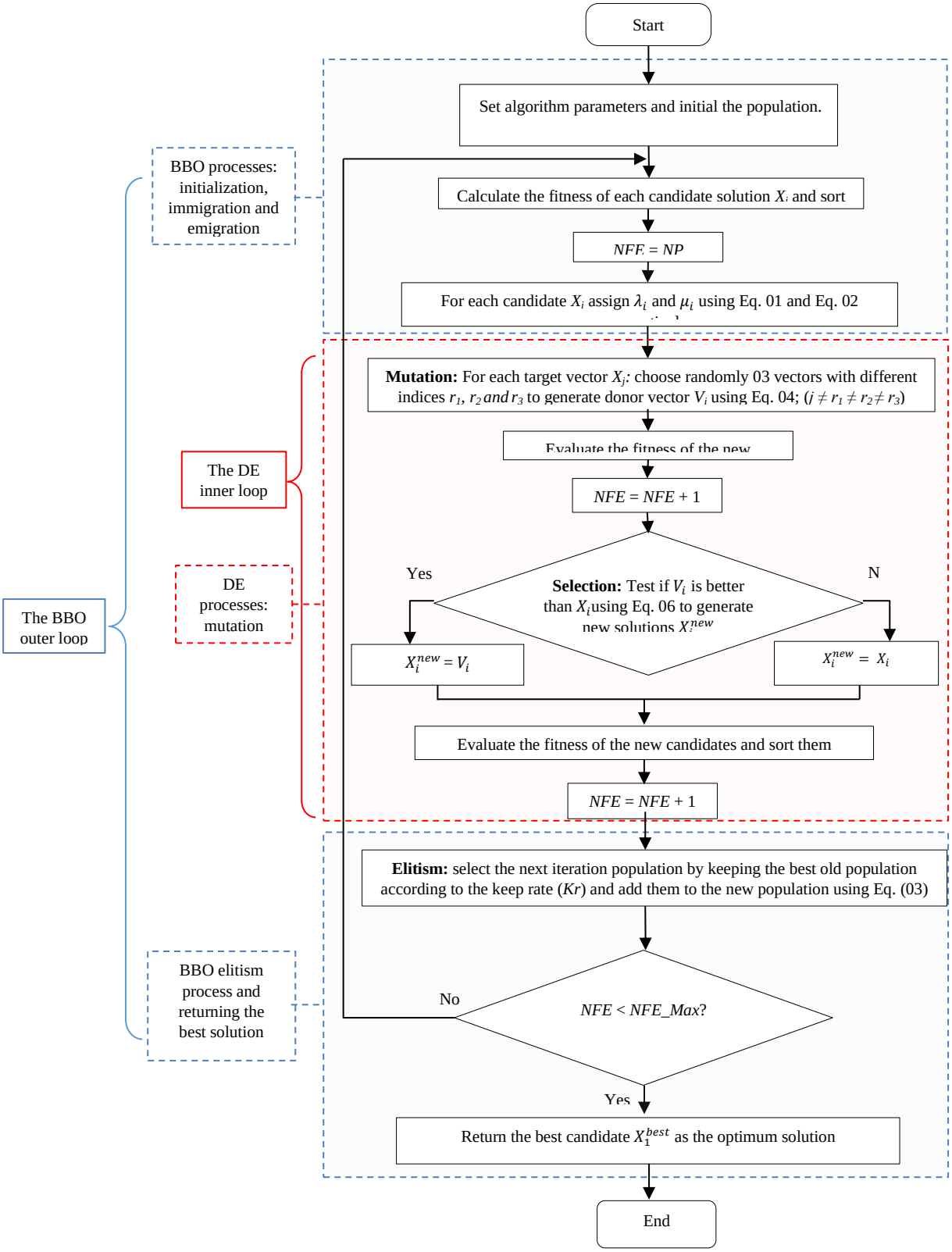

Fig. B.2 Flowchart of the NLBBODE optimizer

B. 3: Pseudo codes and flowchart of the DSCE algorithm

B3.1 Main routine of DSCE:

1: Define problem aspects: *Ob(x)*, *Dim*; *LB*, *UB*;
2: Set the SCE algorithm parameters: *p*, *m*, *s=p*m*, *q*, α and β.
(p = number of complexes, *m* = number of points in each complex; Compute sample size *s=p×m);* Set the DE algorithm parameters: (F_{min}, F_{max}, *CrP*),
3: Initialize the population and calculate the fitness of each candidate.
4: *NFE = NP*
5: **While** *NFE < NFE_Max* **do**
6: **for** *i* =1 to *NP* **do**
7: **Mutation:** For each target vector X_i*:* choose randomly 4 vectors with different indices r_1, r_2, r_3 and r_4 to generate donor vector V_i using Eq. 35
8: **End for**
9: Sort the new population and update the best solution (X_1=X_{best})
10: **for** *j*=1 to *s* **do**
11: Form Complexes $A^k \in D$ from the new sorted population:
$D = \{(A^k)\ ,\ k=1,\ldots s\}$; $A^k = \{X_1^k, X_2^k, \ldots, X_m^k\}$
12: **for** *k*=1 to *p* **do**
13: Evolve each complex A^k using **CCE subroutine**
14: **end for**
15: Replace A^k, *k* = 1,…, *m*, into *D* ($D^{old} \leftarrow D^{new}$)
16: **Crossover:** perform crossover on the best point X_{best} using eq. 24
1: **Selection**: **if** $Ob(U_i) < Ob(X_i)$ **then**
2: $X_i^{new} = U_i$
3: **else** $X_i^{new} = X_i$
4: **end if**
5: Evaluate fitness of the new solution
6: *NFE = FNE* +1
7: **end for**
8: Evaluate the fitness of the new points X_i^{new}
9: *NFE = FNE* +1
10: Sort the new points
11: Return the best points X_1^{best} as the best vector of PV parameters model
12: **end while**

B3.2 Subroutine CCE:

1: Initialization: Select *q*, α, β, where $2 \le q \le m$, $\alpha \ge 1$, $\beta \ge 1$.
2: **for** *j*= 1 to β **do**
3: Assign a triangular probability distribution to each element from complex *A*: $P_i = 2(m+1-i)/[m\,(m+1)]$, *i*=1,…, *m*.
4: Select *q* points as parents from *A* according to P_i.
5: Store them in sun-complex *B* and their relative positions in *A* in *L*.
6: **for** *k* = 1 to α **do**

Sort B and L in order of increasing *Ob(x)*.
  Compute the centroid *g* of $u_1,\ldots, u_{q-1}$ and let u_q be the worst point in B:

$$g=\frac{1}{q-1}\sum_{k=1}^{q-1}u_k$$

  Compute $u_r = 2g - u_q$ (reflection phase)
  if $u_r \in [LB, UB]$ then
    Compute $Ob(u_r)$ and go to 14
  else Generate a point u_z at random in *H*. Set $u_r = u_z$
  Compute $Ob(u_z)$.
  $NFE = FNE + 1$
  if $Ob(u_r) < Ob(u_q)$ **then**
    Set $u_q = u_r$ and $Ob(u_q) = Ob(u_r)$ and go to 23
  else Compute $u_{ic}=(g + u_q)/2$ (reflection step) and $Ob(u_{ic})$
  $NFE = FNE + 1$
  if $Ob(u_{ic}) < Ob(u_q)$ **then**
  Set $u_q = u_{ic}$ and $Ob(u_q) = Ob(u_{ic})$ and go to 23
  else Generate a point u_z at random in H.
  Compute $Ob(u_z)$, Set $u_q=u_z$, $Ob(u_q) = Ob(u_z)$
  $NFE = FNE + 1$
  end if
  end if
  end if
 end for
end for

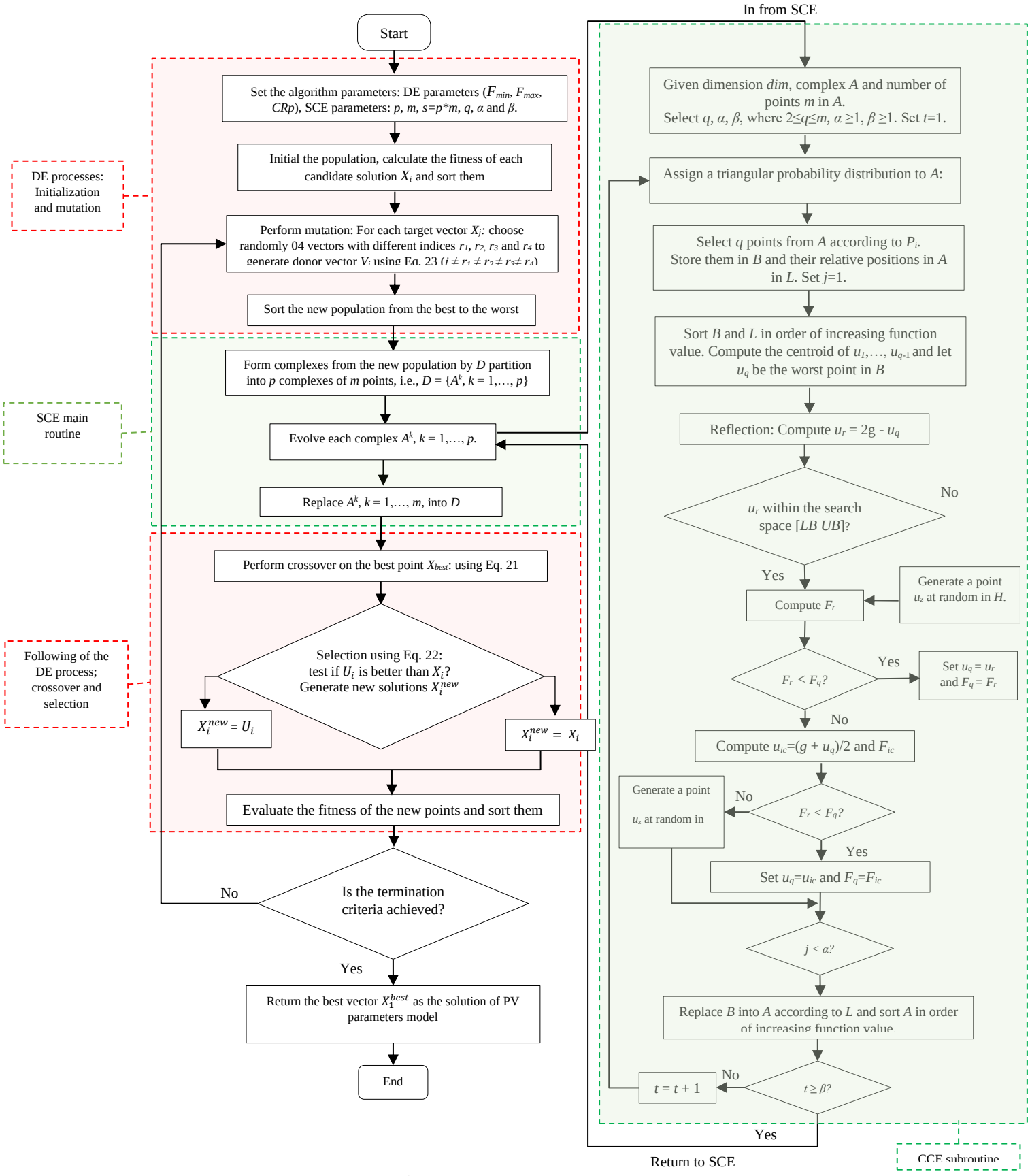

Fig. B.3. Flowchart of DSCE algorithm

References

1. Abbass, Kashif, et al. "A review of the global climate change impacts, adaptation, and sustainable mitigation measures." *Environmental Science and Pollution Research* (2022): 1-21.
2. Olabi, A. G., and Mohammad Ali Abdelkareem. "Renewable energy and climate change." *Renewable and Sustainable Energy Reviews* 158 (2022): 112111.
3. Mehrabadi, Reza Allahdadi, Mohsen Parsa Moghaddam, and Mohammad Kazem Sheikh-El-Eslami. "Generation expansion planning in multi electricity markets considering environmental impacts." *Journal of Cleaner Production* 243 (2020): 118611.
4. IRENA (2022), *Renewable Energy Statistics 2022*, International Renewable Energy Agency, Abu Dhabi. ISBN 978-92-9260-446-2.
5. Ni, Jiaxin, et al. "Dynamic performance investigation of organic Rankine cycle driven by solar energy under cloudy condition." *Energy* 147 (2018): 122-141.
6. Al-Hilfi, Hasanain AH, Ahmed Abu-Siada, and Farhad Shahnia. "Estimating Generated Power of Photovoltaic Systems During Cloudy Days Using Gene Expression Programming." *IEEE Journal of Photovoltaics* 11.1 (2020): 185-194.
7. IEA (2022), Solar PV, IEA, Paris https://www.iea.org/reports/solar-pv, License: CC BY 4.0
8. Awadallah MA. Variations of the bacterial foraging algorithm for the extraction of PV module parameters from nameplate data. *Energy Conversion and Management.* 2016; 113: 312–20.
9. J. Siecker, K. Kusakana, and B. P. Numbi, A review of solar photovoltaic systems cooling technologies, *Renewable and Sustainable Energy Reviews.* 2017; 79:192–203.
10. Siddiqui, M. U., et al. "A comprehensive review on multi-physics modeling of photovoltaic modules." *Energy Conversion and Management* (2022): 115414.
11. A. Mehmood, H. A. Sher, A. F. Murtaza and K. Al-Haddad, "Fault Detection, Classification and Localization Algorithm for Photovoltaic Array," *IEEE Transactions on Energy Conversion*, (2021); 36: 2945-2955.
12. Lahcene Rouani, Mohamed Faouzi Harkat, Abdelmalek Kouadri, Saad Mekhilef. Shading fault detection in a grid-connected PV system using vertices principal component analysis, Renewable Energy, 2021; 164: 1527-1539.
13. M. Ma, Z. Zhang, P. Yun, Z. Xie, H. Wang and W. Ma, "Photovoltaic Module Current Mismatch Fault Diagnosis Based on I-V Data, "*IEEE Journal of Photovoltaics*, (2021); 11: 779-788.
14. A. Mellit, G.M. Tina, S.A. Kalogirou. "Fault detection and diagnosis methods for photovoltaic systems: A review", *Renewable and Sustainable Energy Reviews*, (2018); 91: 1-17.

15. M. C. Chang and S. -I. Liu, "An Indoor Photovoltaic Energy Harvester Using Time-Based MPPT and On-Chip Photovoltaic Cell," in IEEE Transactions on Circuits and Systems II: Express Briefs, 2020; 7:2432-2436.
16. Adel Mellit, Soteris Kalogirou. Assessment of machine learning and ensemble methods for fault diagnosis of photovoltaic systems, Renewable Energy, 2022; 184: 1074-1090.
17. Siva Ramakrishna Madeti, S.N. Singh. Modeling of PV system based on experimental data for fault detection using kNN method, Solar Energy, 2018; 173:139-151.
18. N. Gokmen, E. Karatepe, B. Celik, S. Silvestre, "Simple diagnostic approach for determining of faulted PV modules in string-based PV arrays," Solar Energy, 2012: 86, pp 3364–3377.
19. Mellit A, Tina GM, Kalogirou SA. Fault detection and diagnosis methods for photovoltaic systems: A review. Renewable and Sustainable Energy Reviews. 2018; 91:1-7.
20. Aram M, Zhang X, Qi D, Ko Y. A state-of-the-art review of fire safety of photovoltaic systems in buildings. Journal of Cleaner Production. 2021; 308:127239.
21. Adel Mellit, Soteris Kalogirou, Handbook of Artificial Intelligence Techniques in Photovoltaic Systems, Academic Press, 2022, pp183-226.
22. Omdahl TP, editor. Reliability, Availability, and Maintainability: RAM: Dictionary. American Society for Quality Control; 1988.
23. Puig, Vicenc, and Silvio Simani, eds. Diagnosis and Fault-tolerant Control 1: Data-driven and Model-based Fault Diagnosis Techniques. John Wiley & Sons, 2021.
24. Gallardo-Saavedra S, Hernádez-Callejo L, Duque-Pérez Ó. Analysis and characterization of PV module defects by thermographic inspection. Revista Facultad de Ingeniería Universidad de Antioquia. 2019; 93:92-104.
25. Rossi, D., Omana, M., Giaffreda, D., & Metra, C. Modeling and Detection of Hotspot in Shaded Photovoltaic Cells. IEEE Transactions on Very Large-Scale Integration (VLSI) Systems, 2015; 23(6): 1031-1039.
26. Djordjevic S, Parlevliet D, Jennings P. Detectable faults on recently installed solar modules in Western Australia. Renewable energy. 2014; 67:215-21.
27. Alam MK, Khan F, Johnson J, Flicker J. A comprehensive review of catastrophic faults in PV arrays: types, detection, and mitigation techniques. IEEE Journal of Photovoltaics. 2015; 5:982-97.
28. Zhao Y, Ball R, Mosesian J, de Palma JF, Lehman B. Graph-based semi-supervised learning for fault detection and classification in solar photovoltaic arrays. IEEE Transactions on Power Electronics. 2014; 30:2848-2858.

29. P. Dunbabin BEIS. Fire and solar PV systems-investigation and evidence. Bre National solar center. Report n° P100874-1004. 2017.
30. Ying-Yi Hong, Rolando A. Pula, Methods of photovoltaic fault detection and classification: A review, Energy Reports, 2022: 8, 5898-5929.
31. Pillai DS, Rajasekar N. A comprehensive review on protection challenges and fault diagnosis in PV systems. Renewable and Sustainable Energy Reviews. 2018; 91: 18-40.
32. Mandal RK, Kale PG. Assessment of different multiclass SVM strategies for fault classification in a PV system. In Proceedings of the 7th International Conference on Advances in Energy Research 2020 (pp. 747-756). Singapore: Springer Singapore.
33. Chang M, Chen C, Hsueh CH, Hsieh WJ, Yen E, Ho KL, Chuang HP, Lee CY, Chen H. The reliability investigation of PV junction box based on 1GW worldwide field database. In 2015 IEEE 42nd Photovoltaic Specialist Conference (PVSC) IEEE. 2015 pp. 1-4.
34. Naveen Venkatesh S, and V Sugumaran. "Fault diagnosis of visual faults in photovoltaic modules: A Review", International journal of green energy 2021; 18: 37-50.
35. Tsanakas JA, Chrysostomou D, Botsaris PN, Gasteratos A. Fault diagnosis of photovoltaic modules through image processing and Canny edge detection on field thermographic measurements. International Journal of Sustainable Energy. 2015; 34(6): 351-72.
36. Haque A, Bharath KV, Khan MA, Khan I, Jaffery ZA. Fault diagnosis of photovoltaic modules. Energy Science & Engineering. 2019; 7:622-44.
37. T. Takashima, J. Yamaguchi, K. Otani, K. Kato, M. Ishida, Experimental studies of failure detection methods in PV module strings, IEEE 4th World Conference on Photovoltaic Energy Conference. 2006; 2: 2227-2230.
38. Fadhel S, Delpha C, Diallo D, Bahri I, Migan A, Trabelsi M, Mimouni MF. PV shading fault detection and classification based on IV curve using principal component analysis: Application to isolated PV system. Solar Energy. 2019; 179:1-0.
39. Houssein A, Heraud N, Souleiman I, Pellet G. Monitoring and fault diagnosis of photovoltaic panels. In2010 IEEE International Energy Conference 2010; 389-394. IEEE.
40. Hachana O, Tina GM, Hemsas KE. PV array fault Diagnostic technique for BIPV systems. Energy and Buildings. 2016; 126:263-74.
41. Mellit A, Kalogirou SA. Artificial intelligence techniques for photovoltaic applications: a review. Prog Energy Combust Sci 2008; 34: 574-632.

42. Mellit A, Kalogirou S. Artificial intelligence and internet of things to improve efficacy of diagnosis and remote sensing of solar photovoltaic systems: Challenges, recommendations and future directions. Renewable and Sustainable Energy Reviews. 2021; 143: 110889.
43. Mere A. Structural and Electrical Properties of Spray Deposited Copper Indium Disulphide Films for Solar Cells. Tallinna Tehnikaülikooli Kirjastus; 2006.
44. Hersch P, Zweibel K. Basic photovoltaic principles and methods. Solar Energy Research Inst. (SERI), Golden, CO (United States); 1982 Feb 1.
45. Fraas LM, O'Neill MJ. History of solar cell development. In Low-cost solar electric power 2023 Jul 26 (pp. 1-12). Cham: Springer International Publishing.
46. Allouhi A, Rehman S, Buker MS, Said Z. Up-to-date literature review on Solar PV systems: Technology progress, market status and R&D. Journal of Cleaner Production. 2022 Aug 15; 362: 132339.
47. C.A. Gueymard, D.R. Myers, Solar radiation measurement: progress in radiometry for improved modeling, in Modeling Solar Radiation at the Earth's Surface, Springer, Berlin, Heidelberg, 2008, pp. 1–27.
48. Sen Z. Solar energy fundamentals and modeling techniques: atmosphere, environment, climate change and renewable energy. Springer Science & Business Media; 2008 Mar 28.
49. Iqbal M. An Introduction to Solar Radiation, an Introduction to Solar Radiation.
50. Zhang T, Yang H. High efficiency plants and building integrated renewable energy systems: Building-integrated photovoltaics (BIPV). Handbook of Energy Efficiency in Buildings: A Life Cycle Approach; Elsevier: Amsterdam, The Netherlands. 2018:441-595.
51. Philipps S, Warmuth W. Photovoltaics report fraunhofer institute for solar energy systems. ISE with Support of PSE GmbH November 14th; Fraunhofer ISE: Freiburg, Germany. 2019.
52. International Renewable Energy Agency website: https://www.irena.org//media/Files/IRENA/Agency/Publication/2019/Nov/IRENA_Future_of_Solar_PV_summary_2019.pdf?la=en&hash=A626155A0775CC50427E23E7BE49B1AD2DD31073.
53. NREL website: https://www.nrel.gov/pv/cell-efficiency.html.
54. Mughal S, Sood YR, Jarial RK. A review on solar photovoltaic technology and future trends. International Journal of Scientific Research in Computer Science, Engineering and Information Technology. 2018 Apr;4(1):227-35.
55. IEC 61836 Solar Photovoltaic Energy Systems -Terms, Definitions and Symbols. 2007.

56. Zhao D, Qian M, Ma J, Yamashita K. Photovoltaic generator model for power system dynamic studies. Solar Energy. 2020; 210:101-14.
57. Santiago Silvestre, Chapter 7 - Strategies for Fault Detection and Diagnosis of PV Systems, Advances in Renewable Energies and Power Technologies, Elsevier, 2018; Pages: 231-255.
58. National Institute of Standards and Technology; webpage: https://csrc.nist.gov/glossary/term/model.
59. Precup R, Kamal T, Hassan SZ. Solar photovoltaic power plants. Singapur : Springer. 2019.
60. Bikaneria J, Joshi SP, Joshi AR. Modeling and Simulation of PV Cell using One-diode model. International journal of scientific and research publications. 2013; 3(10):1-4.
61. King DL, Boyson WE, Kratochvil JA. Photovoltaic Array Performance Model. Albuquerque, New Mexico: Sandia National Laboratories; 2004.
62. Ridha HM, Hizam H, Mirjalili S, Othman ML, Ya'acob ME, Ahmadipour M. Parameter extraction of single, double, and three diodes photovoltaic model based on guaranteed convergence arithmetic optimization algorithm and modified third order Newton Raphson methods. Renewable and Sustainable Energy Reviews. 2022; 162: 112436.
63. Xu C, Sun X, Liang Y, Huang G, Yu F. An analytical effective-diode-based analysis of industrial solar cells from three-diode lumped-parameter model. IEEE Transactions on Electron Devices. 2021 Apr 14; 68(6):2753-8.
64. Shockley W. The Theory of p-n Junctions in Semiconductors and p-n Junction Transistors. Bell system technical journal. 1949 Jul;28(3):435-89.
65. Salam Z, Ishaque K, Taheri H. An improved two-diode photovoltaic (PV) model for PV system. In2010 Joint International Conference on Power Electronics, Drives and Energy Systems & 2010 Power India 2010; (pp. 1-5). IEEE.
66. Ishaque K, Salam Z, Taheri H. Accurate MATLAB Simulink PV System Simulator Based on a Two-Diode Model, Journal of Power Electronics. The Korean Institute of Power Electronics; 2011. p. 179-87.
67. Elbaset AA, Ali H, Abd-El Sattar M. Novel seven-parameter model for photovoltaic modules. Solar energy materials and Solar cells. 2014; 130: 442-55.
68. Aoufi B, Hachana O, Sid MA, Tina GM. Precise and fast parameter identification of mono-crystalline, poly-crystalline, and mono-facial photovoltaic modules using a new Bat Artificial Bee Colony optimizer. Journal of Computational Electronics. 2022; (2): 491-512.

69. Nishioka K, Sakitani N, Uraoka Y, Fuyuki T. Analysis of multicrystalline silicon solar cells by modified 3-diode equivalent circuit model taking leakage current through periphery into consideration. Solar energy materials and solar cells. 2007; 91(13): 1222-7.
70. Ćalasan M, Aleem SH, Zobaa AF. A new approach for parameters estimation of double and triple diode models of photovoltaic cells based on iterative Lambert W function. Solar Energy. 2021; 218: 392-412.
71. International Electrotechnical Commission, Technical Specification IEC TS 61836: Solar photovoltaic energy systems - Terms, definitions and symbols, 2016.
72. Hachana O, Aoufi B, Tina GM, Sid MA. Photovoltaic mono and bifacial module/string electrical model parameters identification and validation based on a new differential evolution bee colony optimizer. Energy Conversion and Management. 2021; 248: 114667.
73. Khan F, Al-Ahmed A, Al-Sulaiman FA. Critical analysis of the limitations and validity of the assumptions with the analytical methods commonly used to determine the photovoltaic cell parameters. Renewable and Sustainable Energy Reviews. 202; 140: 110753.
74. Ridha HM, Hizam H, Mirjalili S, Othman ML, Ya'acob ME, Ahmadipour M. Novel parameter extraction for Single, Double, and three diodes photovoltaic models based on robust adaptive arithmetic optimization algorithm and adaptive damping method of Berndt-Hall-Hall-Hausman. Solar Energy. 2022; 243: 35-61.
75. Navarro MA, Oliva D, Ramos-Michel A, Haro EH. An analysis on the performance of metaheuristic algorithms for the estimation of parameters in solar cell models. Energy Conversion and Management. 2023; 276: 116523.
76. Ćalasan M, Aleem SH, Zobaa AF. On the root mean square error (RMSE) calculation for parameter estimation of photovoltaic models: A novel exact analytical solution based on Lambert W function. Energy conversion and management. 2020; 210: 112716.
77. Calasan M, Nedic A. Experimental testing and analytical solution by means of Lambert W-function of inductor air gap length. Electric Power Components and Systems. 2018; 46(7): 852-62.
78. Dehghanzadeh A, Farahani G, Maboodi M. A novel approximate explicit double-diode model of solar cells for use in simulation studies. Renewable energy. 2017; 103: 468-77.
79. Abualigah L, Hanandeh ES, Zitar RA, Thanh CL, Khatir S, Gandomi AH. Revolutionizing sustainable supply chain management: A review of metaheuristics. Engineering Applications of Artificial Intelligence. 2023; 126: 106839.

80. Yang X-S. A new metaheuristic bat-inspired algorithm. Nature inspired cooperative strategies for optimization (NICSO 2010), Springer, 2010; 65-74.
81. D Karaboga, B Basturk, A powerful and efficient algorithm for numerical function optimization: artificial bee colony (ABC) algorithm, Journal of global optimization, 2007; 39:459-471.
82. Meirelles L, Deotti P, Luiz J, Pereira R, Chaves I. Parameter extraction of photovoltaic models using an enhanced Lévy flight bat algorithm. Energy Conversion and Management, 2020; 221:113114.
83. Aoufi B, Hachana O, Sid MA, Tina GM. NLBBODE optimizer for accurate and fast modeling of photovoltaic module/string generator and its application to solve real-world constrained optimization problems. Applied Soft Computing. 2023; 145: 110597.
84. Chen, Xu et al. "Biogeography-Based Optimization with Covariance Matrix Based Migration." Applied Soft Computing, 2016; 45:71-85.
85. Gong, W., Cai, Z. & Ling, C.X. DE/BBO: a hybrid differential evolution with biogeography-based optimization for global numerical optimization. Soft Comput, 2010; 15:645-665.
86. Shukla AK, Sudhakar K, Baredar P. Simulation and performance analysis of 110 kWp grid-connected photovoltaic system for residential building in India: A comparative analysis of various PV technology. Energy Reports. 2016 Nov 1; 2: 82-8.
87. Chen Z, Wu L, Cheng S, Lin P, Wu Y, Lin W. Intelligent fault diagnosis of photovoltaic arrays based on optimized kernel extreme learning machine and IV characteristics. Applied energy. 2017; 204: 912-31
88. Vinod, Kumar R, Singh SK. Solar photovoltaic modeling and simulation: As a renewable energy solution. Energy Reports. 2018; 4: 701-12.
89. Fara L, Craciunescu D. Output analysis of stand-alone PV systems: modeling, simulation and control. Energy Procedia. 2017; 112: 595-605.
90. Cheng-En Ye, Cheng-Chi Tai, Yu-Pei Huang, Jun-Jia Chen. Dispersed partial shading effect and reduced power loss in a PV array using a complementary SuDoKu puzzle topology, Energy Conversion and Management, 2021; 246: 114675.
91. Nabil Karami, Nazih Moubayed, Rachid Outbib, General review and classification of different MPPT Techniques, Renewable and Sustainable Energy Reviews, 2017; 68:1, 1-18.

92. Kashif Ishaque, Zainal Salam. A review of maximum power point tracking techniques of PV system for uniform insolation and partial shading condition, Renewable and Sustainable Energy Reviews, 2013; 19: 475-488.
93. Hegazy Rezk, Mazen AL-Oran, Mohamed R. Gomaa, Mohamed A. Tolba, Ahmed Fathy, Mohammad Ali Abdelkareem, A.G. Olabi, Abou Hashema M. El-Sayed. A novel statistical performance evaluation of most modern optimization-based global MPPT techniques for partially shaded PV system, Renewable and Sustainable Energy Reviews, 2019; 115:109372.
94. Eldeghady GS, Kamal HA, Hassan MA. Fault diagnosis for PV system using a deep learning optimized via PSO heuristic combination technique. Electrical Engineering. 2023 Mar 30:1-5.
95. Garoudja E, Harrou F, Sun Y, Kara K, Chouder A, Silvestre S. Statistical fault detection in photovoltaic systems. Solar Energy. 2017 1; 150: 485-99.
96. Fadhel S, Diallo D, Delpha C, Migan A, Bahri I, Trabelsi M, Mimouni MF. Maximum power point analysis for partial shading detection and identification in photovoltaic systems. Energy Conversion and Management. 2020; 15; 224: 113374.
97. Duan Y. Shuffled Complex Evolution Approach for Effective and Efficient Global Minimization. Journal of optimization theory and applications, 1993; 76: 501–521.
98. Gao X, Cui Y, Hu J, Xu G, Wang Z, Qu J, et al. Parameter extraction of solar cell models using improved shuffled complex evolution algorithm. Energy Conversion and Management, 2018; 157: 460–479.
99. Singer S, Nelder J. Nelder-mead algorithm. Scholarpedia, 2009; 4:2928.